

ESD ACCESSION LIST

TRI Call No. 74426

Copy No. 1 of 2 cys.

ESD-TR-71-229

MTR-2028

MICROWAVE SOLID STATE SOURCES AND INTEGRATED CIRCUITS - FINAL REPORT

B. D. Campbell
P. J. Benson
A. L. Murphy
V. P. Nanda
R. S. Steriti

ESD RECORD COPY

RETURN TO
SCIENTIFIC & TECHNICAL INFORMATION DIVISION
(TRI), Building 1210

JULY 1971

Prepared for

DEPUTY FOR PLANNING AND TECHNOLOGY
ELECTRONIC SYSTEMS DIVISION
AIR FORCE SYSTEMS COMMAND
UNITED STATES AIR FORCE
L. G. Hanscom Field, Bedford, Massachusetts



Approved for public release;
distribution unlimited.

Project 702B
Prepared by
THE MITRE CORPORATION
Bedford, Massachusetts
Contract F19(628)-71-C-0002

A0731756

When U.S. Government drawings, specifications, or other data are used for any purpose other than a definitely related government procurement operation, the government thereby incurs no responsibility nor any obligation whatsoever; and the fact that the government may have formulated, furnished, or in any way supplied the said drawings, specifications, or other data is not to be regarded by implication or otherwise, as in any manner licensing the holder or any other person or corporation, or conveying any rights or permission to manufacture, use, or sell any patented invention that may in any way be related thereto.

Do not return this copy. Retain or destroy.

MICROWAVE SOLID STATE SOURCES
AND INTEGRATED CIRCUITS - FINAL REPORT

B. D. Campbell
P. J. Benson
A. L. Murphy
V. P. Nanda
R. S. Steriti

JULY 1971

Prepared for

DEPUTY FOR PLANNING AND TECHNOLOGY
ELECTRONIC SYSTEMS DIVISION
AIR FORCE SYSTEMS COMMAND
UNITED STATES AIR FORCE
L. G. Hanscom Field, Bedford, Massachusetts



Approved for public release;
distribution unlimited.

Project 702B
Prepared by
THE MITRE CORPORATION
Bedford, Massachusetts
Contract F19(628)-71-C-0002

FOREWORD

This report was prepared under Contract F19(628)-71-C-0002 with The MITRE Corporation, Bedford, Mass. It carries a MITRE Project Number 702B. The project was initiated in FY 69. This report describes the completion of studies on applying microwave integrated circuits and solid state oscillators to future sensor subsystems for Air Force command and control.

REVIEW AND APPROVAL

This technical report has been reviewed and is approved.



ROBERT P. SAVOY
Development Engineering Division
Deputy for Planning and Technology

ABSTRACT

This report describes the completion of the studies, initiated in FY 69, carried out to assess the practicability of applying microwave integrated circuits and solid state fundamental oscillators to future sensor subsystems for radar and communications, including data relay. The X-band eight-element phased array was evaluated, a simple MIC module including a printed antenna was constructed and studies were carried out of avalanche diode oscillator modulation characteristics, MIC IMPATT avalanche diode oscillators, MIC antennas, and MIC evaluation techniques.

ACKNOWLEDGMENTS

This work reported was carried out at The MITRE Corporation, Radar Technology Department, under USAF Contract No. AF19628-68-C-0365, Project 700-B.

The authors are grateful to P. C. Blasi, R. W. LaPorte and R. P. McLean for their technical assistance.

TABLE OF CONTENTS

	<u>Page</u>
LIST OF ILLUSTRATIONS	vi
LIST OF TABLES	x
SECTION I - INTRODUCTION	1
Background	1
Program Objectives	3
SECTION II - SUMMARY AND CONCLUSIONS	5
SECTION III- WORK ACCOMPLISHED	19
Transmitting Phased Array	19
Diode Oscillators and Modulation	47
MIC Transmitting Module	113
MIC Quality Measurements	116
APPENDIX A - MUTUAL COUPLING OF ANTENNA ELEMENTS	123
APPENDIX B - PHASE-CODED INJECTION-LOCKED OSCILLATOR	130
APPENDIX C - SIMPLIFIED DESCRIPTION OF DIODE OSCILLATOR OPERATION	137
REFERENCES	149

LIST OF ILLUSTRATIONS

<u>Figure No.</u>	<u>Title</u>	<u>Page</u>
1	Transmitting Phase Array	6
2	Transmitting Phased Array Module	7
3	MIC Transmitting Module	8
4	Transmitting Phased Array	21
5	High Power IMPATT Oscillator Spectra	23
6	Effect of Isolation on Frequency and Phase Pulling	26
7	Slot-Fed Coaxial Dipole	31
8	Phase Display	32
9	Test Circuit for Measuring Phase and Amplitude of Primary Fields	33
10	E Plane Radiation of Array ($\phi = 0^\circ$)	33
11	Three of the Phased Array Modules	34
12	Part of Antenna Array	37
13	E Plane Radiation Pattern of Dipole with Baffles and Ground Plane	38
14	H Plane Radiation Pattern of Dipole with Baffles and Ground Plane	38
15	E Plane Radiation Pattern of Dipole with Ground Plane (No Baffles)	39
16	H Plane Radiation Pattern of Dipole with Ground Plane (No Baffles)	39
17	Input Impedance of Dipole with Baffles and Ground Plane	40
18	E Plane Radiation Pattern of Array ($\phi = 67.5^\circ$)	42
19	E Plane Radiation Pattern of Array ($\phi = 112.5^\circ$)	42
20	Array Beam Angles	43
21	Calculated E Plane Radiation Pattern of Array ($\phi = 0^\circ$)	44

LIST OF ILLUSTRATIONS - continued

<u>Figure No.</u>	<u>Title</u>	<u>Page</u>
22	Calculated E Plane Radiation Pattern of Array ($\phi = 67.5^\circ$)	44
23	Calculated E Plane Radiation Pattern of Array ($\phi = 112.5^\circ$)	45
24	Smoothed E Plane Primary Pattern of Dipole, In Array, With Baffles	45
25	Calculated and Measured E Plane Radiation Pattern of Array ($\phi = 180^\circ$ Phase Increment)	46
26	Diode Combinations for High Power Outputs	54
27	1/2 W IMPATT Oscillator Cavity	57
28	0.5 W Cavity Oscillator with MIC Output	58
29	Equivalent Circuits of Package at 8280 MHz	60
30	Diode Pill Packages	62
31	Diode Mount Substrate	63
32	MIC Test Jig	65
33	Stub-Tuned MIC Avalanche Oscillator	67
34	Side-Coupled MIC Avalanche Oscillator	69
35	Pulse Spectrum of Transmitter Oscillator	75
36	Typical Bias Curves of Gunn and Avalanche Oscillators	77
37	SPST Switch Response Time	83
38	Circuit for Pulse Injection Locking	84
39	Typical Output from a Phase Detector for a Pulsed Injection Signal	86
40	Transient Response as a Function of Injection Signal	87
41	Bandwidth and Lock Time vs. Lock Gain for Sylvania Avalanche Oscillator	88
42	Measuring Circuit for Binary Phase Code Modulation	90

LIST OF ILLUSTRATIONS - continued

<u>Figure No.</u>	<u>Title</u>	<u>Page</u>
43	Phase Errors of IMPATT Oscillator with Binary Phase Coded Injection Signal	93
44	Computed BPC Oscillator Response	94
45	Phase Differential and Slope vs. Frequency of Injection Signal	98
46	Circuit for Frequency Modulation Tests	99
47	Microstrip T-Dipole on Alumina Substrate	104
48	Microstrip T-Dipole	105
49	"Bow Tie" Microstrip Dipole	106
50	Equivalent Circuit of Dipole and Matching Section	107
51	Equivalence Between Balanced and Unbalanced Microstrip Lines	107
52	Impedance of T-Dipole Connection Sections	109
53	Impedance of T-Dipole Antenna	111
54	E Plane Radiation Pattern of T-Dipole with Ground Plane	112
55	H Plane Radiation Pattern of T-Dipole with Ground Plane	112
56	Impedance of "Bow Tie" Dipole with Ground Plane	114
57	E Plane Radiation Pattern of "Bow Tie" Dipole with Ground Plane	115
58	H Plane Radiation Pattern of "Bow Tie" Dipole with Ground Plane	115
59	Microstrip Ring Resonator	120
60	Phase Errors in Injection Locked Oscillator	124
61	Possible Fit to Phase Curve	126
62	Effect of Non-Uniform Phase Steps	127
63	Antiphase Leakage Signals	127

LIST OF ILLUSTRATIONS - concluded

<u>Figure No.</u>	<u>Title</u>	<u>Page</u>
64	Locked Oscillator Transient Response	133
65	Phase Modulation	134
66	Locked Oscillator Phase for 90° Phase Code	136
67	Operation of IMPATT Oscillator	140
68	Operation of Gunn Oscillator	143
69	Gunn Oscillator Current Waveform	145
70	Operation of LSA Oscillator	145

LIST OF TABLES

<u>Table No.</u>	<u>Title</u>	<u>Page</u>
1	Typical Array Oscillator	20
2	Typical Phase Shifter in Array	24
3	Twin-Circulator Used in Array	27
4	Typical Commercially Available Gunn and IMPATT Oscillators	52
5	High Efficiency and Peak Power Devices	55
6	Typical YIG and Varactor-Tuned Oscillators	79
7	Sylvania Avalanche Oscillator SYA-3200	85
8	Oscillator Response Time to a Pulsed Injection Signal	91
9	Oscillator Response Time to a Binary Phase-Coded Signal	95
10	Measurements on Two Ring Resonators	121
11	Measurements on Linear Resonators	122

SECTION I

INTRODUCTION

BACKGROUND

The program described in this report was initiated in 1969 to meet technology-base needs in the engineering technical areas of microwave fundamental solid state sources and microwave integrated circuits (MIC).

The MITRE "technology base" is provided fundamentally for the purpose of supporting the USAF (ESD) efforts in system definition and acquisition. This base is achieved and updated by pursuing theoretical and experimental advanced techniques in areas identified as critical to future-generation radar and communications systems.

During the last two years, MIC technology has fully emerged as a proven technique and a number of system applications have been reported. The use of the microstrip structure on an alumina substrate is the usual form at higher frequencies but many variations in structure and design detail exist with little or no standardization. There is no question that in many cases this technique offers advantages in cost, repeatability, size and weight, compared with coaxial or waveguide structures. The reliability of the passive components is increased by the structural integrity, making the

active components the limiting factor in reliability. The viability of MIC subsystems and active components in the design of new systems now depends mainly on this factor.

In this same period, the microwave fundamental (negative resistance diode) oscillator has graduated from the laboratory to system use. The avalanche diode oscillator was initially the most advanced and promising device and today is still at the forefront of practical application, together with the Gunn oscillator. Both devices usually require simple circuit configurations and can be produced relatively inexpensively in quantity. Their acceptance rests mainly on proof of reliability.

Because of the above factors, the program was particularly directed to evaluation of MIC microstrip technology together with the avalanche diode oscillator. Emphasis was given to the possible functions of such an oscillator as an element in a phased array system or as a transmitter in a communication system. With the above emphasis it was decided that the design and construction of a small phased array using individual transmitting modules would be a good way to bring together the various areas of study. The specific function of local oscillator was not considered since the successful development of diode local oscillators was already well advanced.

Of interest also was the use of phase-shift keying (PSK) and binary phase code (BPC) modulation in conjunction with an injection locked solid state microwave oscillator. This interest existed because of the studies being carried on at MITRE in this area of signal processing. Whereas previous correlation techniques were limited to short pulse codes such as the 13-bit Barker Code, the use of longer codes has become feasible and offers the advantages of increased energy resolution, target discrimination and clutter suppression. In implementing the long codes, requiring higher bandwidth and higher bit rates, by means of phase-locked microwave oscillators, the phase errors and transient response of the oscillator can impose critical limitations. These factors were therefore given special attention.

PROGRAM OBJECTIVES

The objectives as originally specified were as follows:

- . Investigate microwave solid state fundamental oscillators and their application to future sensor systems.
- . Study the design and associated problems of phased arrays using individual solid state fundamental oscillators for the radiating elements.

- . Assess the practicability of microwave integrated circuits for phase locking, beam steering and other functions in multiple-source phased arrays.
- . Design, fabricate and evaluate a phased array subsystem using solid state sources and microwave integrated circuits.

SECTION II

SUMMARY AND CONCLUSIONS

The studies initiated in 1969 to meet technology-base needs in the areas of microwave solid state sources and integrated circuits were completed.

A simple linear X-band transmitting phased array consisting of eight active elements was designed and evaluated, as a way of bringing together the various areas of study (Figure-1). The latter consisted of a broad study of microstrip passive and active components and of avalanche diode oscillators and modulation techniques.

The transmitting array utilized eight active dipole elements, driven by injection-locked pulse-modulated avalanche diode oscillators. Phase shifting was accomplished by a 4-bit diode-loaded microstrip phase shifter, placed in the injection signal path of each module. Each module (Figure-2) consisted of a phase shifter, a double circulator, a 100 mW cavity oscillator, a monitor coupler and a coaxial-fed dipole, with coaxial connections between the components. Later in the program, a single X-band module was designed and constructed entirely in microstrip (Figure-3) but was not used in the array. This module, measuring 3" x 1" x 1/8", incorporated a 170 mW avalanche oscillator and a photoetched dipole antenna.

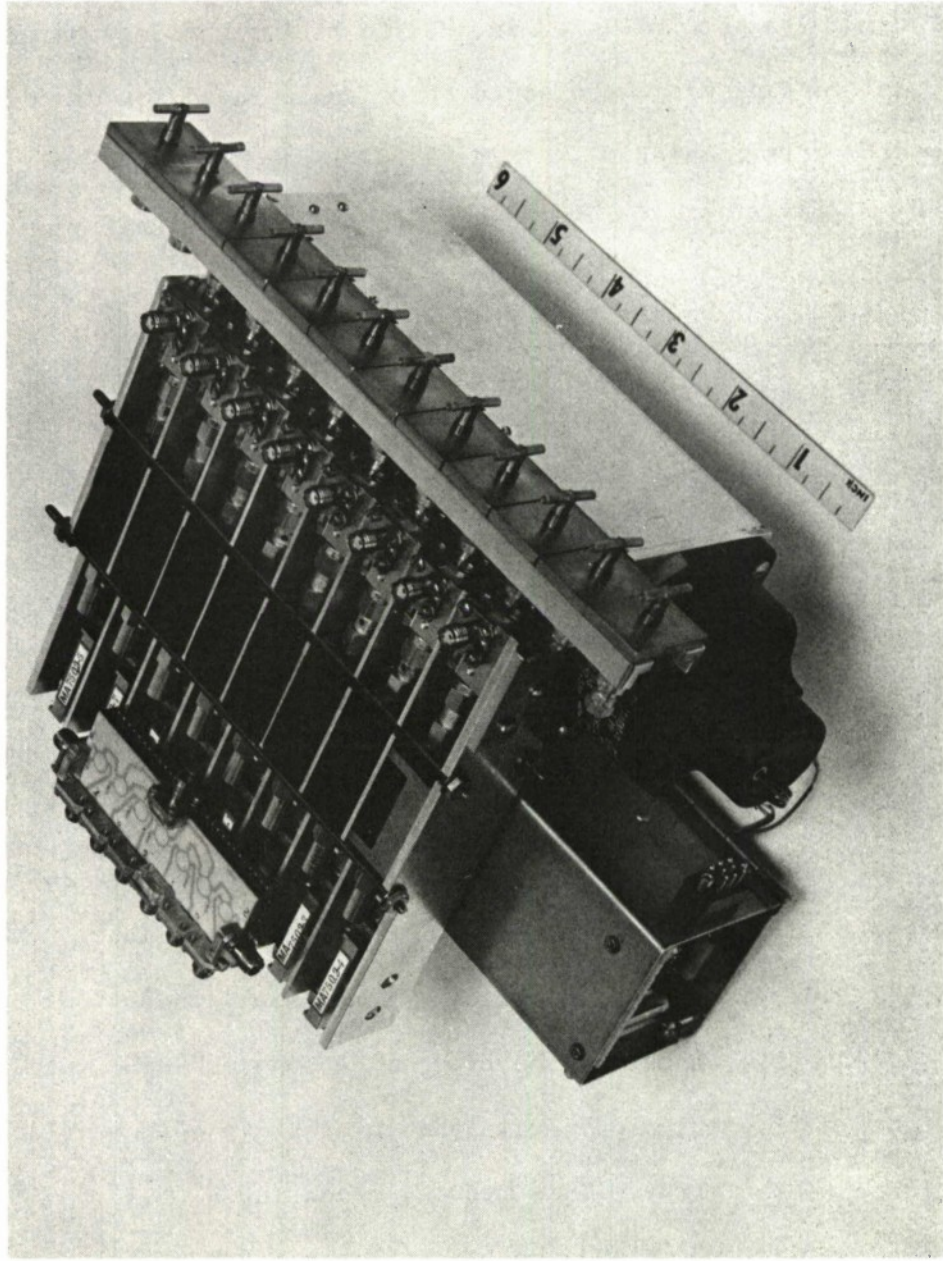


Figure 1. TRANSMITTING PHASED ARRAY

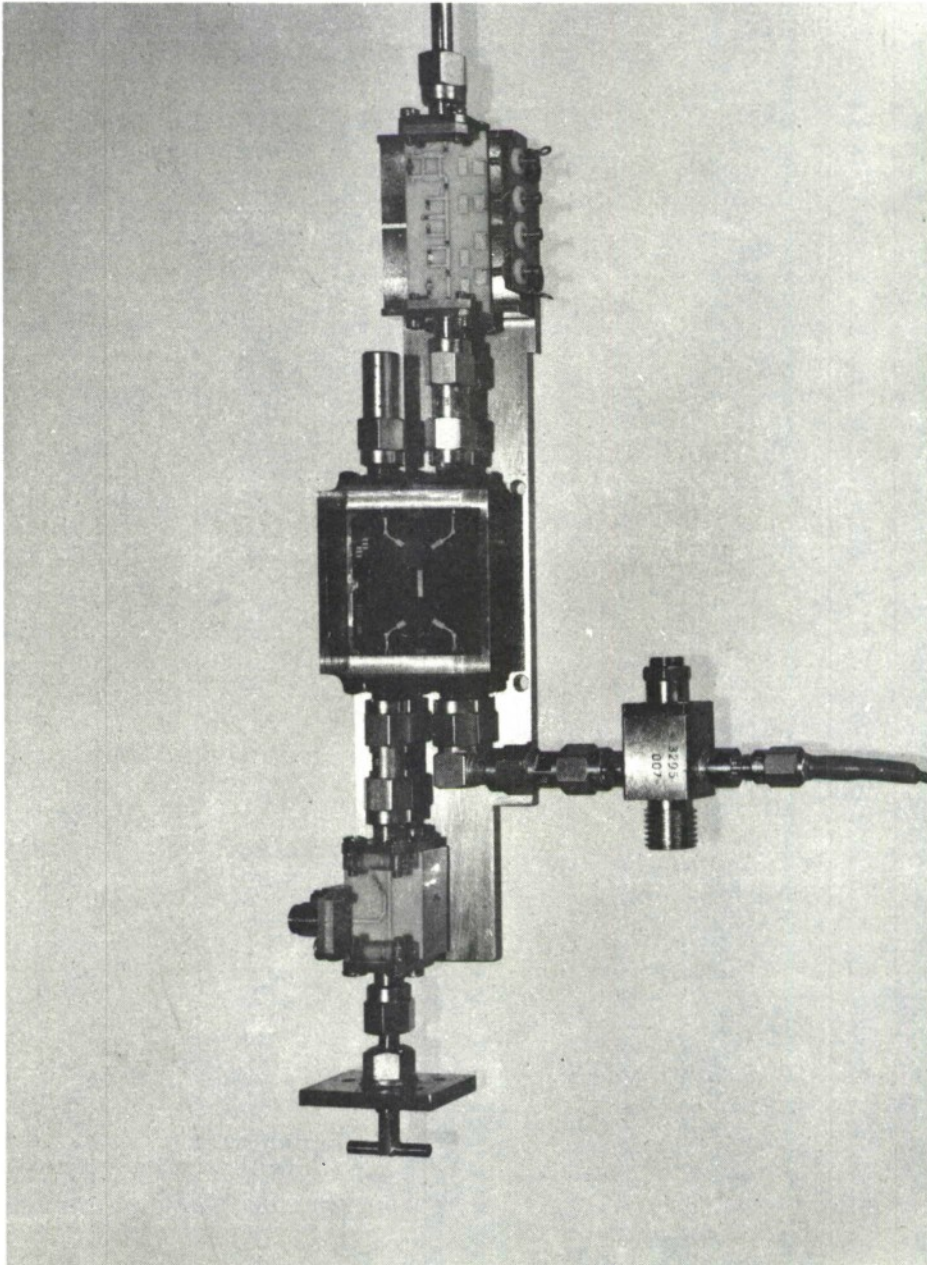


Figure 2. TRANSMITTING PHASED ARRAY MODULE

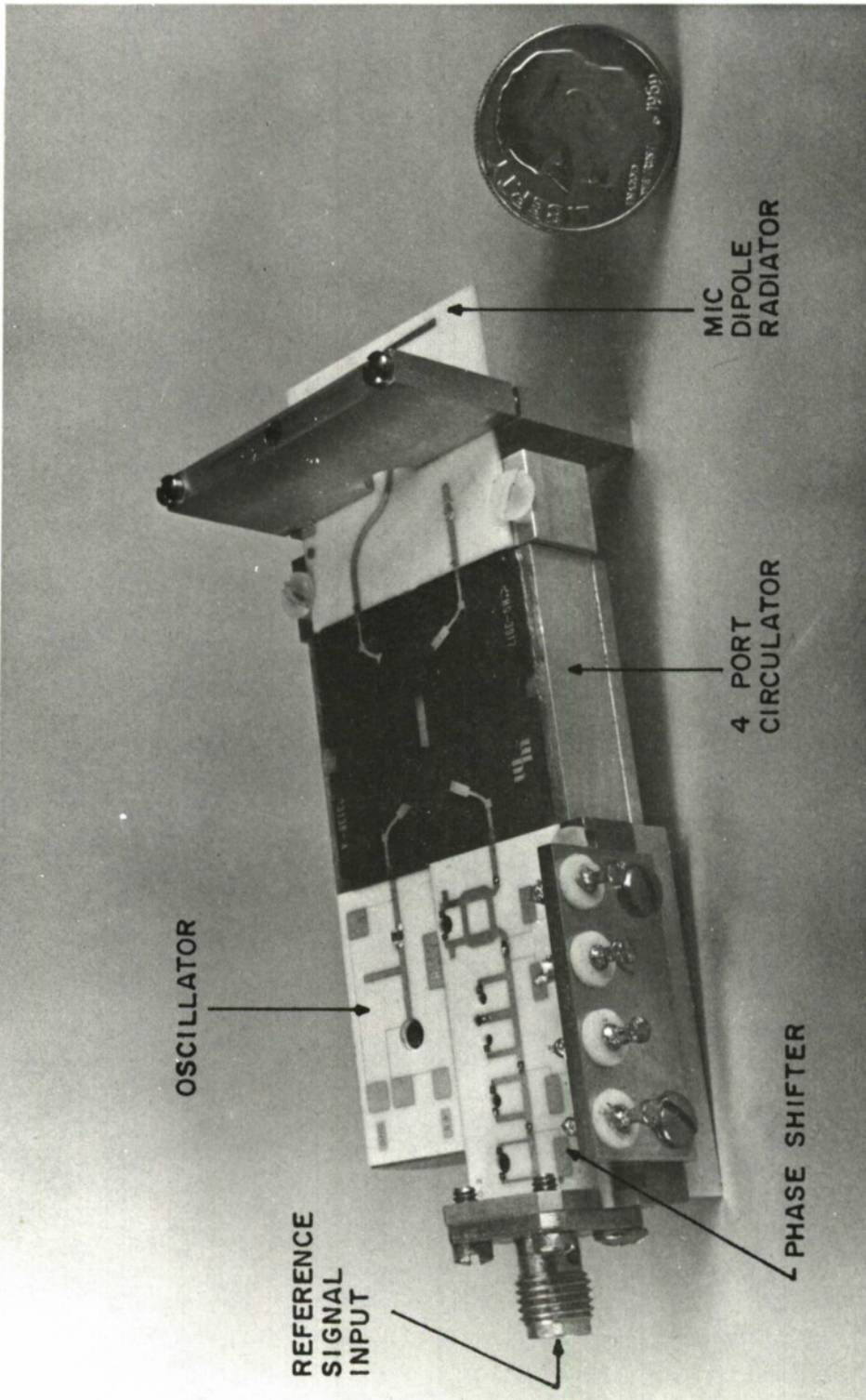


Figure 3 - MIC Transmitting Module

The element spacing of $.55 \lambda$ in the test array was chosen to give accurate beam steering of ± 40 degrees without the appearance of grating lobes. No amplitude weighting was used in the model. The beam patterns and steering angles agreed well with theoretical predictions.

The studies of avalanche diode oscillators were directed to the characteristics of injection-locked oscillators when modulated with pulsed amplitude and digital phase codes. The latter was of special interest since it supported ongoing theoretical studies at MITRE in the area of digital signal processing and long binary phase codes in particular. The phase response time of phase-coded, phase-locked oscillators was studied and confirmed as a limiting factor to binary modulation rates that will be desirable in advanced signal processing systems. Aspects of noise spectra, frequency pulling and errors associated with injection locking were also studied.

Two types of microstrip implementation of avalanche oscillator were considered and models built. One employed a tank circuit with distributed output coupling and the other employed stub matching to the output with a lumped capacitor for DC isolation. The latter oscillator produced .17 W at 3% efficiency, close to the typical values for cavity operation. This unit was also incorporated into the microstrip binary phase-controlled transmitting module described. A .5 W cavity-type avalanche diode oscillator was designed and tested

to obtain some insight into the problems of impedance matching and diode characterization. Previous experience with varactor diode characterization was extended to develop a technique applicable to the negative resistance diode, and equivalent circuits were derived for a diode junction and the impedance transformation of the "standard" pill package. The cavity oscillator used a quarterwave transformer to match the diode to an external microstrip circuit.

The other components designed and/or studied and evaluated included several types of couplers, hybrids, circulators, and diode phase shifters. It was found that, as an example of component design and fabrication problems, the implementation of circulators in microstrip was more easily talked about than accomplished, and after much delay the units received from one of two vendors had poor characteristics. The purchased phase shifters, on the other hand, which had been developed under another contract, were the result of considerable experience in the field and had excellent performance.

Some attention was given to problems of microstrip fabrication and quality control. Early in-house efforts and efforts by one vendor were very poor in several respects, particularly in the photolithography, due to lack of experience. The artwork and photoreduction stages do not contribute significantly to circuit errors when adequate equipment is used, and the photolithographic

processing is very reliable once appropriate controls are established. The adherence of thin-film metallization on alumina substrates can be a problem due to contamination in processing, especially with very smooth substrates (2 micro-inches) and adequate adherence tests need to be established. The variation between dielectric constant of high purity alumina from different vendors and different batches is a source of trouble, usually solved by stockpiling of material for a particular component run. Techniques for measurement of microstrip propagation constant and loss have been evaluated and found to be very convenient and satisfactory for substrate quality control.

The work described above on the array model and the associated techniques has been of considerable value, not necessarily for the design itself, but more from the standpoint of a vehicle for providing a practical basis for the determination of the capability and limitations of solid state microwave oscillators and MIC circuits in actual system applications.

Much of the commentary in the literature has addressed itself to the application of microwave integrated circuit solid state techniques to phased array radars. The arguments supporting these techniques also in general apply to other applications such as (reliable) communications systems and satellite repeaters and telemetering systems. Many of the conclusions are generalized since there are nearly always exceptions, and objective conclusions can

only be made for specific systems whose goals and objectives are clearly defined. The following conclusions are based on the results of this program and views and opinions as expressed in the literature and at various meetings and symposia [1-4, 62,63].

The greatest system needs are for increased reliability and life. This has to be achieved in the face of growing system complexity, especially in large, ground-based phased array systems, to which most of the recent (1969-70) commentary has been addressed.

All-solid-state systems offer the potential of meeting these needs and justify the tremendous effort which is current towards achieving such systems. This potential is far from being realized, however. The reliability of many microwave components using active devices leaves much to be desired and is far from proven. It is usually determined, not by the inherent design of the active devices, when adequately rated, but by the fabrication processes, particularly the bonding of connections. It is exceedingly important that the question of reliability is addressed at early stages of component development. In general the reliability of active devices decreases as the power increases. This trend is a function of increased operating temperature which can result in diffusion of materials, bonding failures and excessive rating on a mean or peak power basis. Claims for power output of microwave devices obtained under laboratory conditions are sometimes colored by optimism and are not

obtainable under reliable operating conditions. A second unreliability factor is the interconnection of passive devices, for example capacitor chips and component substrates. Manual bonding techniques are commonly used and are subject to many faults including errors of judgment where all factors are not controlled or correctly set.

An associated need is for minimum or zero maintenance. The trend is to incorporate automatic monitoring and self-checking circuits.

For phased array radars, the use of individually driven radiating elements by means of distributed solid state power sources, although necessary because of the power limitations of the solid state sources, has great merit from the reliability standpoint. The use of amplifiers or phase-locked oscillators as transmitters appears to be a most promising approach. The miniaturization of solid state transceiver modules allows them to be within the antenna assembly, thereby reducing the system losses and increasing overall detection capability. This technique allows what is commonly termed a "graceful deterioration" of a system as power modules fail, since each failure produces only a small perturbation of system performance. The common parts of the system, operating at low power levels, have to be designed for very high reliability, however.

Because of the high mean powers typical of ground-based long-range radar systems, the efficiency is a dominant factor. At L-band, the transistor and the avalanche diode oscillator have demonstrated efficiencies comparable to high power tube devices such as the magnetron and cross field amplifier. With increasing frequency, however, the tradeoff between the higher efficiencies of the tube devices and the higher basic reliability of the solid state devices tends to favor the former.

Avionics and satellite systems, which require miniaturization and reduced weight as prime factors, have justified the extensive development of high dielectric-constant (ceramic) microwave circuits which result in a linear scaling factor of up to three or four compared to conventional coaxial or waveguide circuits, although the necessity for metal enclosures in most cases negates a good part of the intrinsic savings in size and weight. The fabrication of enclosures can also become a significant cost factor, and development of low-cost metallized plastic moldings or other techniques would be well justified. A microminiaturization bibliography exists^[64,65].

The use of the hybrid microstrip technique with components bonded to photolithographed circuits on ceramic is likely to meet the needs of miniaturized microwave circuits in the foreseeable future. The technique is thoroughly proven and its reliability is determined by the bonding processes and active devices, as discussed elsewhere.

For the ground-based systems, the emphasis is placed on performance (efficiency) and production costs while the question of reduced size is secondary. The high potential reliability of solid state devices is essential for the implementation of the increased complexity and performance demanded by advanced systems. At the same time this complexity must be counteracted by decreased component costs. The future costs of MIC/solid state components, in quantity, can be expected to decrease by an order of magnitude from present small-quantity costs. The cost of the active devices in these components is currently the major factor, but the usual downward trend can be expected to apply as techniques become established.

The choice of solid state microwave transmitters is by no means obvious as the technology is moving so fast. Below S-band, the transistor amplifier was a clear choice until recently, when high pulse powers with good efficiency have also been obtained from TRAPATT oscillators. Transistors delivering 100 watts at 45% efficiency are currently available at L-band. S-band transistors are well under development and if the $1/f^2$ power/frequency dependency established by Johnson and DeLoach is assumed, we might hope for 100 W at S-band. At S-band and above, the use of varactor (step recovery diode) multipliers can provide moderate power with good conversion efficiencies. Varactors capable of 3 W output at X-band and $1\frac{1}{2}$ W at Ku-band are now available. In competition above

S-band are the solid state fundamental (negative resistance diode) oscillators. Avalanche diode oscillators operating in the high efficiency TRAPATT mode are the most promising devices for the future and much laboratory development is going on. 200 W pulse power at 40% efficiency has been obtained at L-band with a single diode^[66] and 1.2 kw pulse power at 26% efficiency was obtained with stacked diodes^[24]. Thirty percent efficiency has been reported for a pulsed X-band oscillator, comparable in efficiency with a transistor/varactor combination. Powers (CW or long pulse) up to 3 W have been reported for X-band avalanche diode oscillators and amplifiers^[22].

Much higher pulse powers, about 1 kW at X-band, are available using LSA diode oscillators, but their mean power limitation requires low duty ratios and short pulses, restricting their application to very short range, high resolution radars. Their low efficiency, typically below 10%, is less important in this case where their power input would be small.

There are many problems remaining to be solved before completely solid state systems of the highest reliability and performance, with minimum cost, are fully realized.

The reproducibility of microwave integrated circuits using hybrid construction, a technique likely to stay for a long time, has to be greatly improved. Although the photolithographed circuits themselves are very reproducible, the trimming and adjusting required to take care of diode variations, etc., needs to be

eliminated or methods developed to make them easily accomplished in production. Active devices need to be characterized in the circuit environment so that the effects of parasitic impedances become negligible. Reduction of parasitics not only improves the impedance matching possible over extended bandwidths but makes the circuits more amenable to calculation, optimization and to computer-aided design.

Much development is still needed to improve heat removal from active devices, using high thermal conductivity heat sinks and substrates, and to transfer heat from these local heat sinks to a heat exchanger.

Improved and low-cost techniques for enclosing and protecting integrated circuits are needed. Standardization of component subunits and dimensions of microstrip should be seriously considered as a means of lowering costs and encouraging the manufacture of standard component building blocks.

Further development of computer-aided design techniques for synthesis procedures will help speed up and reduce the costs of future designs, particularly if some parameters can be standardized.

With the rapid development of solid state circuits at all frequencies, it has become practicable to implement a whole range of new system functions. The development of adaptive and multi-function systems having variable parameters has become feasible.

The trend now made possible is toward completely digital systems using digital signal processing and digitally generated waveforms. Up to L-band, all system functions can be performed by solid state devices, using distributed sources to meet RF power requirements. At higher microwave frequencies, however, a tradeoff between efficiency and reliability involving the choice between tubes and solid state devices is still required for high power systems. Apart from this question, the use of solid state devices and microwave integrated circuit techniques can meet all the demands of radar systems.

In conclusion, the work carried out under this program has helped to verify and emphasize the applications of microwave integrated circuit and solid state technology in the areas discussed above.

SECTION III

WORK ACCOMPLISHED

TRANSMITTING PHASED ARRAY

The main emphasis during FY 1969 was given to the design and evaluation of components which were integrated into a small X-band transmitting linear phased array (Figure 1). This simple array was used as an appropriate test model for the design, study and integration of some typical MIC components and solid state oscillators. Fabrication of the array was completed at the end of FY 1969 but a subsequent change was made to the antennas before evaluation, as discussed later. The array patterns and beam steering were measured and agreed well with theoretical computations.

The array (Figure 1) consisted of eight transmitting modules (Figure 2), each containing a coaxially fed dipole as the radiating elements. These elements were spaced .55 wavelength apart, with two additional terminated dummy elements at each end. This spacing was chosen to allow end-fire grating lobes to appear for a beam deflection of 55° resulting in accurate beam steering to over $\pm 40^{\circ}$. Baffles were used between the radiating elements, which were oriented along the axis of the array to provide an E plane radiation pattern in the scanning plane. All active elements were fed with nominally equal amplitudes at a frequency of 9375 MHz.

Figure-4 shows the circuit block diagram of the transmitting array. Out of several possibilities, the circuit configuration shown was chosen for the following reasons:

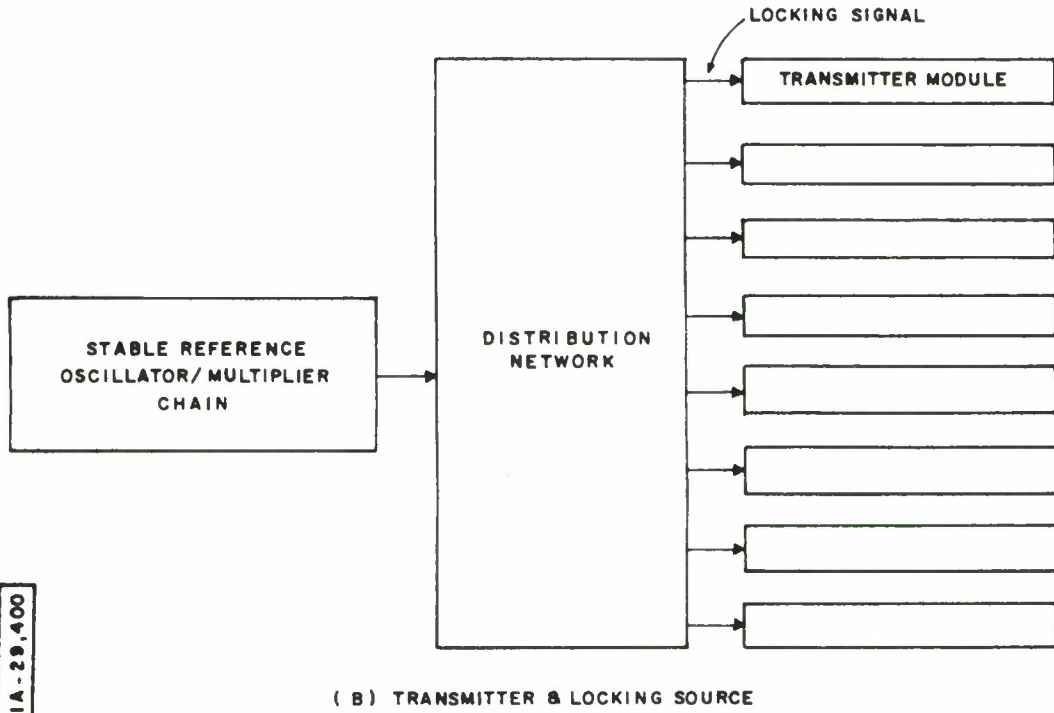
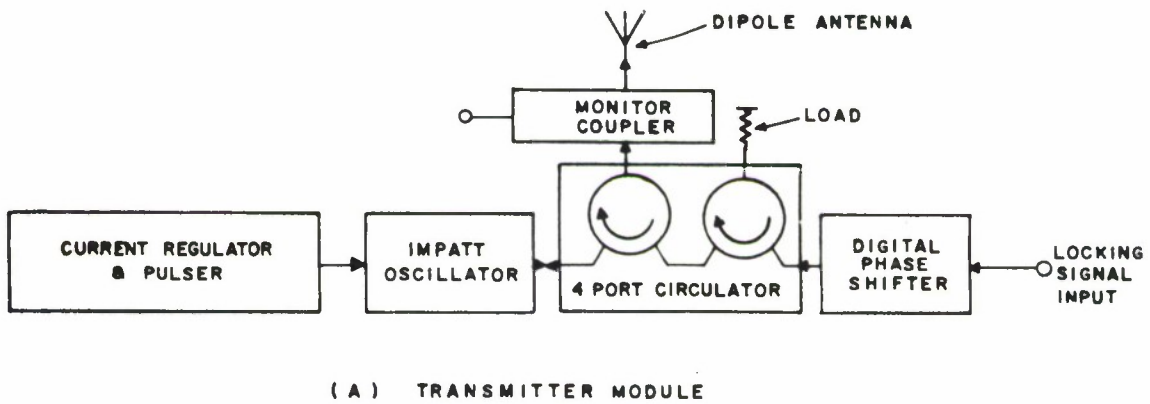
a) An avalanche oscillator operating in its fundamental mode was chosen initially because it represented the most fully developed technique of fundamental solid state microwave power oscillation at X-band and was a likely candidate for initial application to future radar systems. The design theory of these oscillators is well established and many types are commercially available, although their reliability is uncertain.

The oscillators used in the array model were commercial coaxial cavity units giving 0.1 W, CW output. Table 1 gives data for a typical unit, although there was considerable spread of characteristics, especially in the value of Q.

TABLE 1

Typical Array Oscillator

Frequency (tunable)	9375 MHz
Power	0.1 W
Efficiency	4%
Bias Voltage	88 V
Bias Current	28 mA
Q	50



IA-29,400

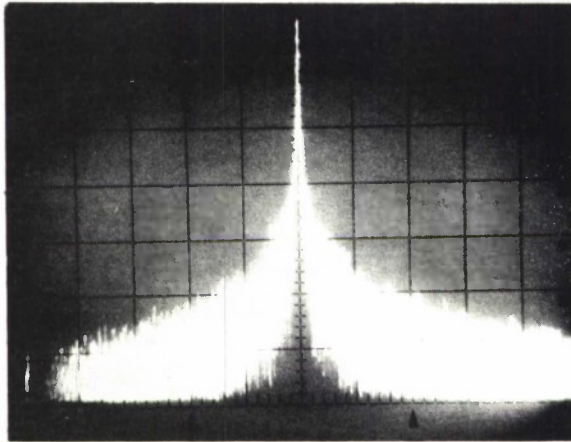
Figure 4. TRANSMITTING PHASED ARRAY

b) The injection-locking technique used to establish the phase coherency necessary between the oscillators of the array, was chosen because it is a straightforward, reliable and well-established technique with a sound theoretical basis. This technique, which is reviewed in a later section, is basically a synchronization process where the output signal is phase locked to a relatively small input (injection) signal to within a small phase error.

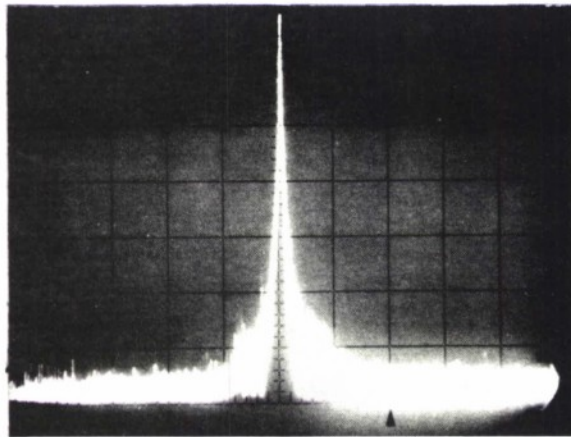
In addition to phase locking the oscillators of the array, the injection source also reduced the FM noise of the free running oscillator. This reduction in the noise sidebands is shown in Figure-5.

c) The choice of digital rather than analog phase-switching was chosen in accordance with contemporary design philosophy based on integrated circuit design and computer-controlled beam steering. Two types of diode-switched phase shifters have been developed under various programs, being either switched line-length (time delay) devices or reactively loaded circuits producing switched phase shifts. A device of the latter class fabricated in microstrip was chosen because of its availability and the compatibility of its parameters with our requirements. Table 2 gives data on a typical unit.

An alternative design using phase-shift control in a magnetized ferrite microstrip substrate was considered initially but such devices were in were too early a state of laboratory development



(a) UNLOCKED



(b) INJECTION LOCKED

FREQUENCY: 10,370 MHz
LOCKING LEVEL: -23 dB

IA-29,585

Figure 5. HIGH POWER IMPATT OSCILLATOR SPECTRA

TABLE 2

Typical Phase Shifter in Array

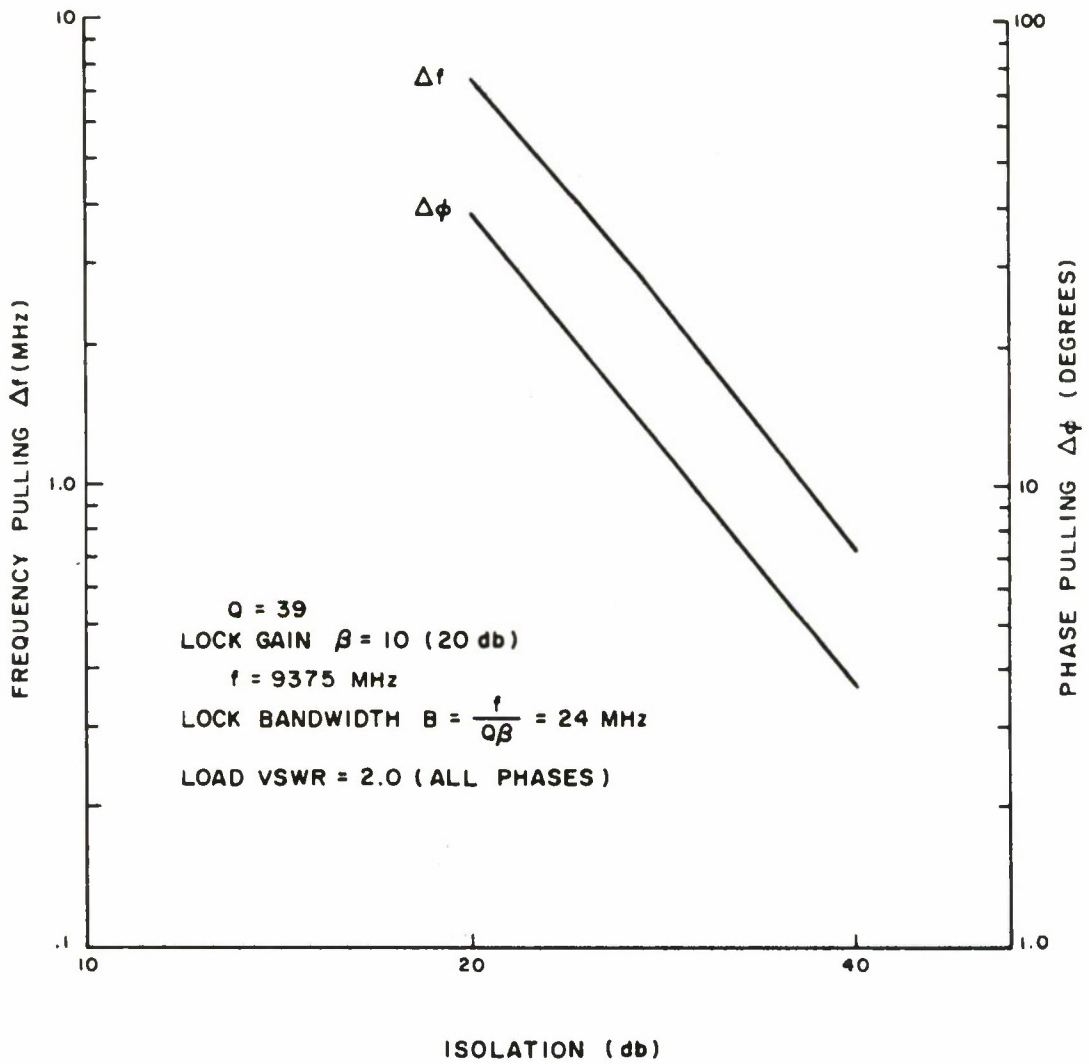
Number of bits	4
Phase Unit (min. phase increment)	22½ degrees
Frequency	9375 MHz
Input and Output Impedance	50 ohm
Construction	Microstrip, chrome-gold on 0.02 inch alumina substrate.
Insertion loss	2.2 to 3.0 dB
Input and Output VSWR	1.20 to 1.65
Absolute Phase Error	± 3°
Phase Tracking Error	± 10° (specified)
Response Time to Control Signal	200 ns max. (specified)

At this time, such ferrite devices are still not available but are a future possibility, particularly at X-band or above, where they offer potentially lower loss than their diode counterparts.

The use of phase-shift control of the low-level injection-locking signal offers the particular advantage of not reducing the efficiency by introducing the phase shifter loss into the transmitter output path. In the circuit arrangement used, neither the phase shifter loss nor its power handling capacity are of major importance. The circuit can be extended to transmit/receive operation by frequency side-stepping the phase-shifted injection signal to generate a local oscillator signal for reception.

d) The twin-circulator configuration was chosen to give high isolation between each phase-shifter and the associated oscillator. This was necessary in view of the high standing wave ratio presented by the phase shifter and which varied with its phase-state, causing considerable phase error of the oscillator signal unless high isolation were provided. This is demonstrated by Figure 6, which shows the calculated first order effect of isolation between one oscillator ($Q = 39$) and the source (phase shifter output) having a VSWR of 2. The open loop frequency pulling δf is based on measured data* and the corresponding phase pulling α under injection-locked

*Reference 5, p.28 and Figure 17.



IA-32,703

Figure 6 EFFECT OF ISOLATION ON FREQUENCY & PHASE PULLING

conditions is calculated from Equation B1, Appendix B. These curves demonstrate the need for high isolation, typically 40 dB.

As discussed in a later section, the isolation of the single circulator section between the oscillator and the antenna was considered at the time to be adequate for this model. A practical system might in some circumstances require the extra isolation provided by a triple-circulator arrangement.

Table 3 gives typical data on one twin-circulator.

TABLE 3

Twin-Circulator Used in Array

Frequency	9375 MHz
Impedance at Ports	50 ohm
VSWR at Ports	1.5 max.
Insertion loss between adjacent ports	0.8 dB
Isolation between adjacent ports	25 dB typ., 15 dB min.
Isolation between doubly isolated ports	> 41 dB typ.

e) The use of multiple hybrids to provide the power split of the injection signal was chosen because of the isolation provided. The latter was necessary to minimize relative phase errors in the injection signals from the divider, due to impedance interactions. The splitter is shown at the rear of the array (Figure 1).

f) A coaxial-fed dipole of conventional design was used for the radiating element (Figure-7) because of the convenient transformation to the associated circuits and because of the possible implementation in microstrip format, making a completely integrated module a possibility. Such a module was subsequently demonstrated and is described in a later section.

Figure 2 shows a photograph of one transmitting module comprising (left to right) the phase shifter, circulator, oscillator (top), monitor coupler, and antenna.

A control and indicator panel using a matrix of lamps (Figure-8) was used to provide a manually switched control and graphical display of the phase-states of the eight phase shifters controlling the transmitted outputs and, thus, the phase slope across the array. This panel was also valuable in the boresighting procedure as described in a later section.

Boresighting

The boresighting procedure consisted of adjustment of the individual phase shifter states to give approximately equal-phase excitations of the dipole elements. The test circuit used (Figure-9) consisted of a small horn antenna placed several feet from the array in the far field, and a phase bridge which used the common injection-signal source as the phase reference.

Since no phase-trimming adjustments were incorporated into the system, the phase shifters were used for this purpose. The

phase shifters were adjusted so that the radiated fields from the individual elements had equal phases to within the quantization error of half the phase unit. This error was 11.25 degrees for the phase unit of 22.5 degrees ($360/2^4$ degrees for the four-bit phase shifter). The RMS value (standard deviation) of the phase errors, measured after completion of the above adjustments, was 9.5 degrees.

A visual display of the phase states across the array was provided by a matrix of indicator lamps (Figure 8) activated by the binary phase-control switches seen at the bottom of the panel. Each column of lamps corresponded to one module of the array, with the vertical positions corresponding to the relative phase shifts. By appropriate connections, the indicated relative phase shifts were all set to zero (top and bottom rows) after the boresighting was completed. Subsequent beam steering was obtained by stepping the phase-shifter states to give an approximately linear phase slope across the array, as visually indicated by the lamps. The setting shown by Figure 8 corresponds to an average phase slope of 15 phase units (337.5 deg.) across the array (14 deg. beam deflection).

The test circuit was also used to measure the relative amplitudes of the individual radiated fields. The amplitude distribution varied by 10% RMS and 2.5 dB peak to peak, due mainly to output power variations from the oscillators. This degree of amplitude modulation of the power distribution was acceptable for the model whose

theoretical $\sin X/X$ radiation pattern had first sidelobes of -13.2 dB. The sidelobes corresponding to any one sinusoidal component of amplitude modulation across the array with modulation index m (modulation/carrier ratio) would have amplitude $m/2$. For example, if the measured amplitude distribution had a single sinusoidal component of 10% (pessimistic), then $m = .1$, giving a pair of -26 dB sidebands. For a practical system with amplitude tapering across the array to produce reduced sidelobes, a correspondingly tighter specification would be placed on the allowable amplitude variation across the array.

With the boresight adjustments made as described above, the measured boresight pattern (Figure-10) agreed well with the theoretical pattern. The half-power beamwidth was 12° (as calculated) in the scanning plane, with a first sidelobe level of -12 dB.

Antenna Element Coupling and Modification

Figure-11 shows the major components of three of the eight phased-array modules. The avalanche oscillators are made coherent by injection locking from a common source, and the output phase from each antenna element is determined by the phase shifter. The antenna beam is steered by proper adjustment of the phase shifter which can step the output signal phase from each antenna in 22.5° phase units.

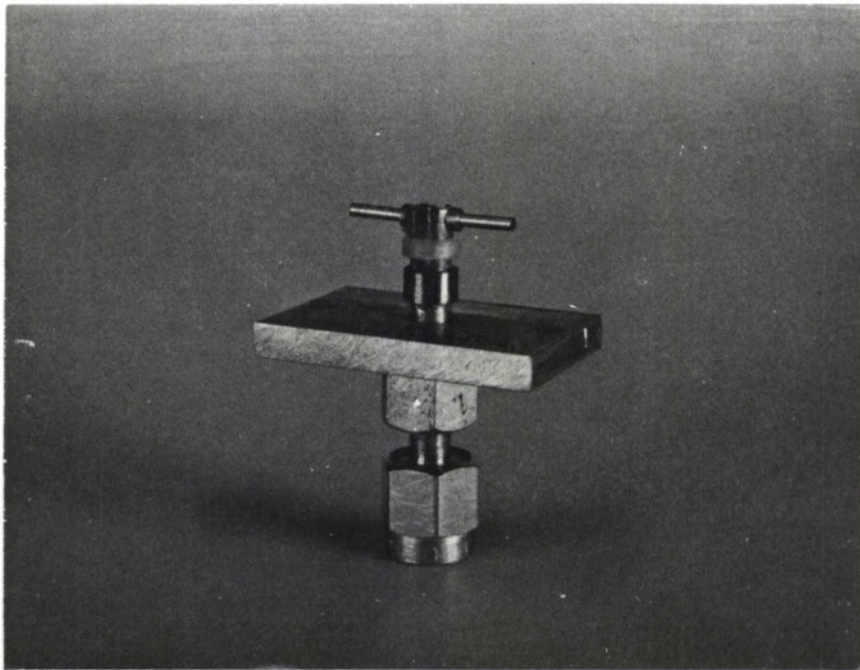
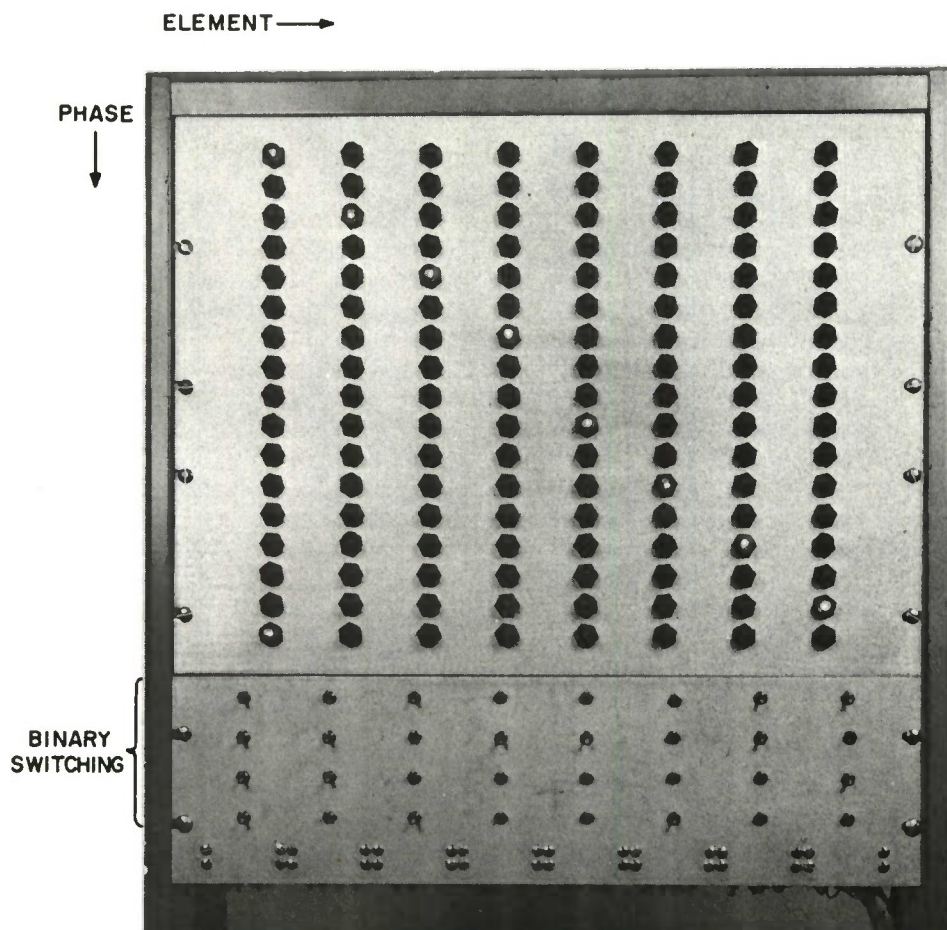


Figure 7 - Slot-Fed Coaxial Dipole



1B-29,568

Figure 8 PHASE DISPLAY

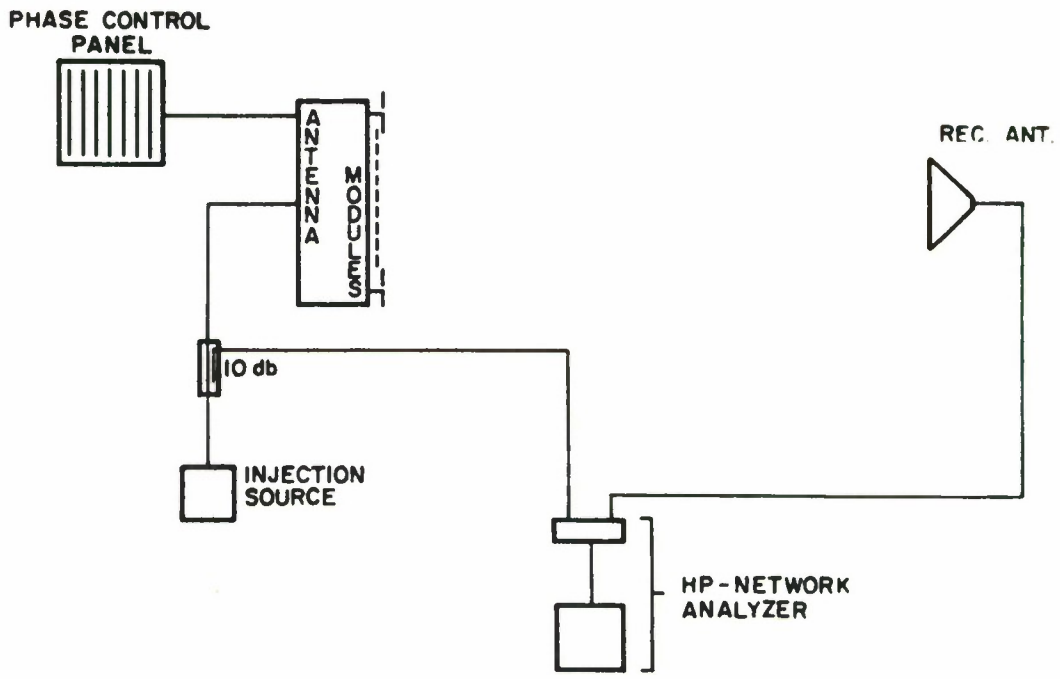
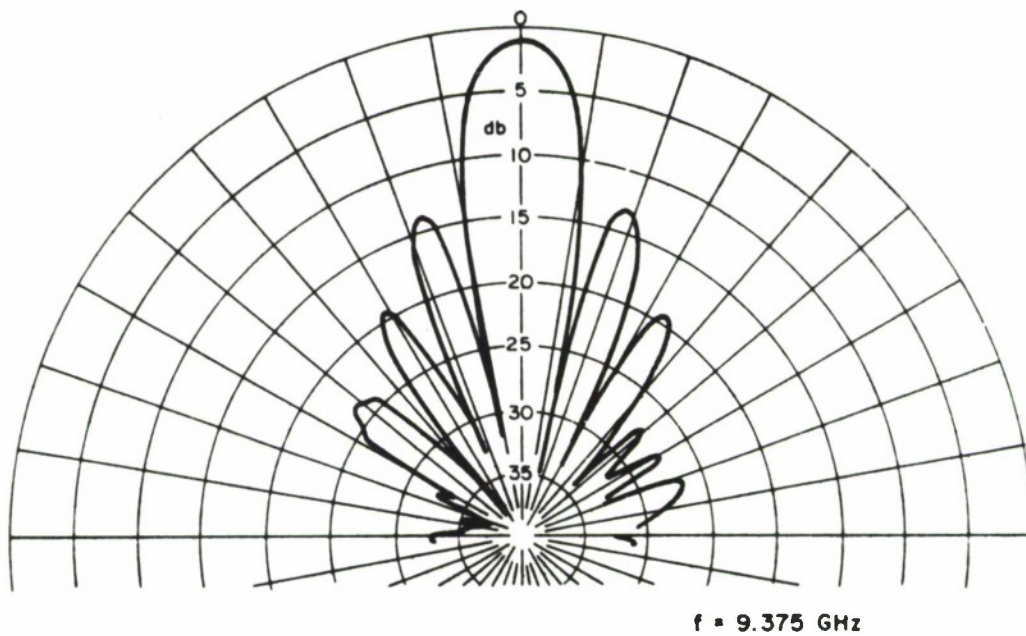
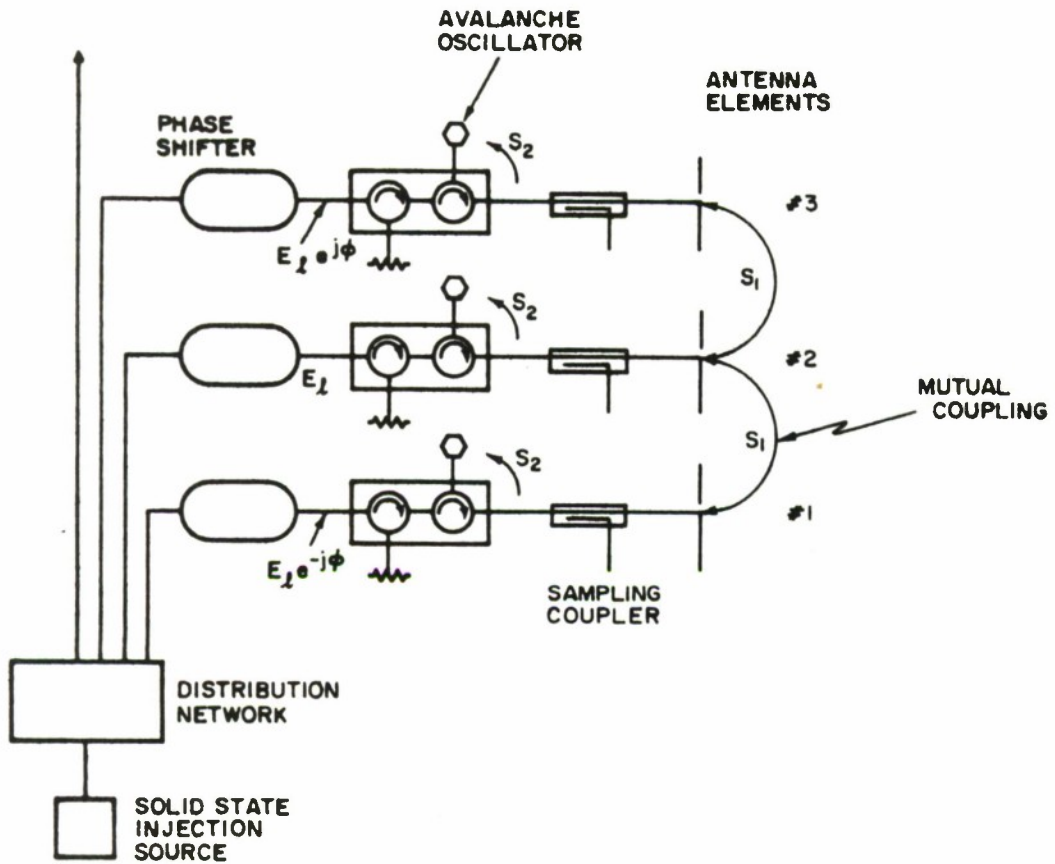


Figure 9 TEST CIRCUIT FOR MEASURING PHASE & AMPLITUDE OF PRIMARY FIELDS



18-32,712

Figure 10 E PLANE RADIATION PATTERN OF ARRAY ($\phi = 0^\circ$)



IA-32,697

Figure 11 THREE OF THE PHASED ARRAY MODULES

To avoid degradation of the array radiation pattern sidelobes and, to a lesser extent, errors in beam steering, it is important that excessive phase errors are not introduced into the oscillator outputs. Inadequate isolation between the oscillators and the antenna elements, together with high mutual coupling between these elements, can result in large absolute phase errors, which if unequal, can result in significant phase fluctuations across the array. These effects can be pronounced when phase-locked oscillators are used, as in the model described, and are discussed in more detail in Appendix A. Preliminary tests with the original array showed the coupling between adjacent elements in the array (coupling S_1 , Figure-11) to be -16 dB as predicted by theory^[6]. The circulators, which were the only commercial units available at the time, had a minimum isolation (coupling S_2 , Figure 11) of only 15 dB at the operating frequency of 9375 MHz. With the injection-locked oscillators of 20 dB gain (power out/locking power in), the leakage signal between adjacent modules was only 11 dB below the injection level. This could produce between zero and 29 deg. absolute phase error, according to the phasing, which is a function of the path lengths. This effect was confirmed by measuring the effect of phase change in one transmitting module upon the phase of the adjacent module. To avoid the cost and particularly the time-delay of incorporating new circulators with increased isolation, the expedient was used of

decreasing the antenna coupling by using baffles between the dipole elements. This reduced the coupling by an additional 10 dB to provide -25 dB isolation. Figure 12 is a photograph of the partly disassembled array showing the isolation baffles between the dipole elements. The coupling could also have been reduced by increasing the injection level.

Principal plane radiation patterns of a dipole element in the array environment are shown in Figures 13 and 14. The presence of the baffles broadens the radiation patterns, as seen by comparing the patterns with those taken without the baffles (Figures 15 and 16). The gain of the dipole with baffles was 4.5 dB. An impedance plot over the band 9.0 to 9.8 GHz is shown in Figure 17. The maximum VSWR was 1.6.

Scanning Performance

Beam deflection was produced by setting the differential phase shifts, relative to their initial boresight states, to approximate the linear phase slope required across the array. The beam deflection φ is given by

$$\begin{aligned}\varphi &= \sin^{-1} [\phi / (2\pi D / \lambda)] , \\ &= \sin^{-1} [\phi \text{ deg} / 198 \text{ deg}]\end{aligned}\tag{1}$$

for the element spacing $D = .55 \lambda$ for the model, where λ is the wavelength and the differential phase shift ϕ is approximated by the nearest possible phase step, in multiples of 22.5 deg.

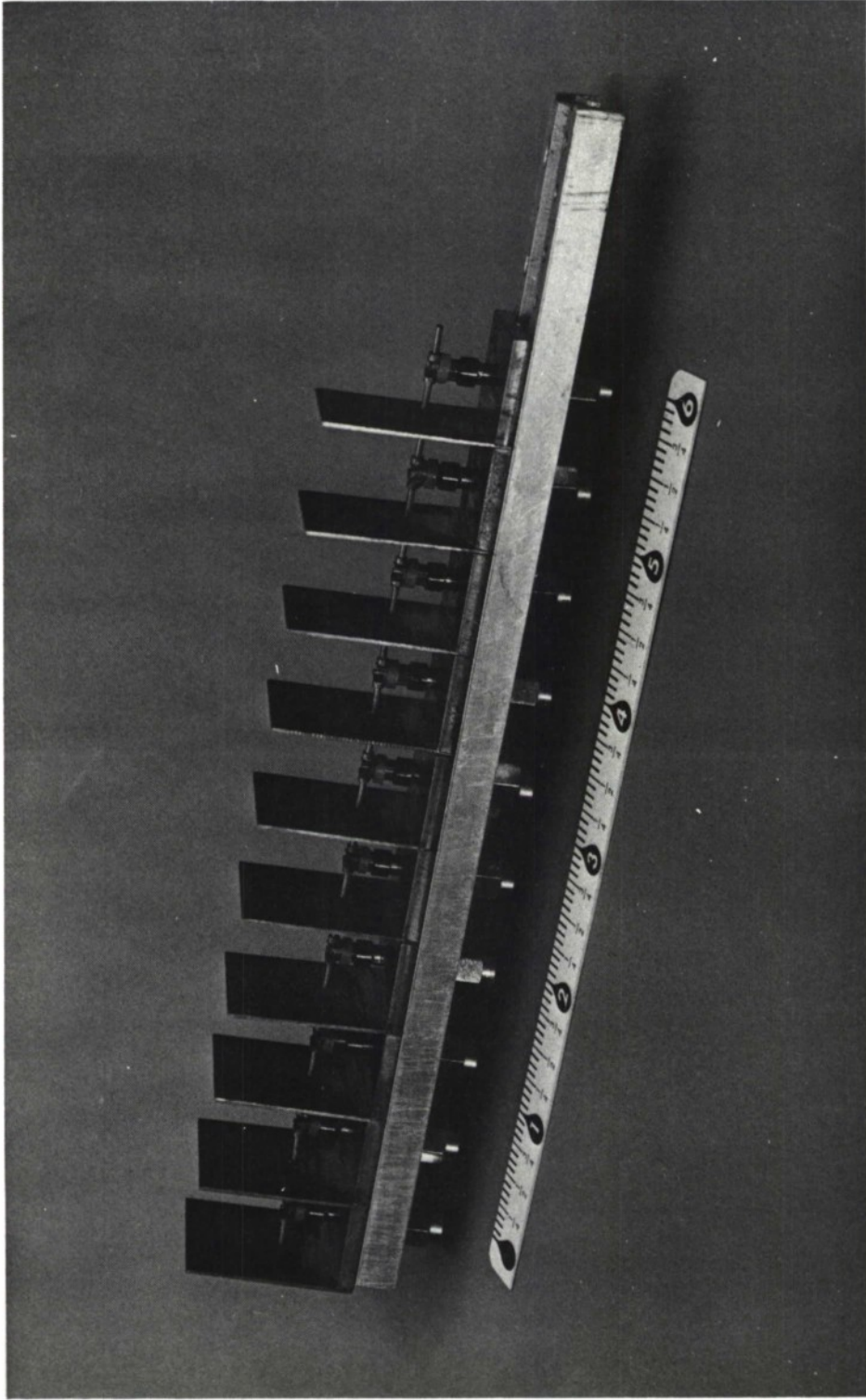
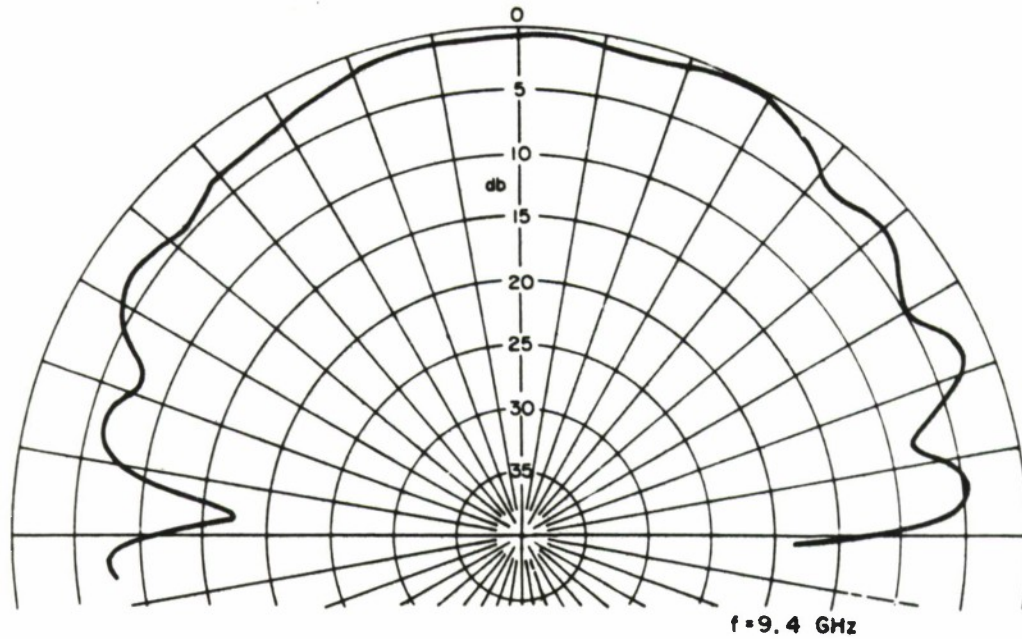
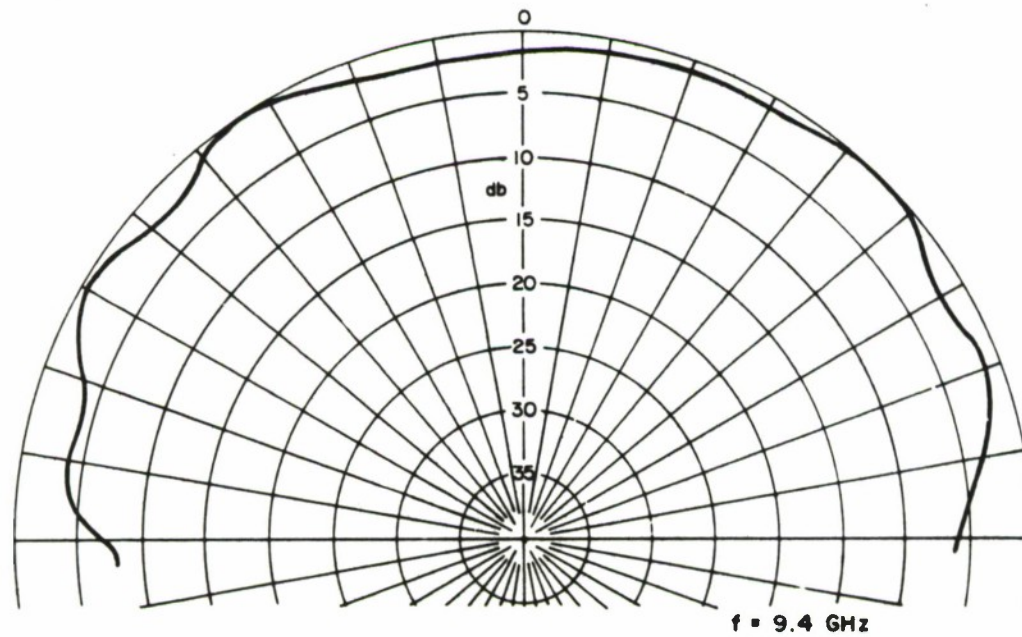


Figure 12 - Part of Antenna Array



**Figure 13 E PLANE RADIATION PATTERN OF
DIPOLE WITH BAFFLES & GROUND PLANE**



**Figure 14 H PLANE RADIATION PATTERN OF
DIPOLE WITH BAFFLES & GROUND PLANE**

IB-32,710

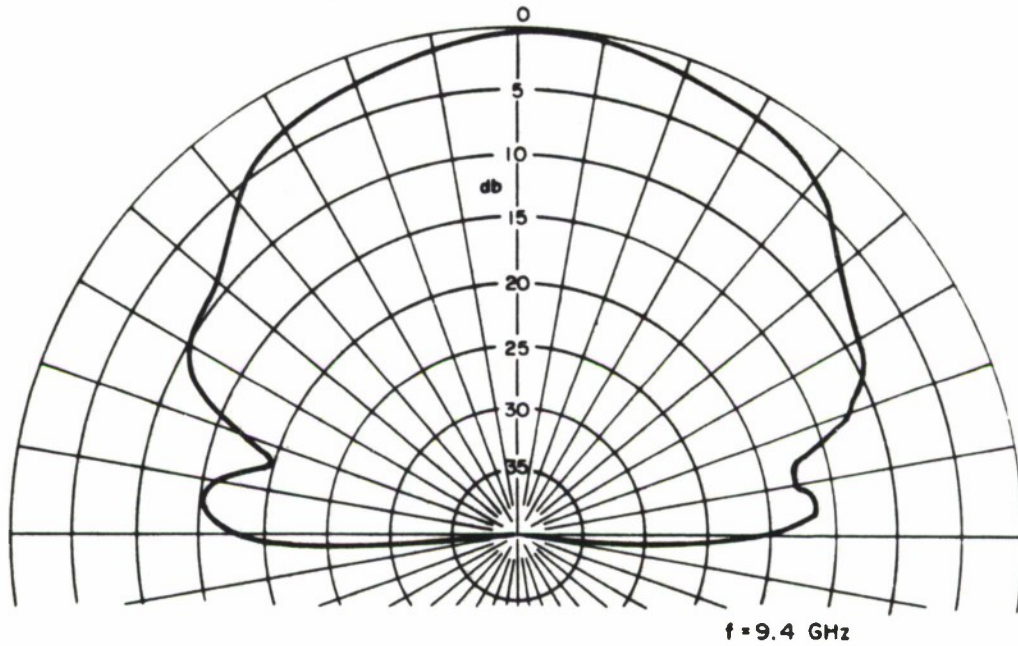


Figure 15 E PLANE RADIATION PATTERN OF DIPOLE WITH GROUND PLANE (NO BAFFLES)

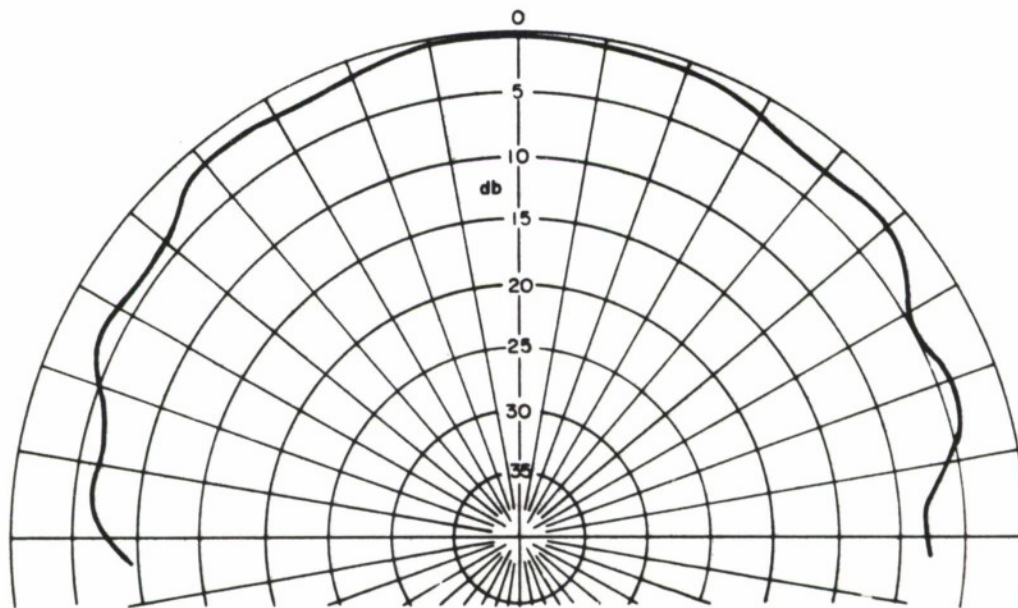
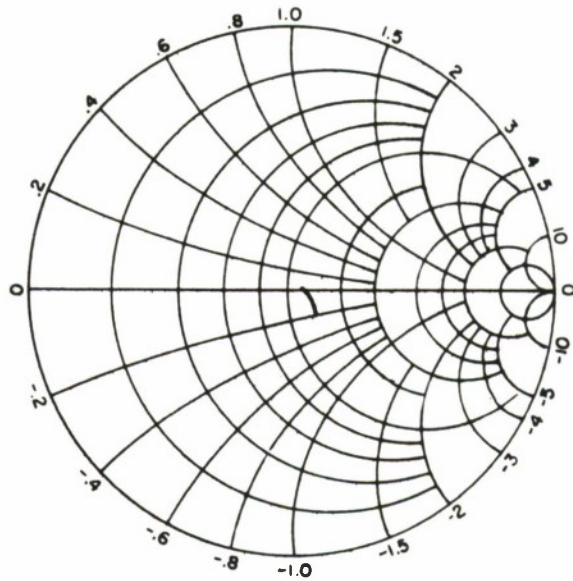


Figure 16 H PLANE RADIATION PATTERN OF DIPOLE WITH GROUND PLANE (NO BAFFLES)

18-32,711



$f = 9.0 \text{ TO } 9.8 \text{ GMz}$

REF. PLANE : INPUT CONNECTOR

1A-32,677

Figure 17 INPUT IMPEDANCE OF DIPOLE WITH BAFFLES & GROUND PLANE

Radiation patterns were measured for values of phase differential ϕ between 1 and 8 units (22.5 to 180 deg). Figure-18 shows the pattern for $\phi = 67.5$ deg.; $\varphi = 20$ deg.; and Figure-19 corresponds to $\phi = 112.5$ deg.; $\varphi = 34$ deg. A comparison of measured and calculated beam deflections is given in Figure-20 and shows good agreement up to 40 deg. beam angle.

To validate the measured patterns, a computer was programmed to calculate the ideal patterns. Using the principle of pattern multiplication^[7] the pattern of an array of eight isotropic sources was multiplied by the pattern of a single element to obtain the actual array pattern. A sine function was used to approximate the element pattern giving a far field from the array in the direction φ of

$$E(\varphi) = \frac{1}{N} \cdot \frac{\sin \frac{NM}{2}}{\sin \frac{M}{2}} \cdot \sin \varphi, \quad (2)$$

where N is the number of elements, φ is the angle with respect to the direction of the array and M is given by

$$M = \frac{2\pi D}{\lambda} \cos (\varphi - \phi), \quad (3)$$

and $\sin \varphi$ is the assumed primary pattern.

For the model, with $N = 8$ and $D/\lambda = .55$,

$$E(\varphi) = \frac{\sin \varphi}{8} \cdot \sin \left[\frac{1.382 \cos (\varphi - \phi)}{.1728 \cos (\varphi - \phi)} \right]. \quad (4)$$

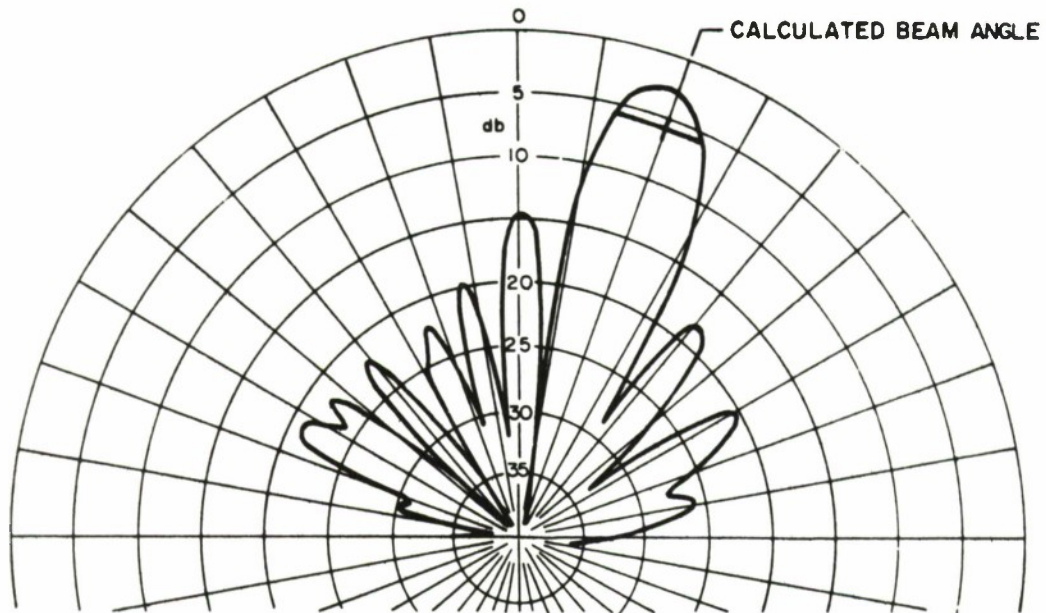


Figure 18 E PLANE RADIATION PATTERN OF ARRAY ($\phi = 67.5^\circ$)

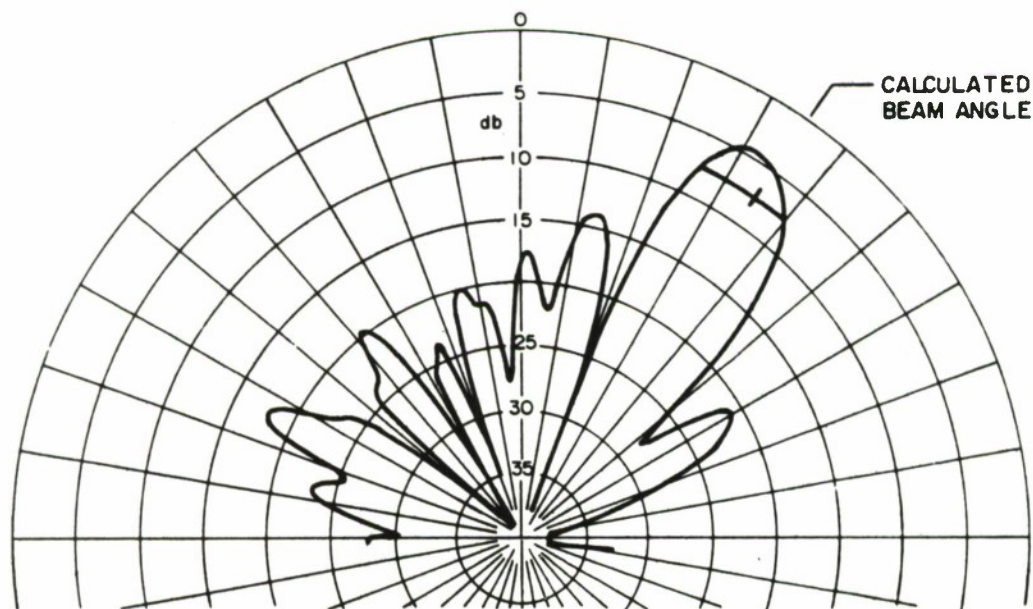
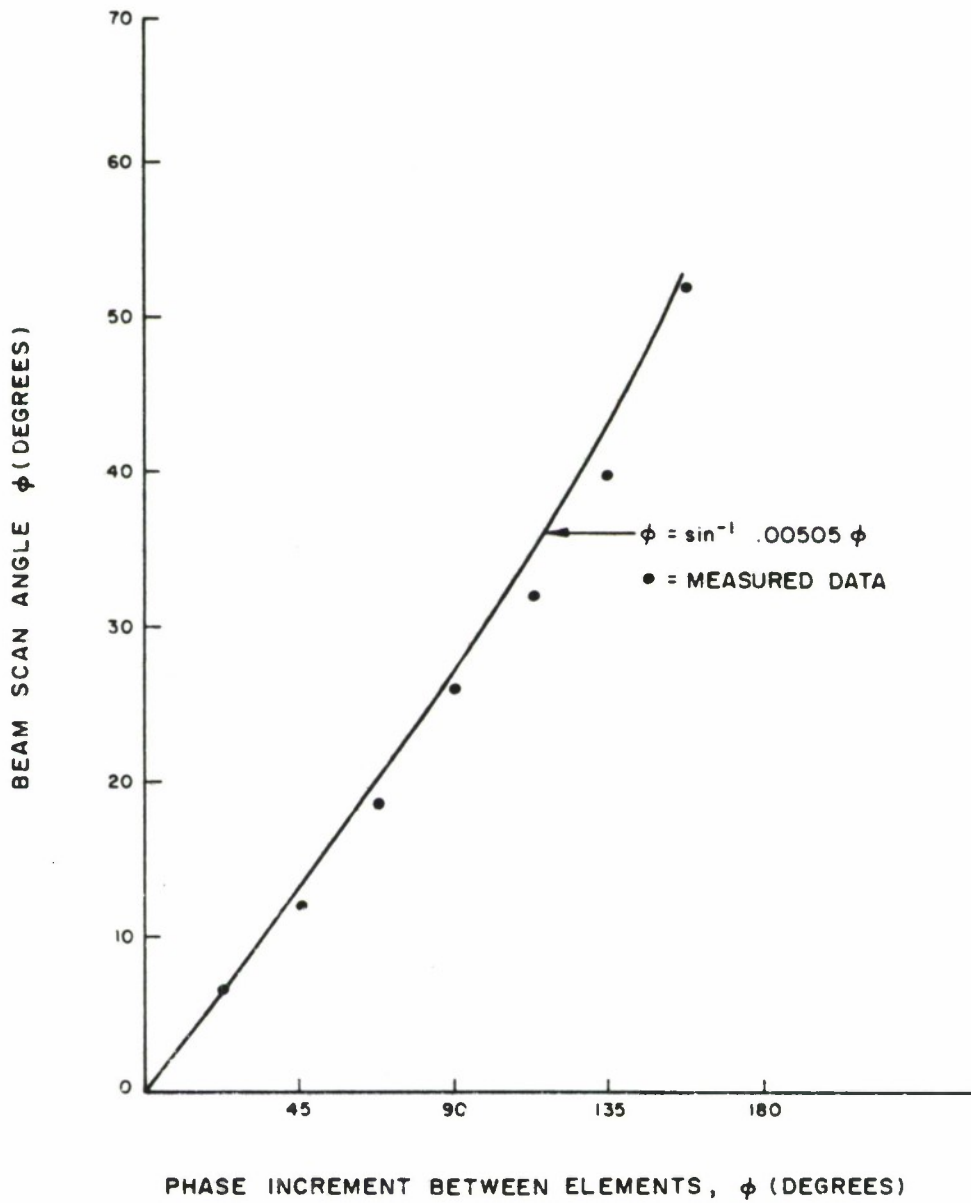


Figure 19 E PLANE RADIATION PATTERN OF ARRAY ($\phi = 112.5^\circ$)

18 - 32,704



1A - 32, 699

Figure 20 ARRAY BEAM ANGLES

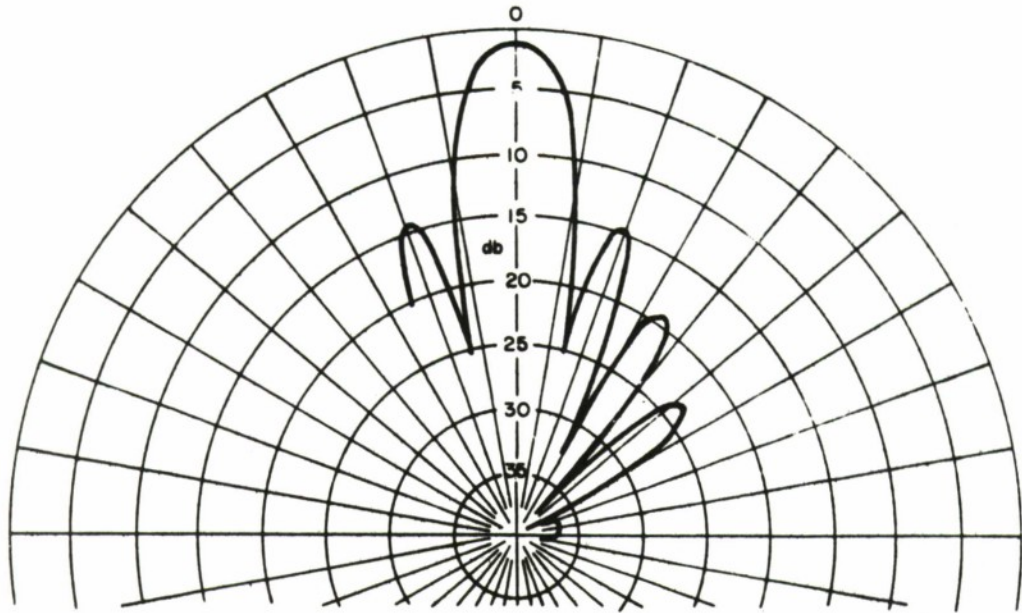
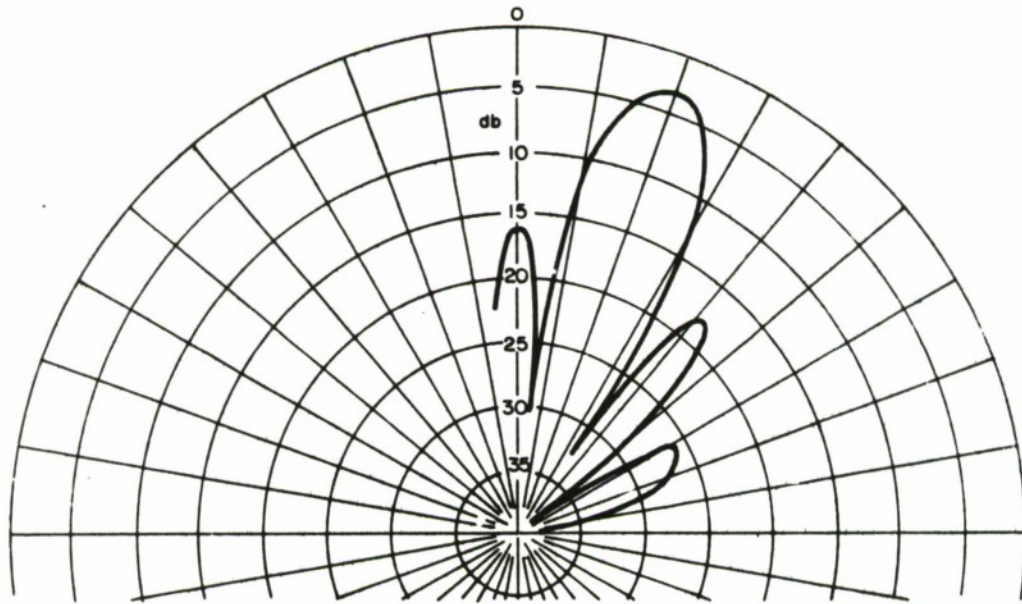


Figure 21 CALCULATED E PLANE RADIATION PATTERN OF ARRAY ($\phi=0^\circ$)



18-32,705

Figure 22 CALCULATED E PLANE RADIATION PATTERN OF ARRAY ($\phi=67.5^\circ$)

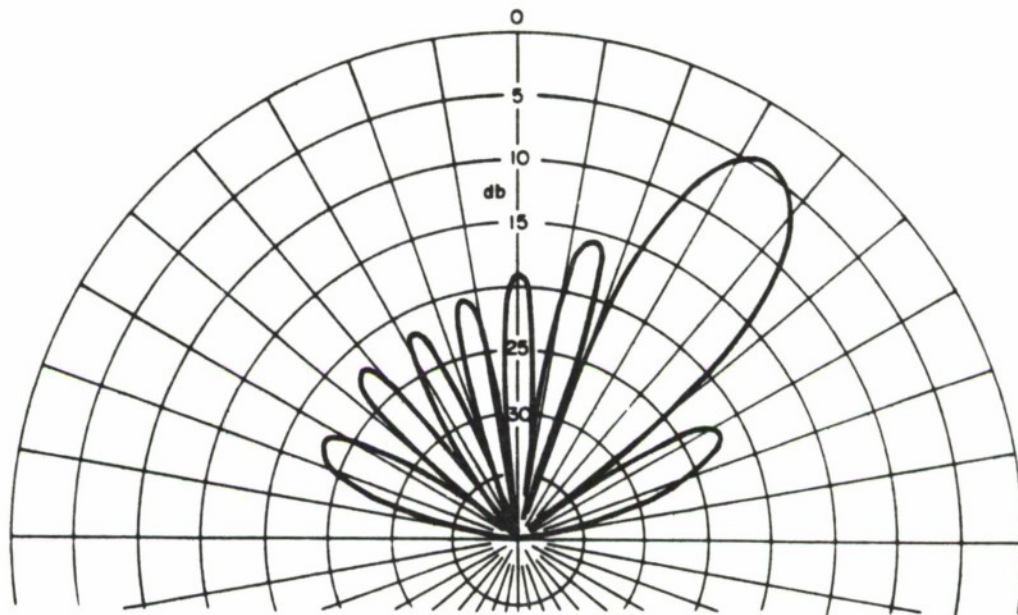


Figure 23 CALCULATED E RADIATION PATTERN OF ARRAY ($\phi=112.5^\circ$)

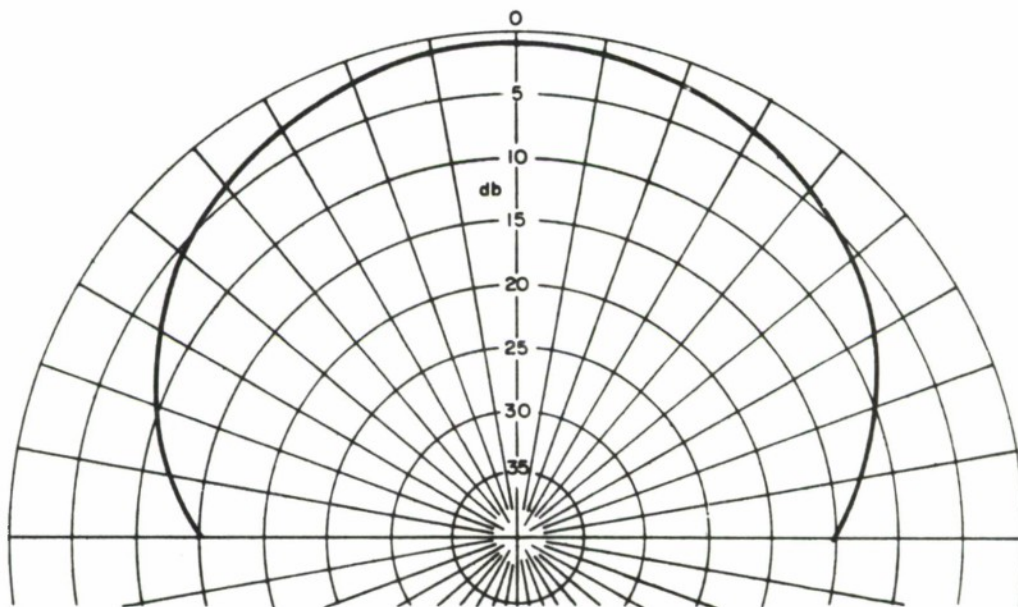


Figure 24 SMOOTHED E PLANE PRIMARY PATTERN OF DIPOLE, IN ARRAY, WITH BAFFLES

18-32,706

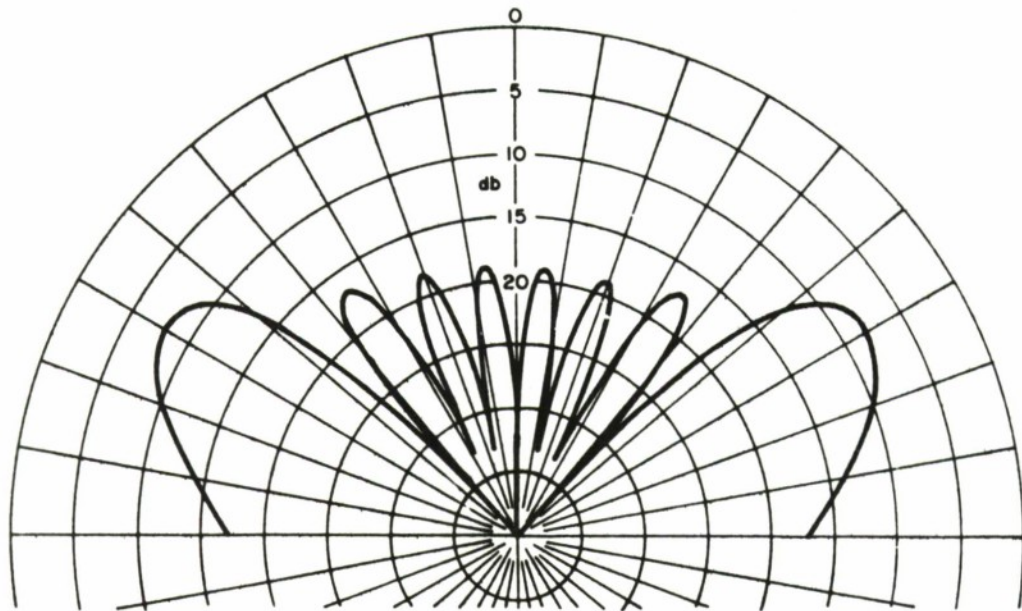


Figure 25-a CALCULATED E PLANE RADIATION PATTERN OF ARRAY
($\phi = 180^\circ$ PHASE INCREMENTS)

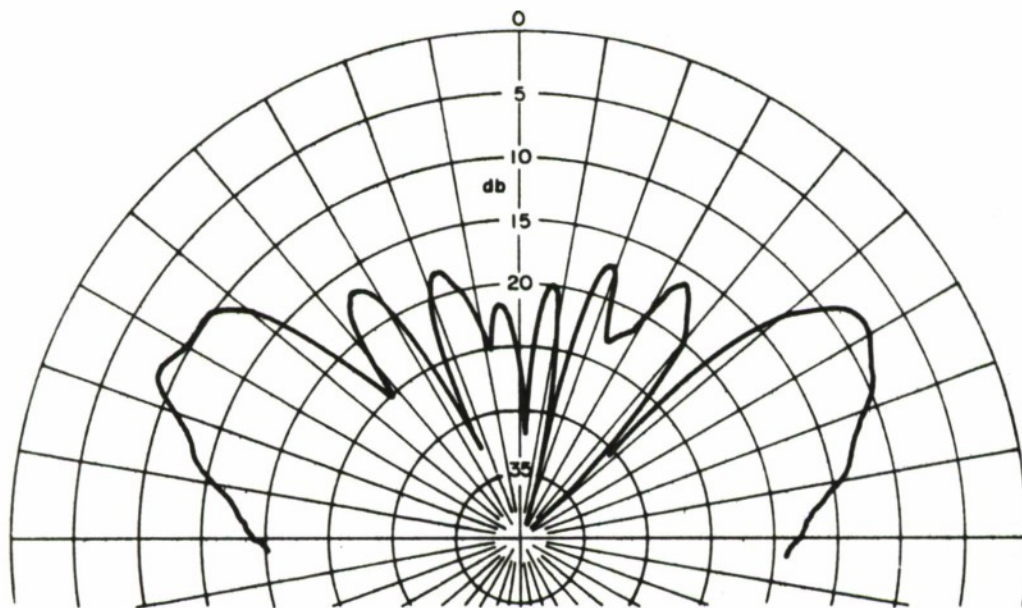


Figure 25-b MEASURED E PLANE RADIATION PATTERN OF ARRAY
($\phi = 180^\circ$ PHASE INCREMENTS)

1B-32,707

The calculated radiation patterns from Equation (4) are shown in Figures 21 through 23 and show satisfactory agreement with the corresponding measured patterns, Figures 10, 18 and 19.

The comparison of computed and measured radiation patterns was also extended to large beam deflections at which a secondary (grating) main lobe existed. Since the $\sin \varphi$ assumption for the primary pattern failed for angles near zero (in the array direction), the measured primary pattern, with the element assembled in the array, was used instead for these angles. Figure 24 shows the smoothed primary pattern. Using this data to replace the function $\sin \varphi$ in Equation (2), the measured and computed radiation patterns were in good agreement. Figures 25-a and 25-b show, respectively, the measured and computed radiation patterns for 180 degrees phase increment.

DIODE OSCILLATORS AND MODULATION

Background

Microwave diode (negative resistance) oscillators have become fully established for the generation of microwave power and their system application is rapidly growing. The emergence from the laboratory into the real world started only a few years ago and is continuing. The low-efficiency (IMPATT and Gunn) oscillators have been at the forefront and are being closely followed by the higher efficiency (TRAPATT) and high peak power (LSA) devices. IMPATT and Gunn oscillators constitute the great majority of available devices and have been reported extensively in the literature [8-11].

A bibliography of Gunn devices and theory is also available^[12,13].

The predominant reasons for selecting the avalanche diode oscillator for study were given in an earlier section. In addition it was felt that the limited effort available would be best used if directed to the study of different aspects of a specific type of oscillator. The work covered the following general areas:

- . Behavior of the injection-locked oscillator.
- . Principles and problems of oscillator design.
- . Characteristics and techniques of modulation, especially phase coding.

During FY 1969, the main effort was directed to the first two areas, using IMPATT cavity oscillators. Typical characteristics of pulse-modulated injection-locked oscillators were also studied^[5]. In the current year the work was extended to include MIC IMPATT oscillators and phase coding.

Injection phase locking was chosen as a suitable technique for producing phase coherence between the oscillators of the array and studies were therefore made of this technique during FY 1969^[5] to compare practical performance with theoretical predictions. Adler's theory, originally directed to the klystron oscillator, and relating locking bandwidth and phase errors to the circuit Q and injection power level, was found to agree well with experimental results. This theory is discussed in a later section.

In view of the misunderstanding and the confusion between the various oscillators that often exists, a brief and simple description is given of the basic oscillator types in the following sections. A somewhat more detailed description of the fundamental mode (IMPATT) avalanche diode oscillator and the Gunn and LSA oscillators is given in Appendix C.

Fundamental Mode Avalanche Oscillator (IMPATT)

The avalanche diode is so called because it is operated with reverse bias producing a strong enough electric field to induce reverse breakdown by means of the avalanche process (exponential increase of ionization with time, due to molecular impacts). The term IMPATT (impact ionization avalanche transit time) diode is also commonly used. In a simplified explanation of the process, an electric charge is first created in a narrow region at which the electric field is maximum and heavy impact ionization occurs. This charge then moves at constant velocity across a drift zone under the influence of the electric field. The output current then consists of a series of pulses which are delayed and thus shifted in phase relative to the applied voltage. The length of the drift zone is designed to produce a transit time delay of half the RF period. The current is thus out of phase with the applied voltage and power is delivered to the load. The diode also can be said to have a negative RF resistance at this frequency.

High Efficiency Avalanche Oscillator (TRAPATT, ARP)

Whereas the fundamental IMPATT mode operates at low efficiency in the range 2 - 10%, the high efficiency modes of operation can achieve efficiencies approaching 60% (pulsed) and 45% (CW). The latter modes are achieved by operating at a subharmonic of the fundamental transit-time frequency of the avalanche diode. A resonant idler circuit is provided at the fundamental frequency as well as at the desired output frequency. The output frequency is typically between the second and tenth subharmonic of the fundamental frequency. Several theories have been proposed^[11] to explain the high efficiency modes, the most generally accepted description being the TRAPATT (TRapped Plasma Avalanche Triggered Transit) mode^[14]. Another description is the ARP (Avalanche Resonance Pumping) mode, which is a parametric theory^[11].

Gunn Oscillator

Operation of the Gunn diode oscillator is based on a class of semi-conductors that exhibit a mobility (drift velocity of ions/ electric field) having two values, with a transition occurring at a critical value of electric field. Gallium arsenide is the material almost exclusively used at present. The Gunn diode behaves as a resistor until the electric field due to the applied voltage rises above the critical value. At this point the mobility falls from the higher to the lower value, resulting in an accumulation of electrons

in a space-charge domain which grows and travels across the diode to produce an output current pulse. The pulse rate and hence the operating frequency is determined by the transit time, but tuning of the oscillator circuit can affect the position of domain formation in the diode and allow almost an octave tuning band for a given diode. The possible operating frequencies extend above 20 GHz.

LSA Oscillator

Operation of the LSA (Limited Space Charge Accumulation) diode oscillator is a specialized mode of operation of a Gunn diode. The essential difference is that space charge accumulation, characteristic of the Gunn diode, is only allowed to form partly, hence the name. By applying a bias field which is much larger than the mobility transition threshold and allowing the AC field to build up initially so that the total field dips below the threshold, the space charge accumulation is dissipated. The field remains above the threshold for most of the cycle and most of the bulk of the device (rather than a small region) exhibits negative resistance. The advantages are that high peak powers can be obtained because of the extended negative resistance region and that the device is not transit-time limited like the other three oscillators described.

Performance Status

Various versions of IMPATT and Gunn diode oscillators, which operate in their low efficiency (2-10%) fundamental mode, are available commercially. Table 4 presents data on some typical devices.

Table 4

Typical Commercially Available Gunn and IMPATT Oscillators

<u>Mode</u>	<u>Frequency (GHz)</u>	<u>P out (MW) CW</u>	<u>Bias</u>		<u>Efficiency</u>
			<u>Volts</u>	<u>Ma</u>	
IMPATT (Varian)	8 - 12.4	100	85	30	5
	8 - 10.0	1000	100	200	5
Gunn (Monsanto)	4 - 8.0	35	11	400	0.8%
	8 - 12	9	9	200	0.5%
	8 - 12	100	12	800	1%

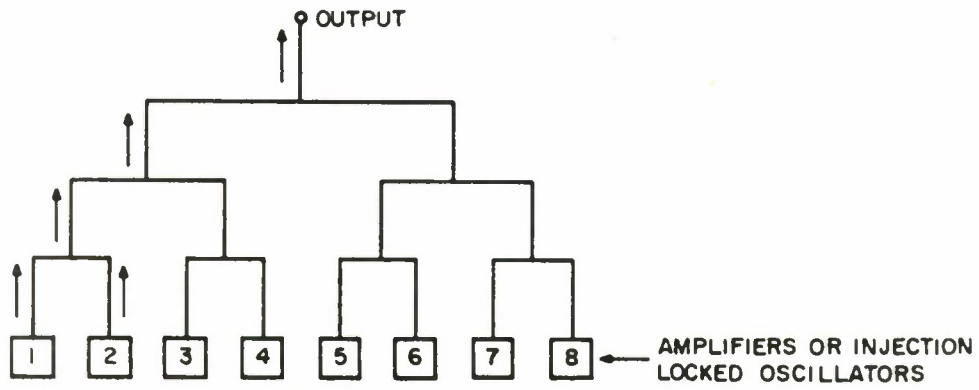
Note: Multi-diode avalanche devices of the future may be capable of delivering 100 W CW at 8 GHz.

Considerable and continuing effort has gone into the theory and development of oscillators having higher efficiency and power output, operating pulsed and CW^[15-20]. The TRAPATT mode avalanche diode oscillator probably represents the most advanced and promising high microwave frequency device that is becoming available^[14]. Table 5 outlines some laboratory results of the higher efficiency modes and these data represent what might be available in the future.

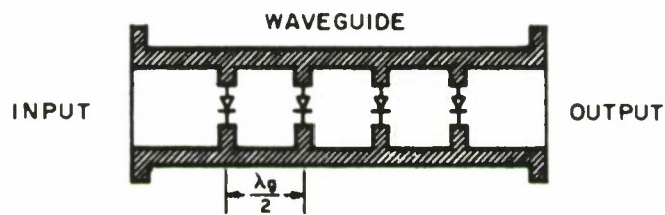
Various techniques have been reported for overcoming the power limitations of individual diode oscillators and amplifiers by means of power-combining circuits^[21]. One form is the arrangement of diodes in series or parallel arrays. For example, five diode wafers have been paralleled to produce 2.8 watts (CW) at X-band in the IMPATT mode^[22], and three series-connected diodes have produced 4.5 watts (CW) at 13 GHz^[23]. Five diodes have been stacked in series and operated in the TRAPATT mode to give pulsed power of 1.2 KW at 1.1 GHz with an efficiency of 25.6%^[24].

Another form is the combination of individual oscillators using hybrid couplers (Figure 26-a). To insure that the oscillators are synchronized, a common locking signal is used (as in the array design of the previous section), or alternatively the mutual coupling between ports can be used to provide the locking signals required^[25].

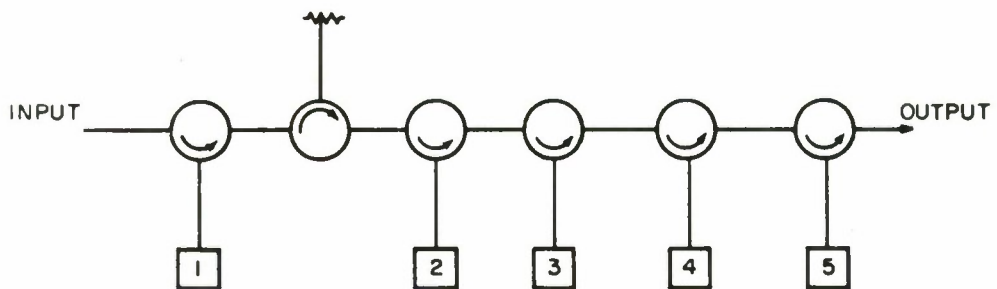
A third form is the arrangement of diodes in periodic structures, such as that shown in Figure 26-b. As a locked



a) HYBRID - COUPLED POWER COMBINER



b) PERIODIC STRUCTURE AMPLIFIER



c) CIRCULATOR COUPLED DIODE AMPLIFIER

1A-32,698

Figure 26 DIODE COMBINATIONS FOR HIGH POWER OUTPUTS

Table 5

High Efficiency and Peak Power Devices

<u>Diode</u>	<u>Peak Power</u>	<u>Frequency</u> <u>(GHz)</u>	<u>Efficiency</u> <u>(%)</u>	<u>Laboratory</u>
Avalanche TRAPATT	200 watts 10 watts 200 watts	1 8.6 2	40 25 30	RCA Sperry
Gunn	140 watts	2	30	RCA
Gunn (LSA)*	6 KW	1.8	15	Cayuga
Gunn (LSA)	2 KW	7	5	Cayuga
Gunn (LSA)	3 KW	3.5	7.3	Cayuga
Transistor	100 W	1.0	40	M.S.C.

*LSA (Limited Space Charge Accumulation) diode. This is a special operating mode for a Gunn diode. The theoretical peak power prediction limit for these devices is 100 KW at 10 GHz and 1 KW at 100 GHz.

Note: Thermal limitations restrict the duty cycle (10^{-4} to a few percent) and the pulse width ($< 2 \mu\text{seconds}$) [9-11].

oscillator, 300 mW at X-band was obtained, and as a power amplifier, 200 mW at 6 dB gain resulted. This experimental circuit achieved 91% of the sum of the individual diode power outputs^[26].

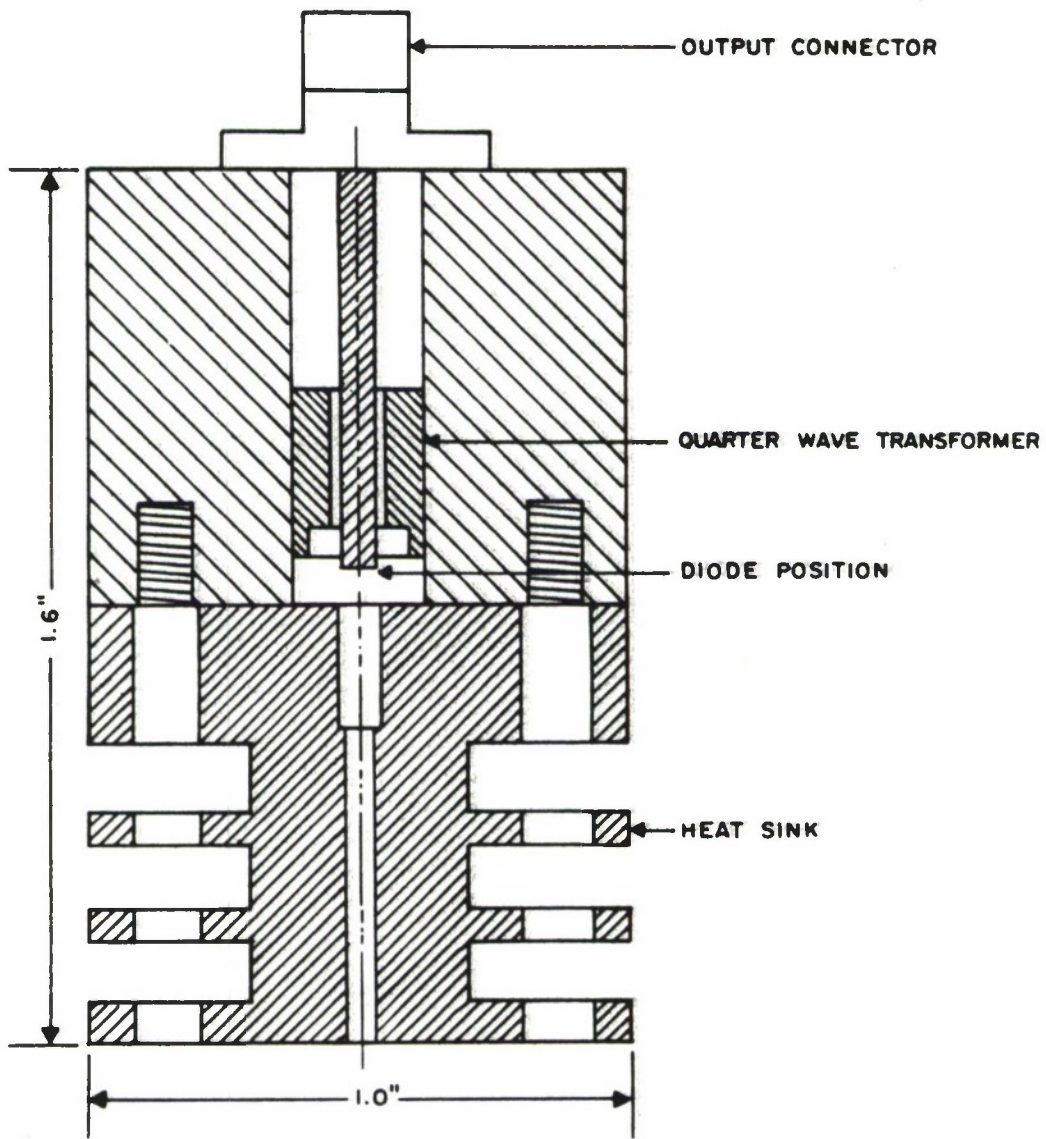
A fourth form uses cascaded low-gain amplifiers to provide power addition as shown in Figure 26-c. One device produced 1 watt output at X-band^[27]. Another similar device employing only three IMPATT diodes yielded 1.85 W (CW) at 6 GHz, which was 90% of the sum of the individual powers^[28].

It is difficult to say at this time which of the above techniques is, or will be, most favored, and it is likely that a combination of the above schemes will provide the highest power.

IMPATT Cavity Oscillators

Several cavity oscillators were designed during FY 1969^[5] in order to appreciate some of the design problems and limitations and to develop a small cavity which might be used in the transmitter array model. One of the most satisfactory design techniques was to use a quarter-wave transformer to match the low impedance of the packaged diode ($\approx -10 \Omega$) to the 50Ω load impedance. Figure 27 shows the arrangement of a 0.5 watt X-band cavity oscillator using this technique.

The cavity oscillator described above was modified to be compatible with MIC external circuits. Figure 28 shows the oscillator connected to an MIC circuit containing a filter providing a DC return



1A-29,583

Figure 27 1/2 W IMPATT OSCILLATOR CAVITY

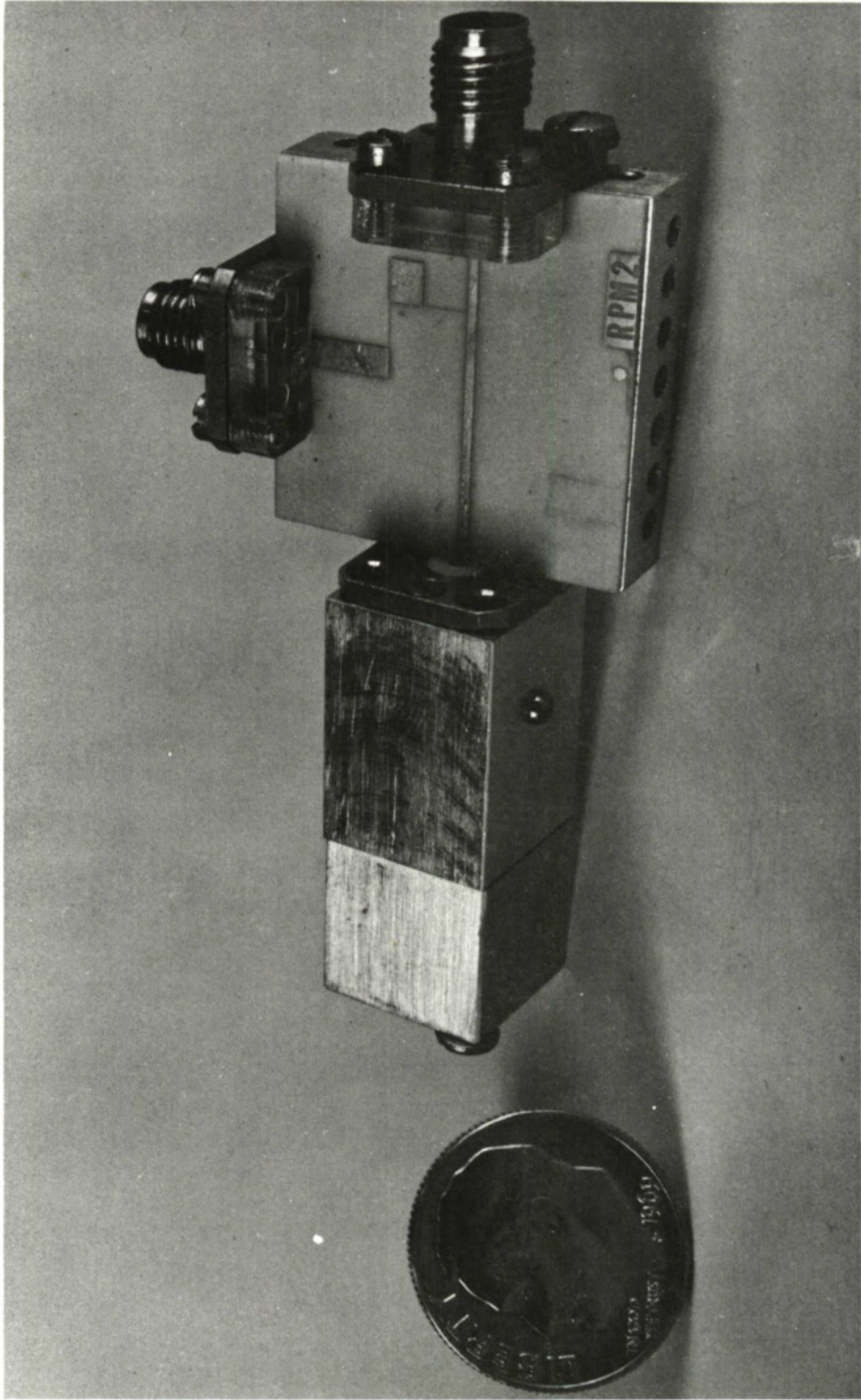


Figure 28 - 0.5 W Cavity Oscillator with MIC Output

to the diode. This configuration represents the sort of arrangement that could be used with a coaxial cavity oscillator/MIC circuit combination. In some applications the use of the coaxial cavity is advantageous. For example, where a low temperature coefficient is required an invar cavity or expansion-compensating arrangement is feasible. The need for a low temperature coefficient can become important where minimum phase errors are required in an injection-locked system, as discussed elsewhere in this report. A coaxial (or waveguide) oscillator cavity may also be appropriate where a second, loosely coupled high Q cavity is used to provide increased stability or AM noise suppression. In such a case, the loose coupling requires a substantial reduction of output power, limiting the applications to reference or local oscillator use.

Diode Characterization

Characterization studies were made during FY 1969^[5] of a typical low power, X-band IMPATT diode to determine the effects of package transformation and to test characterization techniques which would lead to the design of matching transformers for use in IMPATT oscillators. Figure 29 shows two equivalent circuits that may be used to describe the diode package at X-band. The package parasitics can impose serious design constraints and the package tolerances can cause major variations in diode performance at high microwave frequencies.

1A-29,394

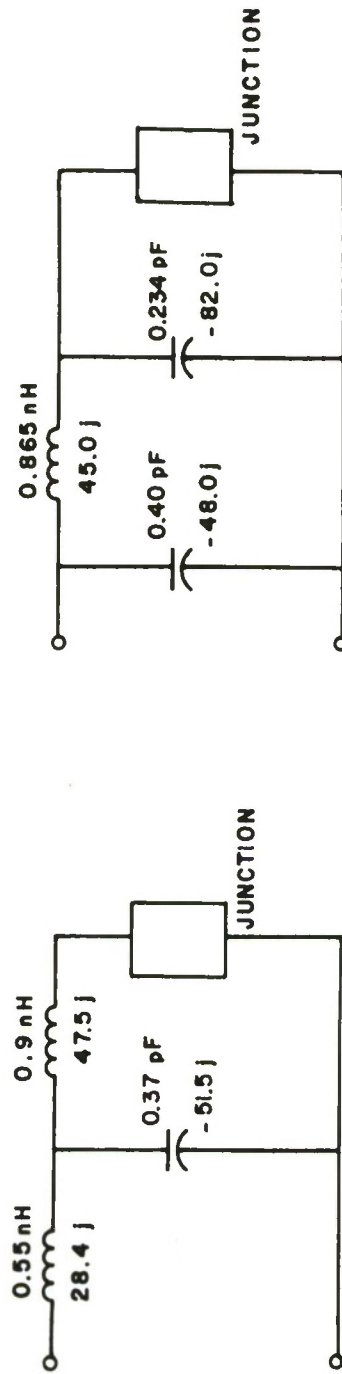


Figure 29 EQUIVALENT CIRCUITS OF PACKAGE AT 8280 mHz

MIC IMPATT Diode Oscillators

The previous work on avalanche diode cavity oscillators and MIC passive component techniques^[5] was extended and brought together in the design of two types of MIC avalanche diode oscillators. This work was carried out in order to obtain a more detailed insight into the merits and problems of MIC technology as applied to solid state oscillators.

MIC Oscillator Circuits

Two oscillators were constructed on metallized substrates of 99.5% purity alumina with 5-10 micro-inches roughness and .025 inch thickness. The plating was 100 Å chromium and .3 mil gold. This type of substrate was used exclusively for all our work.

In the MIC circuits developed in-house a modified pill package diode was used (Figure 30 bottom). The top section of the package was removed to reduce surface wave excitation and stray capacitance. Details are given in the following section. The diode itself was an oxide-passivated mesa epitaxial silicon avalanche diode with a transit time designed for X-band operation^[10,11].

The diode was mounted within a hole bored in the substrate by a diamond drill (in production, an ultrasonic drill would be used). The base plate provided a heat sink to dissipate power up to 6 watts and was bored to accommodate the diode so that the diode flange could make a pressure contact to the circuit. Figure 31



Figure 30 - Diode Pill Packages

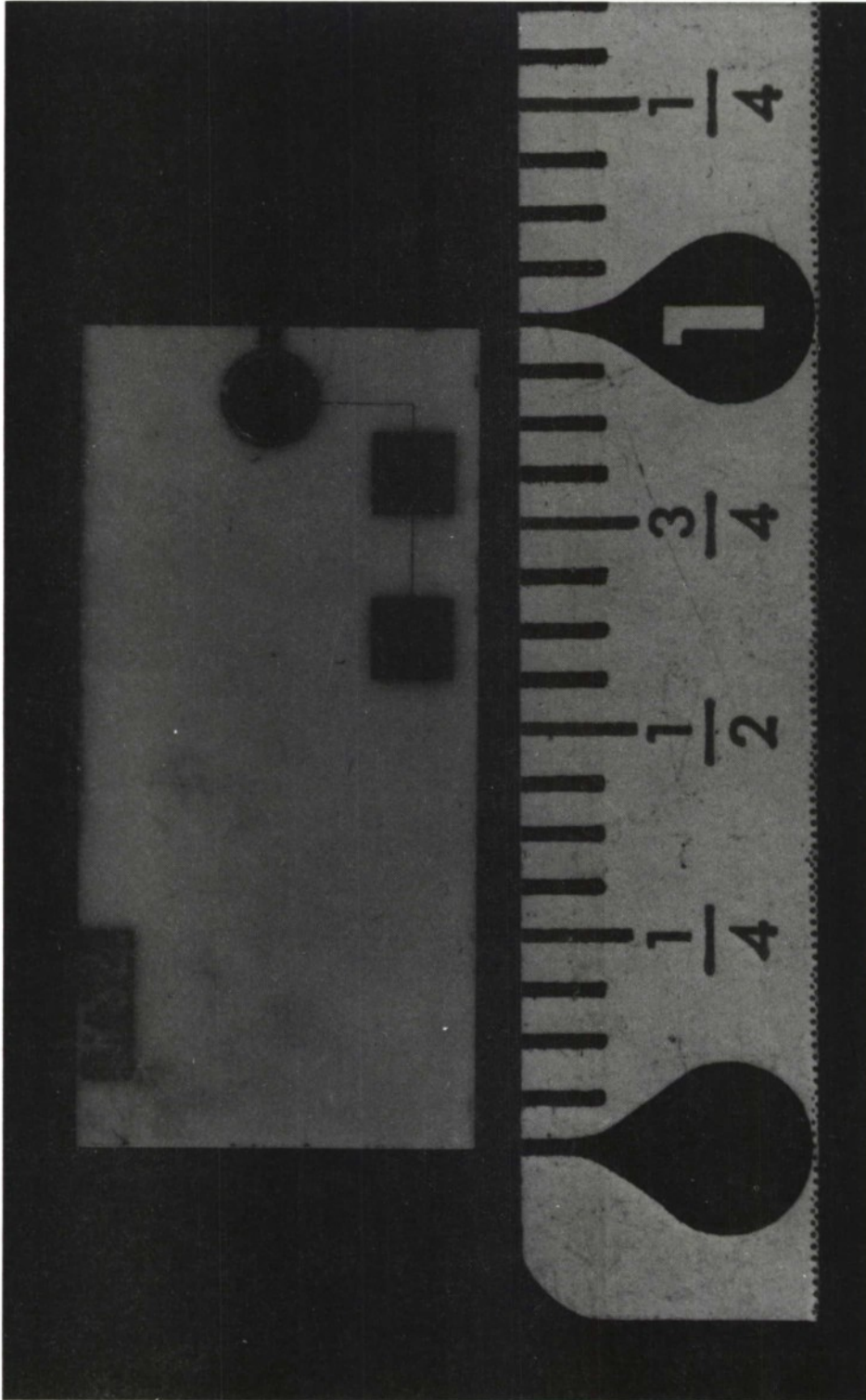


Figure 31 - Diode Mount Substrate

shows a diode mount constructed as described and including a low-pass filter for the DC return. A possible disadvantage of this type of mount is the increase of package capacitance due to the contact ring, although this capacitance may be used to resonate the pill diode inductance. A soft metal washer under slight pressure was used to obtain a low impedance contact as a matter of convenience, although for a reliable construction the pill diode would have to be soldered into the circuit. The latter technique has been used successfully elsewhere [29].

The test jig shown in Figure 32 provided a transition from the microstrip diode mount (Figure 31) to a coaxial line. The jig provided the means by which the diode impedance could be measured while inserted in its alumina holder (its actual operating environment). Optimum impedance loading of the mounted diode for maximum power output was obtained by adjusting a double-stub tuner placed in the coaxial output circuit (Figure 32). This impedance was then measured, using a Hewlett Packard impedance analyzer. The diode impedance was then calculated by taking the negative of this load impedance. The mounted diode impedance at a frequency of 11.2 GHz was typically $-185 + j 68$ ohm measured at an arbitrary reference plane close to the diode (right edge of holder, Figure 31) indicating that the diode is inductive (due to the diode leads) even when inserted in the capacitive MIC mount.

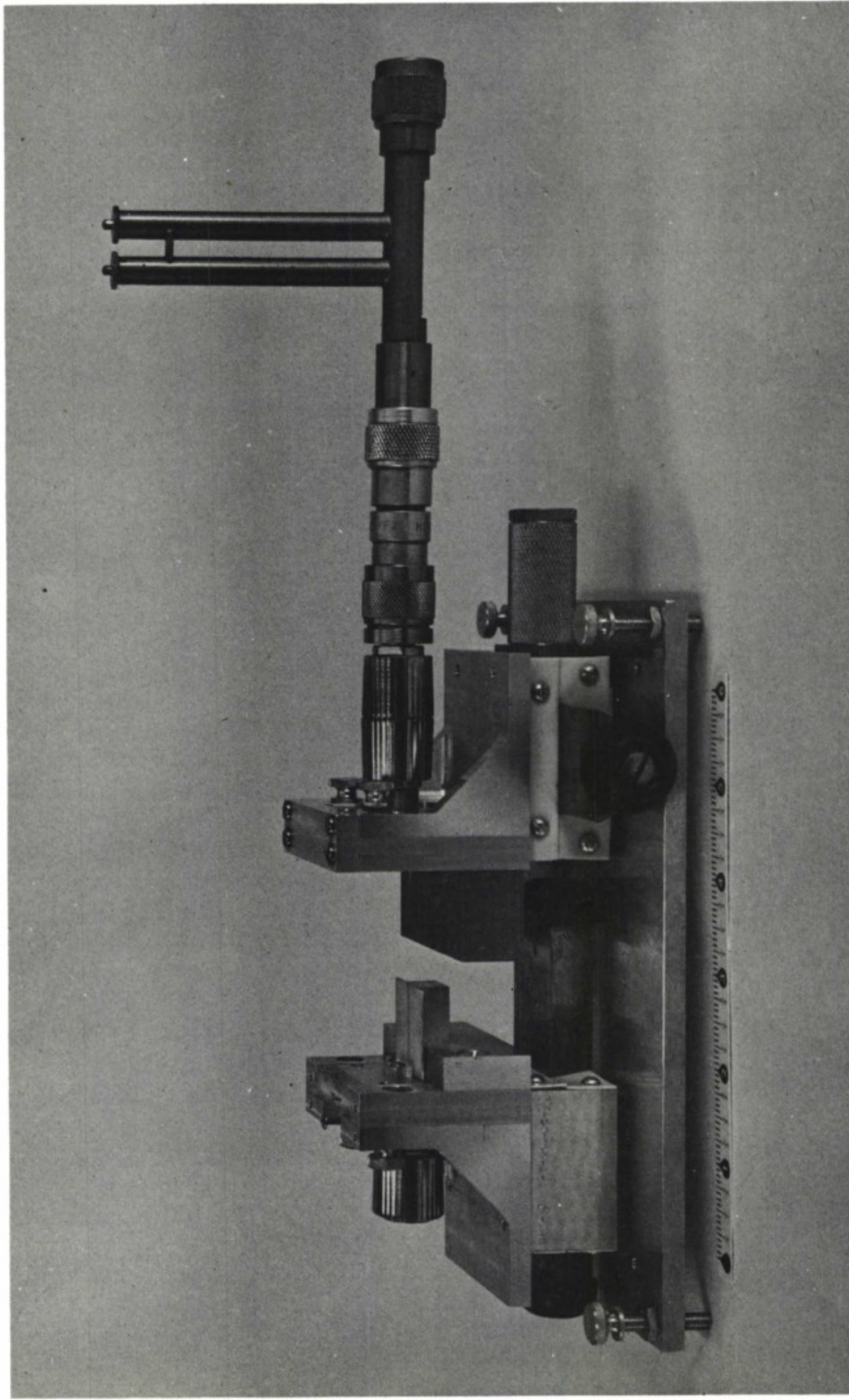


Figure 32 - MIC Test Jig

Figure 33 shows the MIC circuit of a stub-tuned oscillator, before assembly. The center of the ring was subsequently drilled for the diode, as described earlier. A 50 ohm termination was connected to the .024 inch wide transmission line on the right. A 3 pF DC-blocking ceramic capacitor was soldered across the gap in the output line. Matching was accomplished by means of the shunt stub running vertically. This stub provided capacitive loading of the main line at the junction point, whose distance from the diode reference plane was chosen to provide the required load impedance at this plane. Two filters were incorporated in the oscillator, each consisting of cascaded high and low impedance sections. These are seen at the top and left of the substrate. The top section provided a DC ground to the output line to protect the external components (particularly the phase shifter) from damage, in case the series-blocking capacitor should fail. The other section provided a filter for the B+ supply to the diode, the other side of which was grounded via the heat sink.

The above oscillator provided 160 mW output at 11.8 GHz with an efficiency of 3%. The diode was specified at 200 mW with 3% efficiency. A second diode in the same circuit gave 100 mW output. It was found that with this circuit, very little control could be applied to the frequency of oscillation, which was largely determined by the parasitic elements of the mounted diode. The

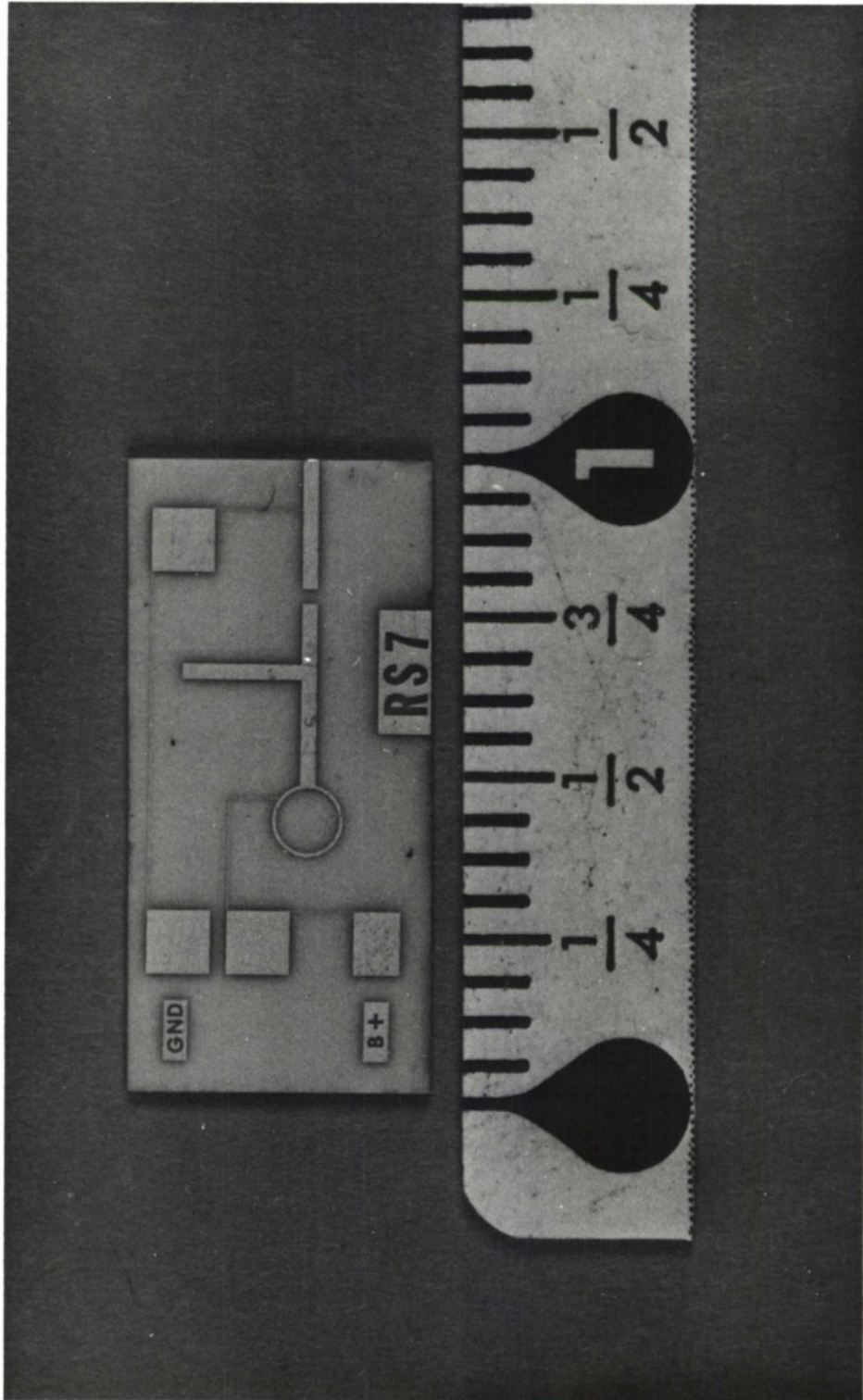


Figure 33 - Stub-Tuned MIC Avalanche Oscillator

above circuit was subsequently integrated into a transmitting module, shown in Figure-3. The latter shows the oscillator completely assembled and bonded to the associated component (circulator).

Figure-34 shows a second type of MIC oscillator that was designed and fabricated in-house. This oscillator used a resonant tank circuit with a distributed coupling to an external load. The tank circuit was approximately a quarter wavelength long with a characteristic impedance of 18 ohms. This circuit provided a higher unloaded Q to the diode than in the previous design and enabled the frequency to be tuned. This was done by changing the resonator length by means of a dental sandblaster although this proved extremely inaccurate for the delicate trimming that was necessary. The coupling gap between the two transmission lines primarily controlled the output transformation and hence the impedance loading. This oscillator was not optimized with respect to output coupling and gave reduced output of 70 mW at 8.8 GHz, with an efficiency of 1.5%. This circuit was considered superior to the previous design, since the higher Q allowed the frequency to be controlled readily and the design was inherently more reliable and simpler to construct, due to elimination of a coupling capacitor.

General Discussion

The advantages of using MIC construction are best discussed in relation to an example. This is done in a later section, for the

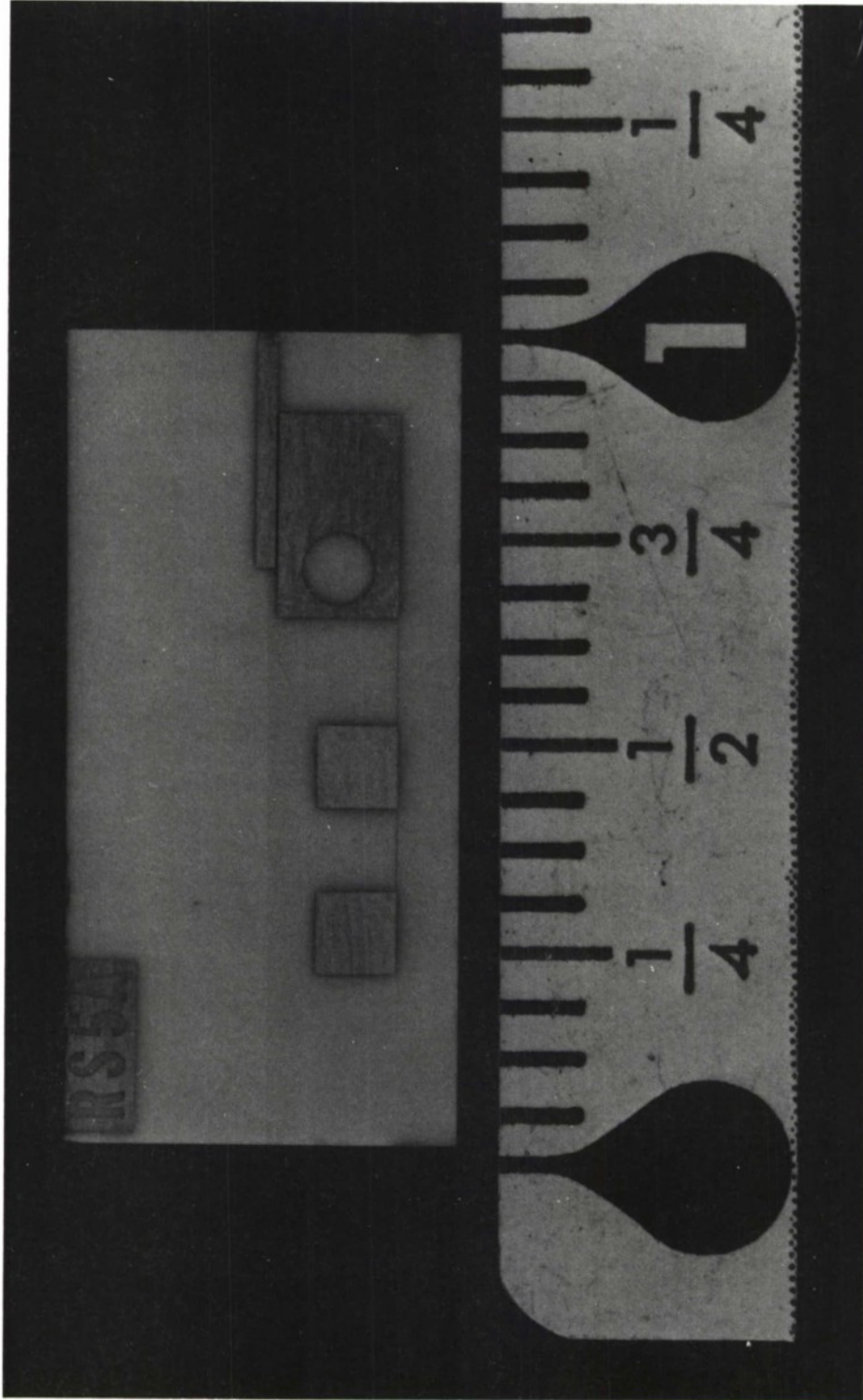


Figure 34 - Side-Coupled MIC Avalanche Oscillator

integrated transmitting module (Figure 3). The following discussion deals mainly with the problems associated with the implementation of MIC solid state power oscillators. These problems can be roughly separated into those of the diode package and those of the oscillator circuit.

There is a basic problem of testing and selecting diodes in packages, pills or mountings appropriate to MIC circuits. Any packaged diode suffers from the problems of impedance transformation through its package, as previously described^[5]. Although for a specific oscillator design at a specific frequency the transformation may be acceptable and even advantageous, the tolerances of the parasitic elements, particularly inductance, offset the advantage of reproducibility in the photo etched circuit. The highly frequency-sensitive transformation may also be a serious disadvantage for a tunable oscillator (or broadband amplifier). Another problem is the difficulty of obtaining a low and reproducible contact impedance between a diode capsule and an oscillator circuit. This requirement can be met by soldering the diode capsule in the circuit. Advantages of a capsule are the amenability to testing and selection and the possible reliability advantage of a hermetically sealed package.

There are also problems with an unencapsulated (chip) power diode operated in a microstrip circuit. Provision of an efficient heat sink becomes a limiting factor for high power oscillators.

Protection or passivation of the diode chip is necessary to ensure reliability. Electrical connections must have low and repeatable parasitic impedances and must not produce damaging mechanical stresses on the diode chip. Finally, the diode should desirably be electrically tested in the microstrip environment under oscillating or equivalent high-level conditions. Although it appears difficult to overcome all of these difficulties, a possible solution may be to fabricate a microstrip package in which the diode chip is mounted in a small MIC module providing a heat sink. Such a module could be comparable in size and cost to a standard pill package, and might consist of a metal-dielectric combination or a solderable substrate of high thermal conductivity, such as beryllia or silicon carbide. The development of integrated diode-MIC oscillators would be facilitated if such electrically tested MIC modules became available. The choice between a miniature cavity and the MIC format for the oscillator sub-unit can only be made for a particular system trade-off. For small production quantities the basic MIC advantages of small weight and size, compared to miniature cavities, may not be sufficient to outweigh the development expense and lack of flexibility (for example, the tuning difficulty). Furthermore, the common and necessary use of metal enclosures around MIC components to prevent radiation and damage, offsets the basic advantages of size, weight and cost. This argument applies particularly to operation at high

microwave frequencies, such as X-band, where radiation and surface wave coupling are serious problems unless appropriate boxes are used.

At lower frequencies such as L-band, the basic MIC advantages may be realized^[24,30,31], since radiation problems are less serious and cheaper mechanical structures can be used in many cases^[32]. Transistor/multiplier circuits may be preferred to fundamental diode oscillators where efficiency is a major factor^[33], but the high efficiency (TRAPATT) avalanche oscillator is a close competitor. For low duty ratio pulsed systems, however, the efficiency may be less important than size, weight and cost factors and the MIC diode oscillator then becomes a more logical choice^[34,35]. At lower frequencies also, the arguments made earlier against the packaged diode on the grounds of package transformation are not necessarily valid, although the contact problem remains.

If a suitable microstrip diode package could be successfully developed and characterized as suggested in an earlier section, then the design problems of an MIC power oscillator at higher frequencies might be considerably reduced and the efficiency increased. This swings the argument in favor of the MIC design, especially for large quantity applications like phased arrays.

A basic disadvantage of MIC (microstrip) construction is the high loss compared with other transmission systems such as coaxial line or waveguide. This disadvantage is normally offset by the improved packaging and consequent decrease in size of components

and by the use of coaxial cables where long interconnections are required. Microstrip has a loss typically of .18 dB/inch or .09 dB/wavelength at X-band. The latter is about 20 times higher than for coaxial line (air dielectric). The difference between the losses shows up in the unloaded Q's of resonant cavities constructed in MIC and coaxial line. The unloaded Q (when very lightly loaded by the source and load impedances) is proportional to the ratio of phase constant $\beta = 2\pi/\lambda$ (phase shift/unit length) to the loss/unit length α (dB/unit length),

$$Q_u = 4.3 \beta/\alpha.$$

The measurement of Q_u is thus used to determine the MIC loss, as discussed in a later section. Unloaded Q's of MIC resonators are typically 200 to 400, compared with several thousand for a coaxial cavity.

In the case of the avalanche oscillator using injection locking, it is usually necessary to load the circuit heavily by the external load so that the power dissipated in the internal loss of the oscillator cavity is small compared with the power delivered to the load resistance. This procedure results in a reduction of the phase errors between oscillators in a system where multiple oscillators are used. By such heavy loading such that the Q becomes, typically, a tenth of the unloaded Q, the loss associated with the microstrip circuit becomes small, typically 0.4 dB.

IMPATT Oscillator Modulation

The majority of applications require amplitude, pulse, frequency or phase modulation. Waveforms of particular interest at MITRE in connection with its ongoing high resolution radar studies are the linear FM pulse ("chirp") waveform and the binary phase coded pulse waveform. Modulation studies made of IMPATT oscillators paid special attention to the characteristics relevant to the latter type of waveform.

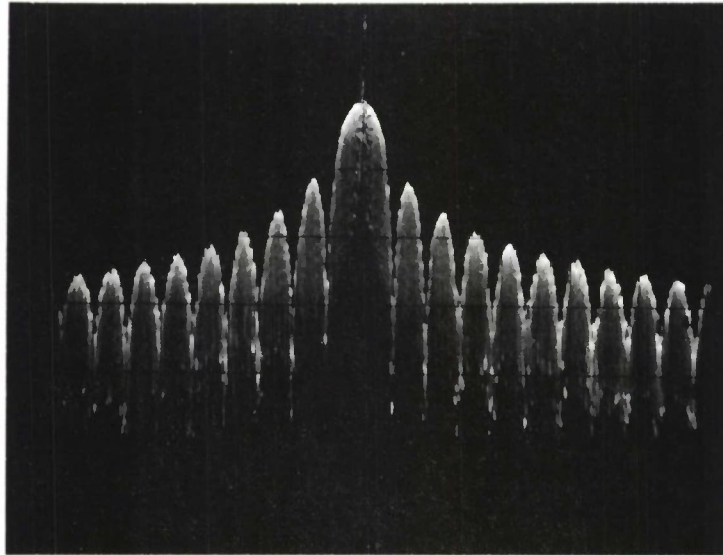
The initial studies of modulation techniques were directed to the simultaneous use of pulse modulation and injection phase locking. This technique was used in the transmitting array model. Oscillator characteristics were measured with pulse modulation, achieved by direct modulation of the oscillator bias. Figure 35 shows the typical pulse spectrum of a transmitter oscillator. The central line is that of the locking signal which can be removed in practice by gating the locking signal synchronously with the oscillator. A problem with this modulation technique is the presence of FM on the signal in the approximately 200 nanosecond period between the onset of oscillation and acquisition of phase lock.

There are four general modulation techniques which are described as follows:

Bias Control

Although diode oscillators do not have the flexibility of some conventional oscillators such as the klystron, proper bias

VERTICAL 10 dB/DIV
HORIZONTAL 100 KHz/DIV



UNIT # 1

PULSE WIDTH: 20 μ SEC
POWER OUTPUT: 100 mW
LOCKING LEVEL: -20 dB

1A-29,502

Figure 35 PULSE SPECTRUM OF TRANSMITTER OSCILLATOR

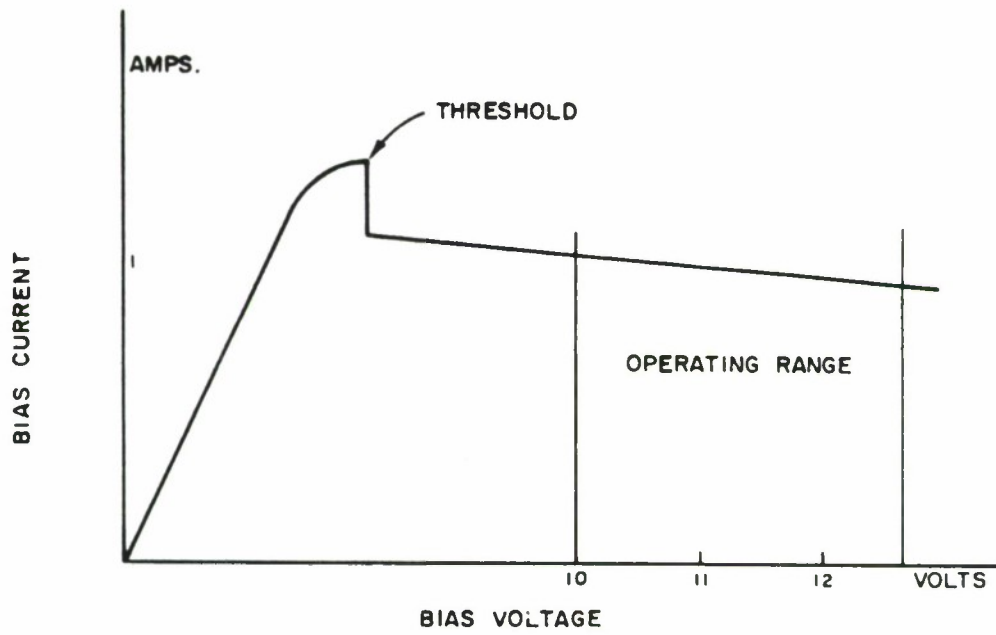
control can be used to obtain pulse and frequency modulation^[36].

Typical bias levels for Gunn and avalanche oscillators are noted in Table 4. Representative current vs. voltage curves are presented in Figure 36 and reveal the changes in AC impedance which take place as a function of bias. For pulse operation therefore, the bias supply has to be capable of switching relatively large DC power levels into a load exhibiting substantial variation in impedance. Oscillators pulsed in this fashion have considerably lower peak power levels as compared to the LSA or TRAPATT mode.

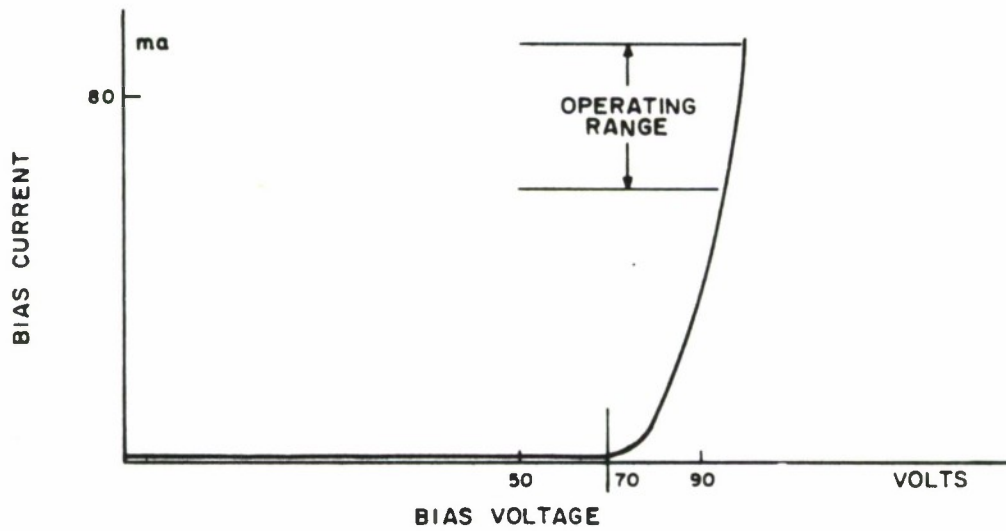
The bias voltage can also be used to control the oscillator frequency, with little power variation, by choosing the appropriate operating conditions. This method has been used to provide electronic tuning and frequency modulation. A typical commercial device (which does not represent the state-of-the-art) produces 40 MHz peak-to-peak frequency deviation at a modulation frequency of 800 KHz.

Electronic Circuit-Tuning

Frequency modulation is usually obtained by electronically tuning the oscillator tank circuit. A commonly used technique is to incorporate the junction capacitance of varactor diode into the tank circuit^[37]. This bias-controlled capacitance is approximately proportional to the square root of the bias voltage for one class of varactor. In frequency modulation experiments using varactor-tuned



(a) GUNN OSCILLATOR



(b) AVALANCHE OSCILLATOR

1A-32,700

Figure 36 TYPICAL BIAS CURVES OF GUNN AND AVALANCHE OSCILLATORS

oscillators, modulation frequencies up to 300 MHz with deviations of ± 120 MHz have been observed with no deterioration of the FM spectra.

A second common method of electronic tuning is to use the magnetic-resonance property of ferromagnetic material to determine the oscillator frequency^[38-41]. A small sphere of yttrium iron garnet (YIG) is normally coupled into the oscillator circuit and behaves as a high Q resonator whose material ferromagnetic resonance frequency is proportional to the internal magnetic field in the sphere. Large tuning bandwidths are obtainable with excellent linearity (as good as .1%) but because of the magnetic driving circuits these devices tune at much slower rates than varactor-tuned oscillators. YIG-tuned Gunn oscillators are commercially available and are commonly used in swept oscillators.

Table 6 lists typical parameters of varactor and YIG-tuned oscillators reported in the literature.

External Modulation

Modulators used externally to the oscillator (i.e., as separate, decoupled, components) can readily provide pulse, amplitude and phase modulation. Frequency modulation is also possible, within limitations, by using modulated phase shifters. The use of external modulators provides design flexibility and can avoid undesirable modulations of the oscillator (i.e., pulling effects) due to impedance

TABLE 6

Typical YIG and Varactor-Tuned Oscillators

<u>Tuning Mechanism</u>	<u>Oscillator</u>	<u>Tuning Bandwidth</u>	<u>Tuning Rate and FM Limit</u>	<u>Power Out</u>	<u>Source</u>
YIG	Gunn	8-12.4 GHz	400 MHz/ms	5 mW min.	Varian
YIG	Avalanche	7.5-10.5 GHz			
Varactor	Gunn	4-8 GHz	N/A	35 mW ± 1.7 dB	Kruse Elect. (Microwave Journal, 10/70)
Varactor	Gunn	300 MHz at X-band	3 GHz/ μ sec (10 MHz FM)	15 mW min.	Varian (Microwave Journal, 10/69)
Varactor	Avalanche	4.1-4.4 GHz	N/A	20 mW ± 0.5 dB	Sperry Rand (MIT, 1/70)

NOTE: These figures do not necessarily represent the state-of-the-art but are typical of what could presently be purchased.

interactions, etc. The independence of the oscillator and modulator(s) allows each circuit to be individually optimized or modified.

A major disadvantage of external modulation is loss of system efficiency. First, the direct attenuation of the microwave signal due to the modulators can cause unacceptable degradation of the signal-to-noise ratio. Second, pulse operation is inefficient since the oscillator runs continuously.

Modulation of Injection-Locking Signal

Frequency and phase modulation are both possible by applying the modulation to the locking signal of an injection-locked oscillator. Injection locking is a technique wherein a small signal injected into an oscillator determines, over a certain bandwidth, the frequency and phase of the oscillator output^[42-52]. A discussion of the technique and experimental results are given in the previous report^[5]. Although injection locking may be considered a form of amplification suitable for CW or FM signals, it can only be used to produce frequency or phase modulation, since any AM on the injection signal is directly converted to PM.

Adler's paper (1946) is commonly accepted as the basis of injection locking^[42]. A brief summary is given in Appendix B. Mackey extended Adler's theory to include the dynamic response of a locked oscillator to modulation of the locking signal^[53]. The

results apply to solid state oscillators, although originally directed to the klystron oscillator. A summary of Mackey's paper is included in Appendix B.

Injection-locking modulation combines some unique properties of its own with some of the desirable properties of external modulation. As with the latter, the separation of the oscillator and the modulated locking signal source allows the oscillator and modulator packages to be optimized separately. This does not imply that the injection modulation signal can be developed independently of the oscillator. The bandwidth of the modulated injection signal is restricted by the lock bandwidth of the oscillator and in general the oscillator and modulation signal would be designed to have compatible bandwidths. To obtain high modulation rates, therefore, the oscillator has to be designed for large lock bandwidths.

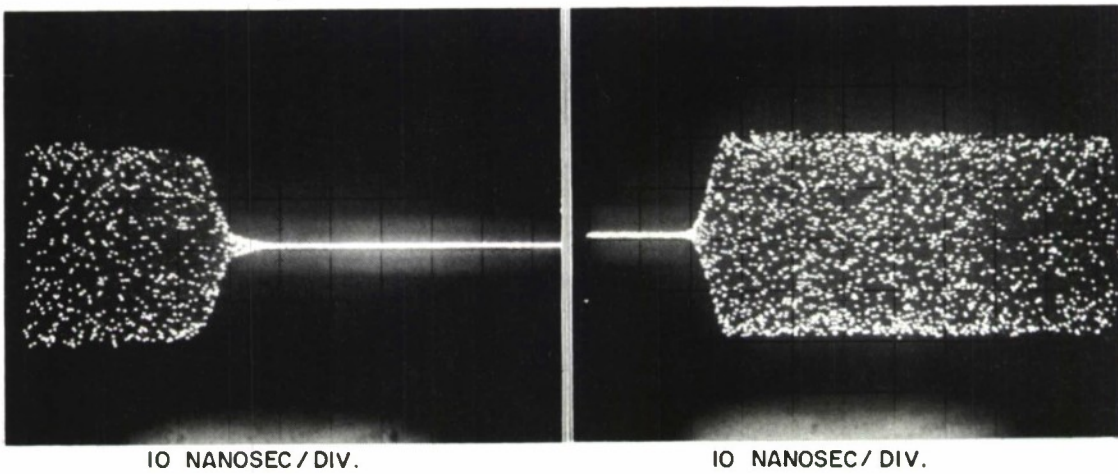
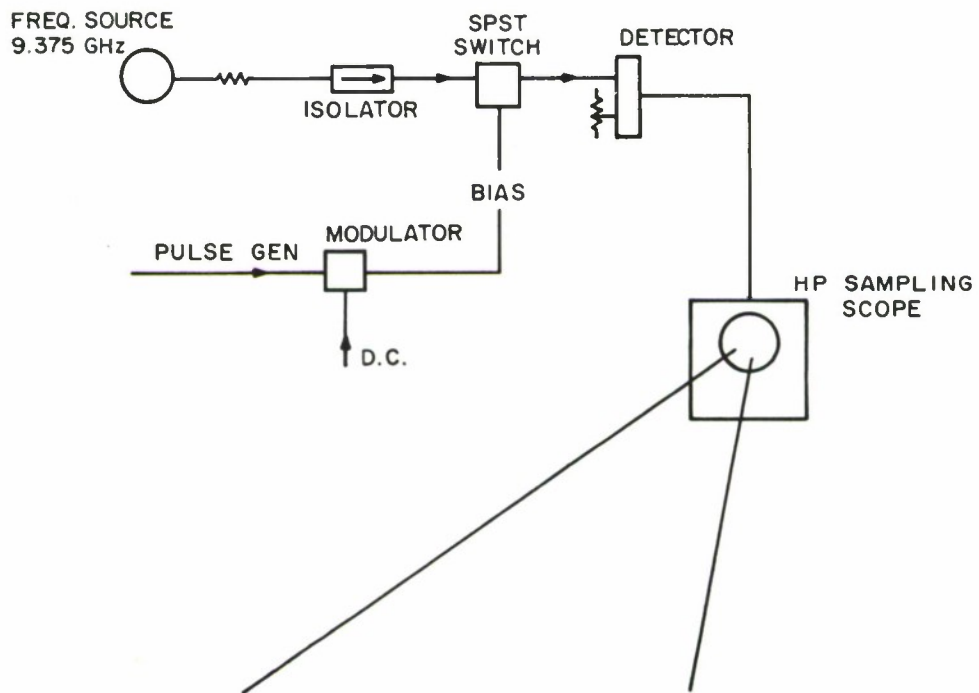
Experimental Work

The study was confined to establishing the characteristics of an avalanche diode oscillator when injection-locked by a modulated signal. Particular interest was centered around binary phase coding (BPC) in which area theoretical work has been carried out at MITRE. In particular, more knowledge was desired on the rates of frequency or PBC modulation which are possible in the injection-locked mode. This mode was chosen for its several advantages, and because the technique had been little discussed in the literature.

Measurements were made of the injection-locking characteristics of avalanche oscillators, using three types of input signal, as discussed in the following sections.

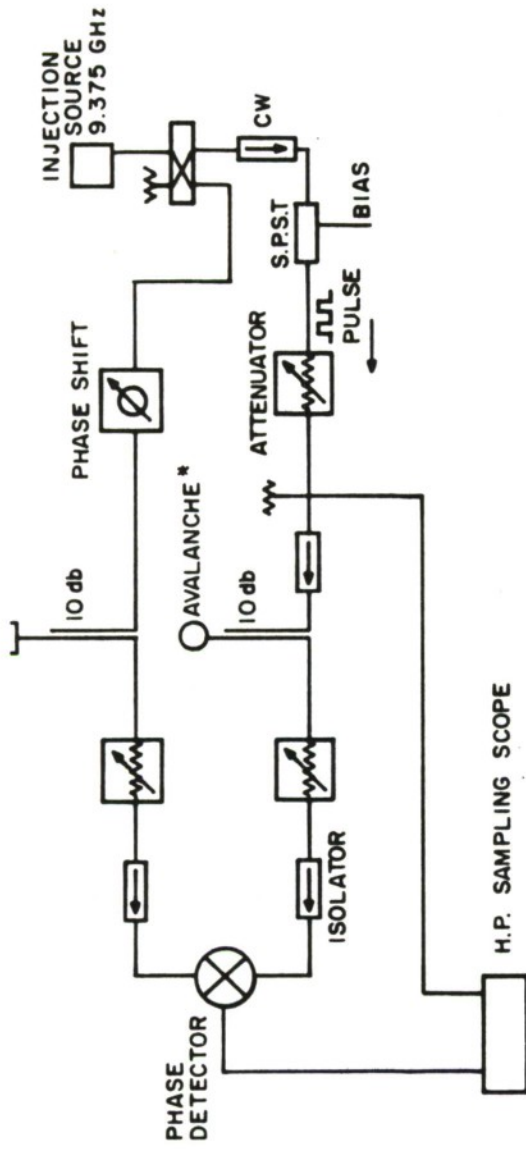
Pulse Modulated Injection Signal. The response time to acquire phase lock was measured using a pulsed injection signal. The experiments were made to verify Mackey's theory (Appendix B, Equation B-2) and to establish experimental techniques required for further work.

Figure 37 shows the test circuits used and also the rise and fall times of the injection pulse. The latter parameters were small enough (< 10 ns) to cause negligible experimental errors in the oscillator response times. This pulsed signal was then injected, using the circuit of Figure 38 into a Sylvania oscillator whose parameters have previously been measured and are listed in Table 7. The single-pole, single-throw switch shown in the diagram was used to pulse modulate the injection signal. This pulsed carrier was then injected into the avalanche oscillator and determined, within the lock range of the latter, the phase and frequency of the oscillator output. The relative phase shift between the oscillator output signal and the injection-locking signal was measured by means of a phase detector (mixer), whose output was proportional to the sine of the phase angle.



1A-32,679

Figure 37 SPST SWITCH RESPONSE TIME



* AVALANCHE OSC

SYLVANIA SYA 3200

FREQ x 9.375 GHz

POUT 14-15 MILLIWATTS

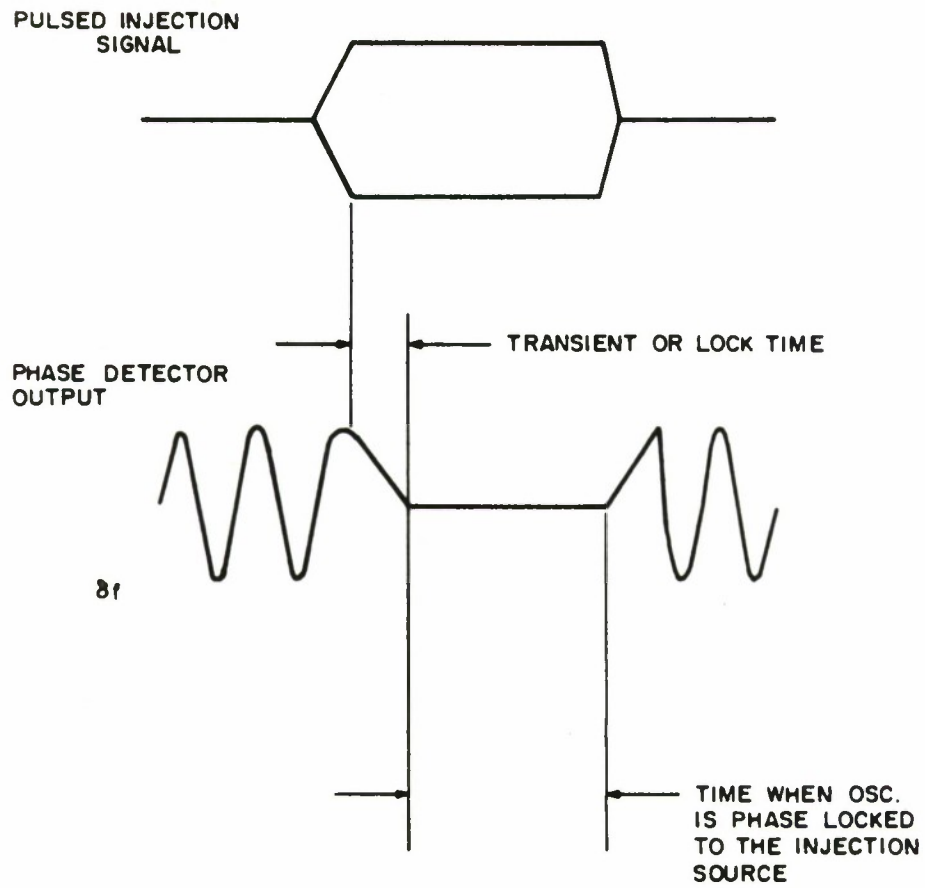
Figure 38 CIRCUIT FOR PULSE INJECTION LOCKING

TABLE 7

Sylvania Avalanche Oscillator SYA-3200

Frequency (f_o)	9.375 GHz
Power Output	\approx 14 - 15 mW
Efficiency	3.5%
Q_{ext}	32

Figure-39 shows a typical output expected from the phase detector and discusses the various parts of the waveform. With bias applied to the oscillator and the circuits adjusted for best operation, the phase detector output was recorded for various levels of injection signal (Figure-40). Using the parameters from Table 7 together with Adler's and Mackey's results, the curve of Figure-41 presents the interrelationships of response time, lock bandwidth, and injection ratio for this oscillator. The response time was obtained from Equation B-6 (Appendix B). Figure-41 is only applicable when the open loop frequency of the oscillator is approximately equal to the frequency of the injection source. The case was not considered for different frequencies, but Mackey does discuss this in his paper^[53]. In general the transient response varies as a function of the frequency difference. The measured transient or lock time (Figure-40) is recorded in Table 8 together

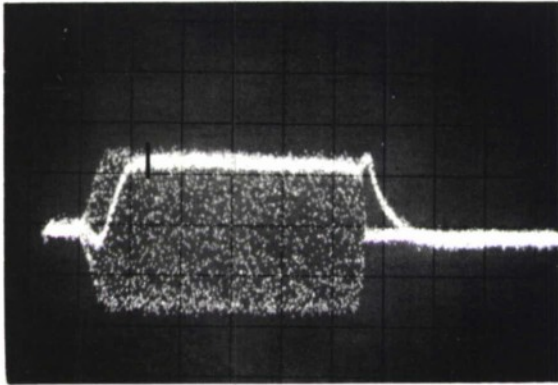


δf = OPEN LOOP FREQUENCY DIFFERENCE BETWEEN OSCILLATOR AND INJECTION SIGNALS.

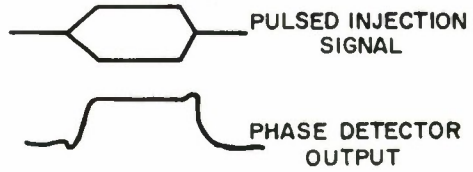
IA-32,702

Figure 39 TYPICAL OUTPUT FROM A PHASE DETECTOR FOR A PULSED INJECTION SIGNAL

VOLTS

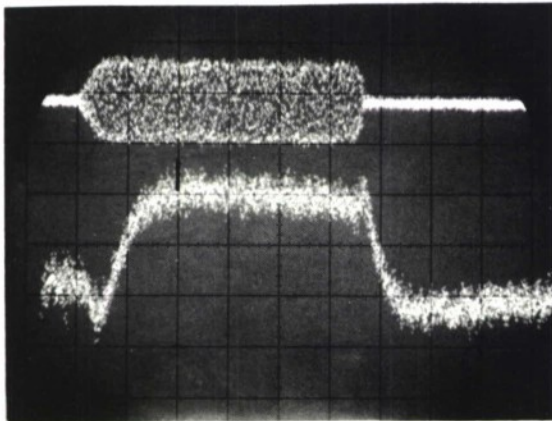


HOR : 20 NANOSEC / DIV.



INJECTION RATIO 9.3 db
 $f_{osc} - f_{lock} \approx \pm 100 \text{ Kc}$

VOLTS



HOR : 20 NANOSEC / DIV.

INJECTION RATIO 15.3 db
 $f_{osc} - f_{lock} \approx 100 \text{ Kc}$

1A-32,660

Figure 40 TRANSIENT RESPONSE AS A FUNCTION OF INJECTION SIGNAL

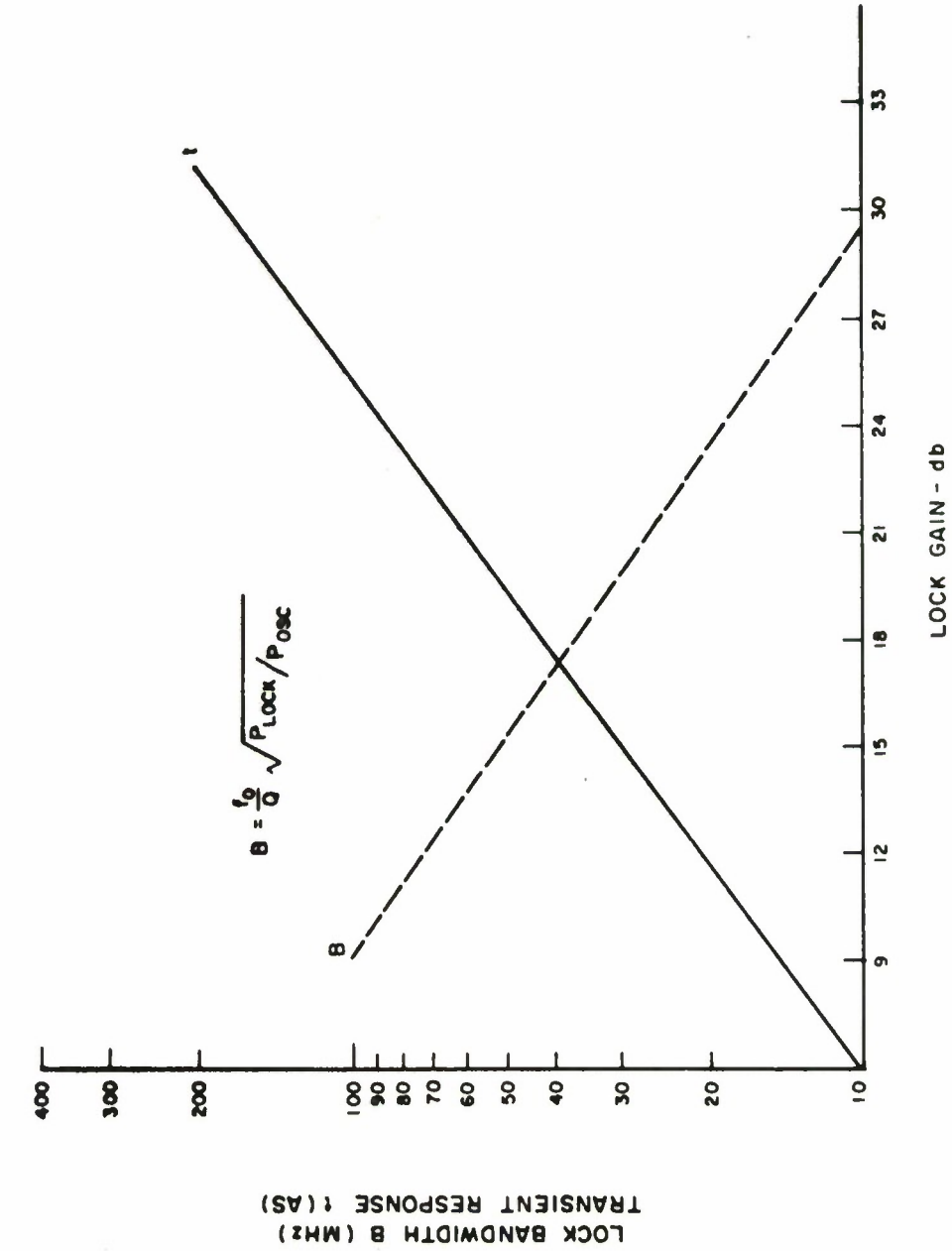


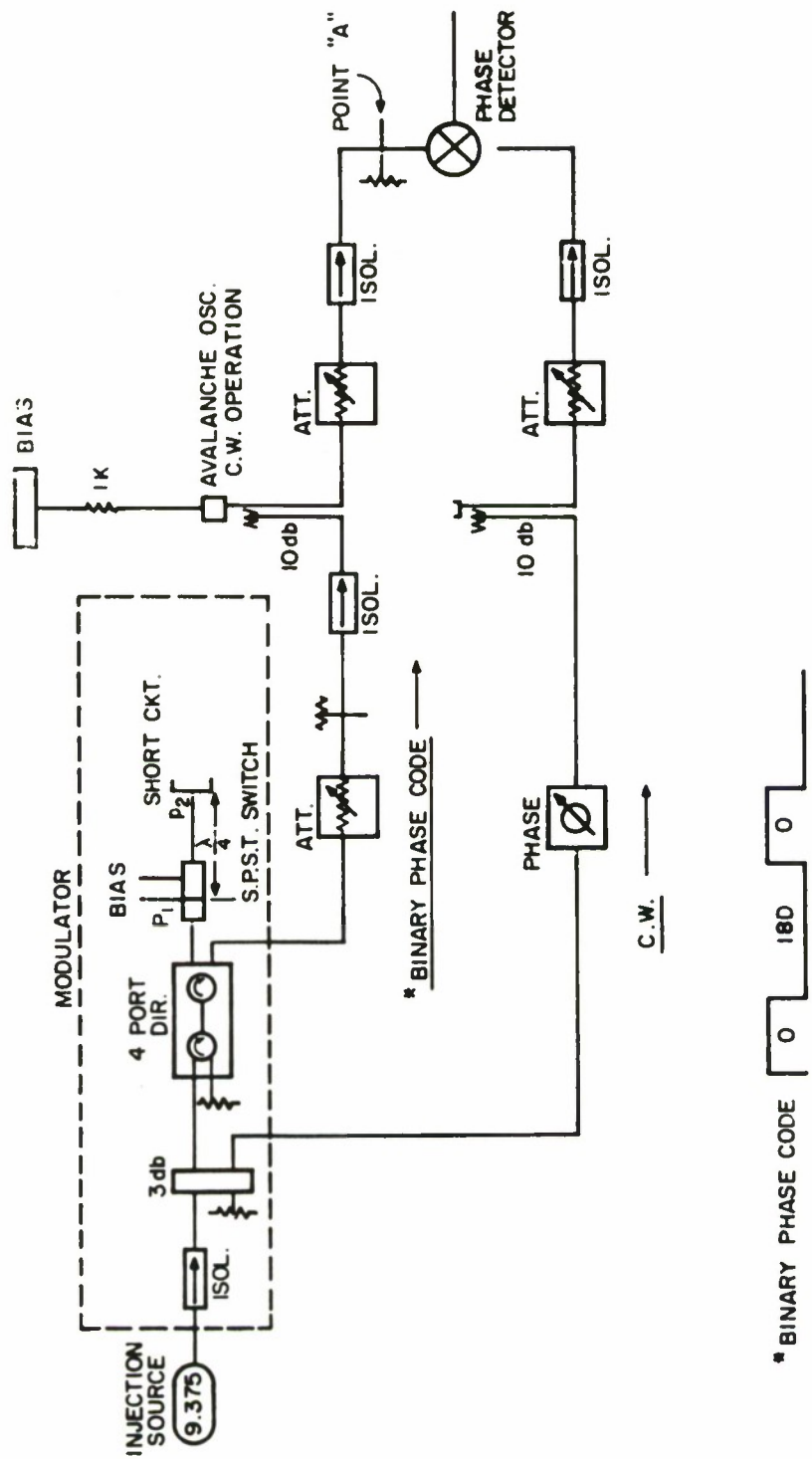
Figure 41 BANDWIDTH AND LOCK TIME VS LOCK GAIN FOR SYLVANIA AVALANCHE OSCILLATOR

IA-32,696

with the approximate response time estimated from Figure 41. Although the experimental data is approximate due to errors in time measurement, the correlation is satisfactory.

Binary Phase Coded (BPC) Injection Signal. The circuit of Figure 42 was used to produce binary phase coded modulation (phase $0 - \pi - 0 - \pi \dots$) of the injection-locking carrier. The code was generated by a digital phase modulator consisting of a ferrite circular and a SPST diode switch terminated by a short circuit. The short circuit position was chosen so that a quarter wave path length was produced between the internal short circuit plane of the switch when closed and the external terminating short circuit plane seen when the switch was opened.

A phase detector was used to measure the oscillator phase error relative to the unmodulated injection signal, after initial calibration. This calibration consisted of replacing the oscillator by a short circuit and minimizing the phase errors (indicated by the phase detector output) by adjusting the short circuit position in the phase modulator. These errors were recorded and found to be small. The phase errors were then measured when the oscillator (as used for the previous measurements) was placed in the circuit. Figure 43 shows the typical phase errors measured using binary phase code modulation. A cessation of oscillation for a short interval (< 20 ns) continually showed up throughout the measurements,



* BINARY PHASE CODE

Figure 42 MEASURING CIRCUIT FOR BINARY PHASE CODE MODULATION

TABLE 8

Oscillator Response Time to a Pulsed Injection Signal

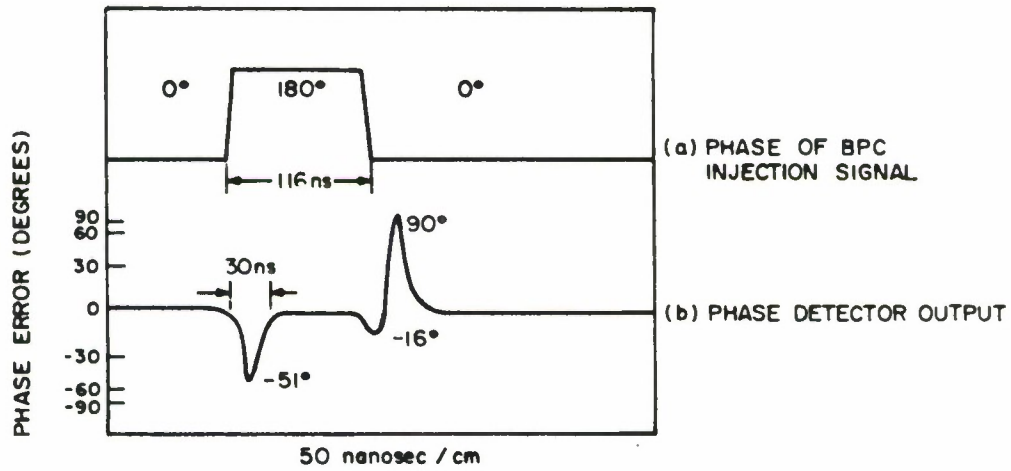
$\frac{P_{\text{lock}}}{P_{\text{osc}}}$ (db)	$ f_{\text{osc}} - f_{\text{lock}} $ (KHz)	Measured Transient Time (ns)	Calculated Transient Time (ns)
9.3	< 100	18	15
12.3	< 100	23	22
15.3	< 100	30	31
21.3	< 100	45	62

and its explanation is uncertain. This effect was independent of pulse width and PRF but was dependent on the degree of phase modulation, the injection ratio, and the difference between the frequencies of the unlocked oscillator and the locking source.

The measured transient response times, for a phase error of approximately 5 degrees, taken from data similar to that of Figure 43 is given in Table 9. The theoretical data, assuming a value of $\pi Bt = 5$ (Figure 41), is also given and again shows good correlation with the measured data.

An exact theoretical calculation of the oscillator response time based on Equation B-6 (Appendix B) taking into account the finite rise time of the injection signal is difficult. A numerical computer solution is straightforward, however. The lagging phase response of the locked oscillator during the input phase "rise time" was computed by approximating the injection signal phase "rise time" by a linear series of phase steps. At the end of this period, the oscillator response was then computed as a function of time. Figure 44 shows the computed oscillator response and also the input phase curve based on the measured data of Figure 40, where a linear phase "rise time" of 8 ns was assumed. For a lock gain of 15 dB, the transient time of 30 ns corresponds to a 5 degree phase error. This error falls to 1 degree in 40 ns.

The transient time clearly provides a limitation to the pulse bit rates which are practical using BPC modulation in an



TEST CONDITIONS :

INJECTION SIGNAL : BPC

INJECTION RATIO : 15 db

FOSC - FLOCK $\leq \pm 100$ KHz

1A-32,692

Figure 43 PHASE ERRORS OF IMPATT OSCILLATOR WITH BINARY PHASE CODED INJECTION SIGNAL

IA - 32, 694

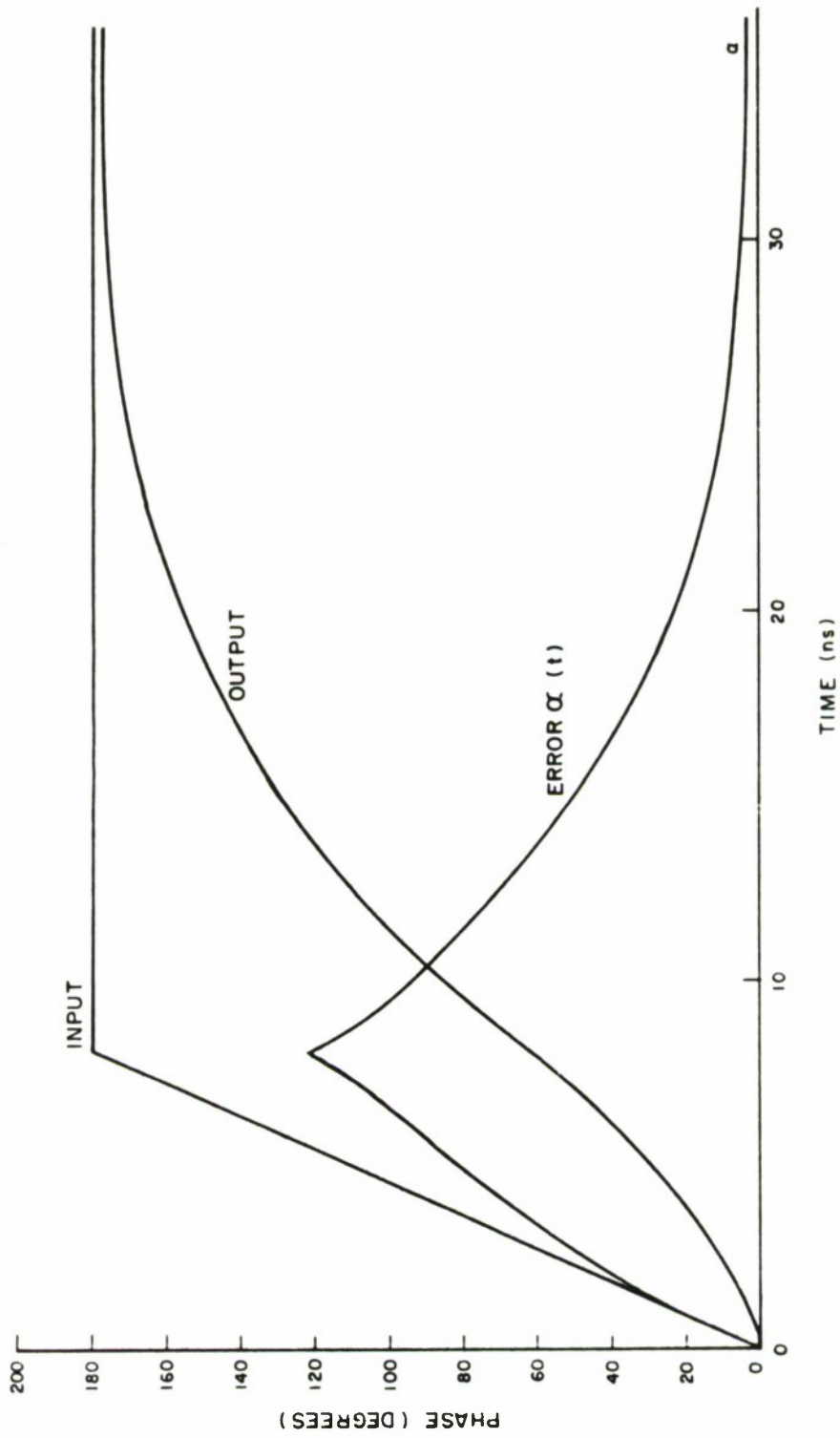


Figure 44 COMPUTED BPC OSCILLATOR RESPONSE

TABLE 9

Oscillator Response Time to a Binary Phase-Coded Signal

Lock Gain P_{osc}/P_{lock} (db)	$ f_{osc} - f_{lock} $ (KHz)	Measured Transient Time (ns)	Calculated Transient Time (ns)
15.1	< 100	30	31
22.6	< 100	70	80
28.6	< 100	115	116

injection-locked oscillator scheme. For high bit rates the locked oscillator requires correspondingly large lock bandwidths, which in turn require very low Q (tightly coupled) circuits and/or low lock gains. The problem is very similar to that of a final amplifier required to handle the high bandwidth of the BPC waveform. In either case, a tradeoff is required between a wideband locked oscillator (or amplifier) preceded by a relatively low power modulator on the one hand, and on the other hand, a narrowband locked oscillator followed by a higher power modulator. In the latter case the loss of the modulator (0.5 - 1.0 dB typ.) is also an important factor.

Frequency Modulated Injection Signal. The interest in this modulation technique was related to the use of linear FM ramp (chirp) waveforms and thus to the FM rate and distortion problems.

There is nothing to suggest that Mackey's theoretical limits, discussed earlier, for the case of discrete changes in the injection signal, would not also apply to a frequency modulated injection signal and thus provide a limit to the FM rate or modulation frequency.

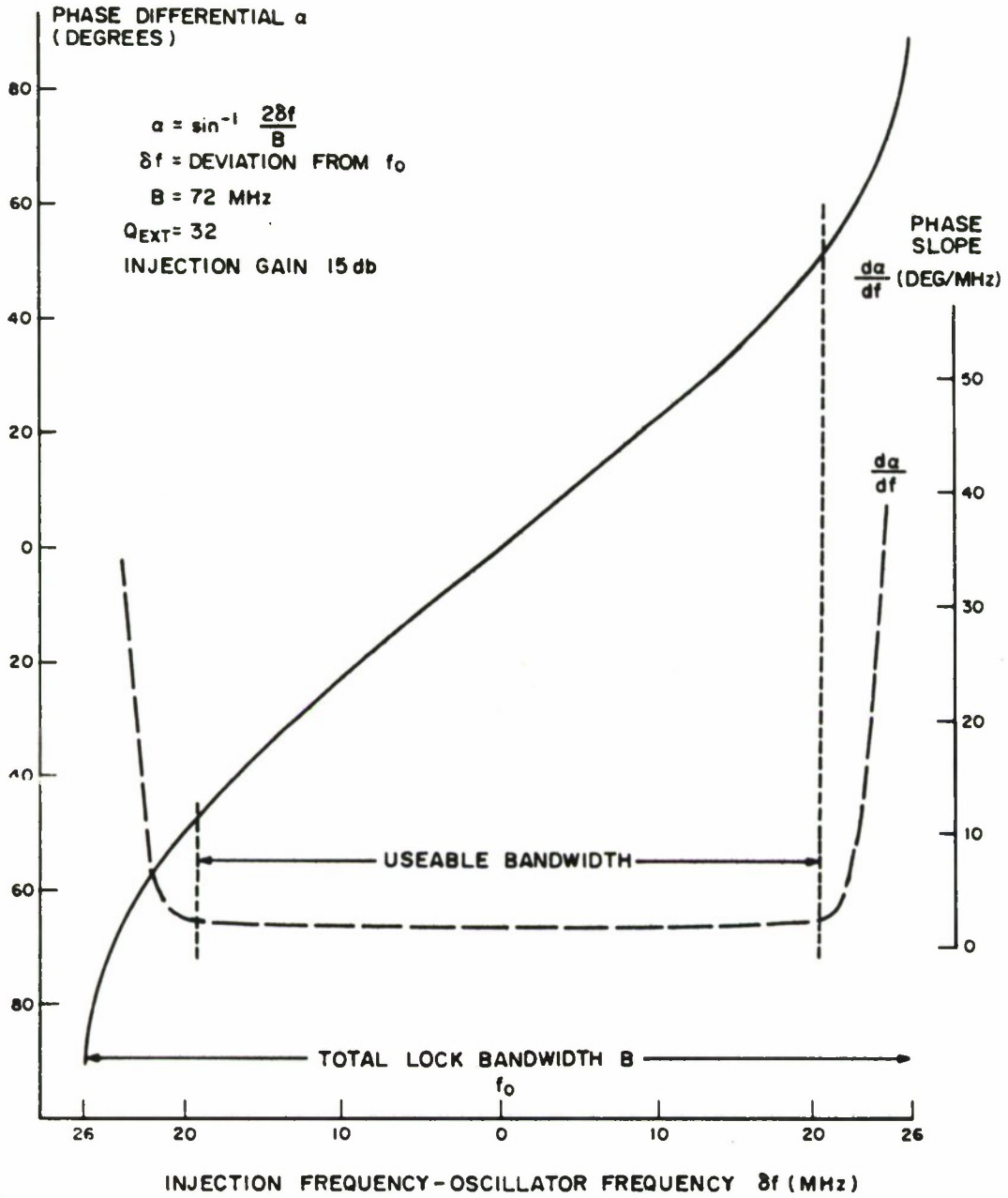
If distortion-free FM signals are desired, the compatibility of the FM signal deviation and bandwidth and the locking bandwidth have to be considered. The bandwidth of an FM wave is approximately twice the sum of the frequency deviation and the modulating frequency.

In order to avoid distortion, the circuits carrying the FM signals should be non-dispersive (linear phase vs. frequency). Figure 45 shows plots of phase and phase slope vs. frequency deviation calculated for the injection-locked Sylvania oscillator, for a fixed lock gain of 15 dB. The locking bandwidth B and hence the phase and phase slope are functions of the injection level (and gain), which therefore determines the usable bandwidth and the distortion.

Figure 45 indicates that as the limits to the locking bandwidth are approached, considerable distortion would occur due to the sinusoidal phase curve. The usable FM bandwidth would therefore be only about 70-80% of the locking bandwidth.

The objective of the experiments was to confirm the above relationships in a semi-quantitative manner. The measurements were made with a sinewave modulated injection signal using the circuit of Figure 46. The signal, obtained using the generator shown at the left, was used to phase lock the avalanche oscillator, and the FM oscillator output and FM injection signals were mixed in a phase detector (or demodulator), whose output was a measure of the phase modulation of the oscillator relative to the injection source.

An explanation of the electrical mechanisms involved is as follows. Since the oscillator was phase locked, the frequency modulation of the injection signal was transferred to the oscillator. Adler's Equation B-1 (Appendix B) shows that, in addition to the FM



IA-32,693

Figure 45 PHASE DIFFERENTIAL AND SLOPE VS
 FREQUENCY OF INJECTION SIGNAL

IA - 32,688

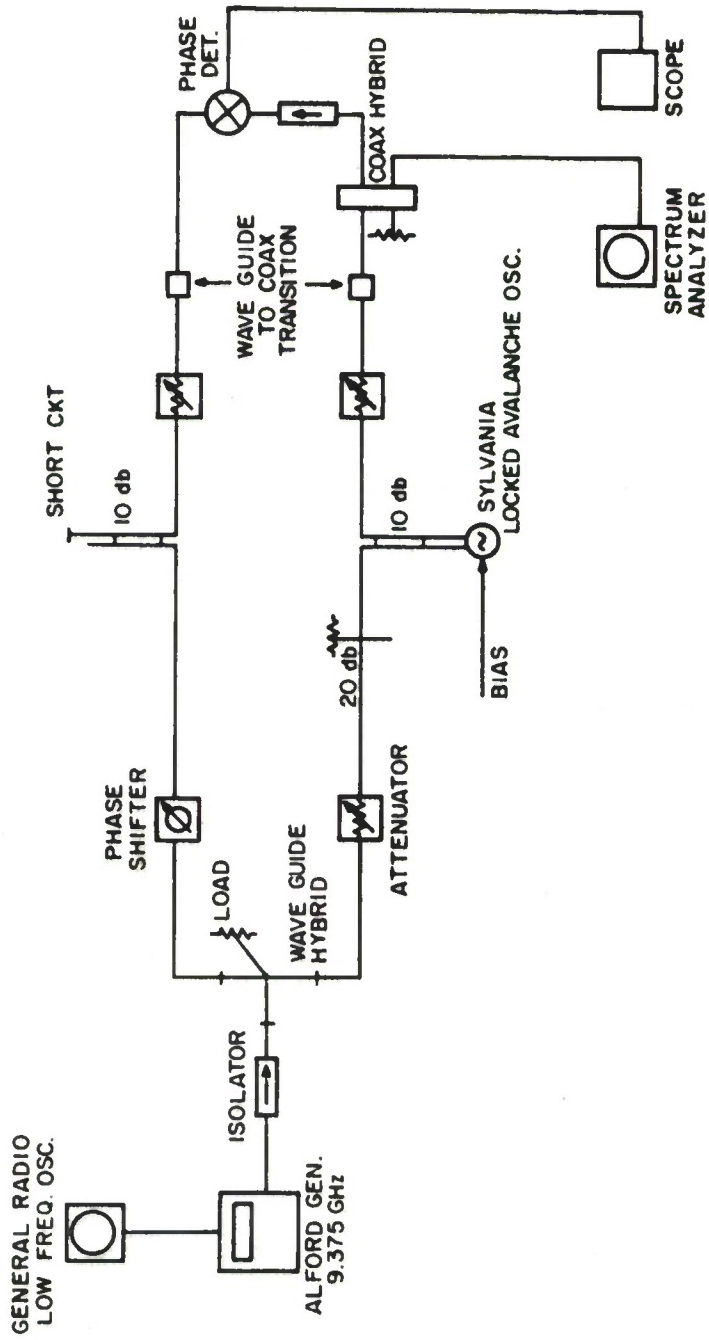


Figure 46 CIRCUIT FOR FREQUENCY MODULATION TESTS

signal forced on the avalanche oscillator, a phase-modulation modulation-distortion term is also produced, given by

$$\alpha(t) = \sin^{-1} \frac{2\delta f(t)}{B} ,$$

where the instantaneous frequency deviation is

$$\delta f(t) = \hat{\delta f} \sin 2\pi f_m t ,$$

giving

$$\alpha(t) = \sin^{-1} \left[\left(\frac{\hat{2\delta f}}{B} \right) \sin 2\pi f_m t \right] ,$$

where $\hat{\delta f}$ is the peak frequency deviation and f_m is the modulation frequency.

$\alpha(t)$ can be expressed as a power series,

$$\alpha(t) = \left(\frac{\hat{2\delta f}}{B} \right) \sin 2\pi f_m t + \frac{1}{6} \left(\frac{\hat{2\delta f}}{B} \right)^3 \sin^3 2\pi f_m t + \dots ,$$

where the distortion increases rapidly as $\left(\frac{\hat{2\delta f}}{B} \right)$ approaches unity.

This is also clear from inspection of Figure 45. The phase error results in an oscillator frequency error f_e , also expressible as a power series, or as an odd harmonic series with a main third harmonic term, of the form

$$f_e = \frac{1}{2\pi} \frac{d\alpha}{dt} = a \sin 2\pi f_m t + b \sin 2\pi (3 f_m) t + \dots$$

For $\left(\frac{2\hat{\delta}f}{B}\right)$ less than 1/2, for example, the third harmonic frequency error is below 1/2% and f_e merely contributes a phase shift to the resultant FM signal.

The above effects were confirmed qualitatively by the experimental measurements. Distortion was measured by observing the change in level of the modulation sidebands as the lock bandwidth was reduced as a result of reducing the injection level (i.e., increasing the lock gain). The limits indicated in Figure 45 corresponded experimentally with a threshold above which the distortion increased seriously. Measurements were made with modulation frequencies up to 8 MHz, which was the limit of the test modulator. The maximum modulation frequency f_m allowable before distortion becomes significant, is hard to express analytically, but a conservative value is given [52] by setting half the modulation period equal to the transient response time (Figure 41). Pull-in can be shown to be essentially complete at a time equal to the reciprocal lock bandwidth

$$t \sim \frac{1}{B} = \frac{QB}{f} . \quad (5)$$

The maximum modulation frequency is then conservatively

$$\hat{f}_m \sim \frac{1}{2t} = \frac{B}{2} . \quad (6)$$

Above this frequency the distortion smoothly increases. Under the experimental conditions used, with $Q = 32$, $f = 9.375$ GHz, $\beta = 15$ dB and $t = 30$ ns (Table 8), the upper frequency limit is $f_m \sim 16$ MHz.

Microstrip Antennas. The extension of the photolithographic technique used for thin film microstrip circuits to include the radiating elements of a system appears an obvious one. If the primary pattern of a dipole is suitable for a given system, for example, in phased array systems or anywhere when a narrow primary beamwidth is not required, a photolithographed dipole can be made integral with the associated microstrip circuits. The principal advantages are cost savings, reproducibility, and ease of integration with associated circuits. The advantages are probably the most fully realized at the higher microwave frequencies, for example, X-band, where the coaxial-fed, fabricated dipole is typically expensive to make. The use of the technique is not new, however, and has been applied to phased-array systems.

Design Basis

The design of a microstrip antenna can be broken down into two parts; the radiating element, and the matching and transition section.

Two versions of a dipole radiating element were developed with different dipole taper angles θ (Figure 47), to determine the effect on bandwidth and radiation patterns. The models, having tapers of 1.4 deg. and 19 deg., are shown in Figures 48 and 49, respectively,

and are referred to as the "T" dipole and the "bow tie" antennas.

The equivalent circuit of the antenna and matching section is given in Figure-50. The dipole impedance is given by

$$Z_d = R_r + R_l + j X_d,$$

where R_r = antenna radiation resistance

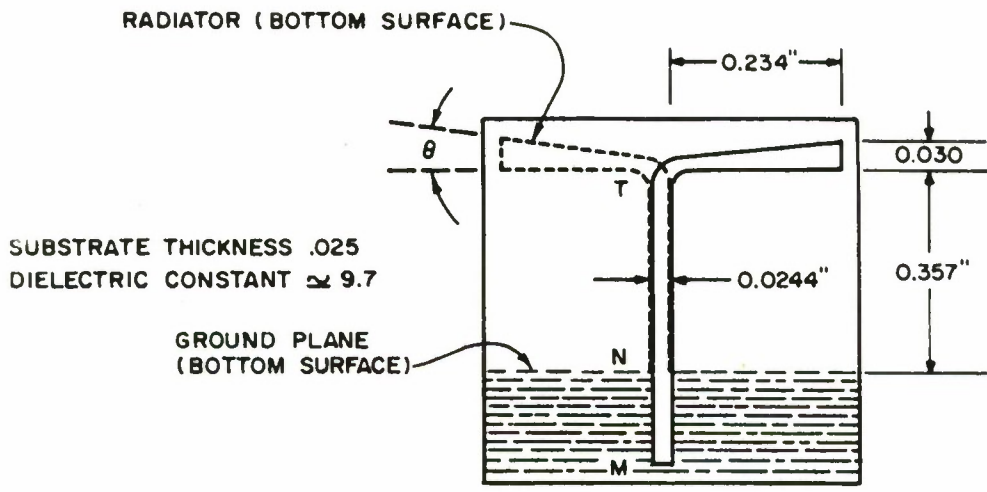
R_l = antenna loss resistance

jX_d = antenna reactance due to self and mutual impedances and reactive end-effects (fringing).

The unbalanced to balanced impedance matching transformer used for the experiments consisted of a simple three-quarter wavelength section of balanced microstrip transmission line connecting the standard 50 ohm microstrip feed circuit to the balanced dipole. The transformer section ideally transforms the termination impedance Z_d to give an input impedance Z_i of

$$Z_i = Z_t^2 / Z_d, \quad (7)$$

where Z_t is the characteristic impedance of the balanced section. It can be seen from the symmetry of the mechanical structure and electric field of the unbalanced line (Figure-51), that a hypothetical ground plane could be placed at XX without disturbing the field. The impedance for substrate thickness h is therefore equal to twice the value for unbalanced microstrip of half the thickness $h/2$.



IA-32,691

Figure 47 MICROSTRIP T-DIPOLE ON ALUMINA SUBSTRATE

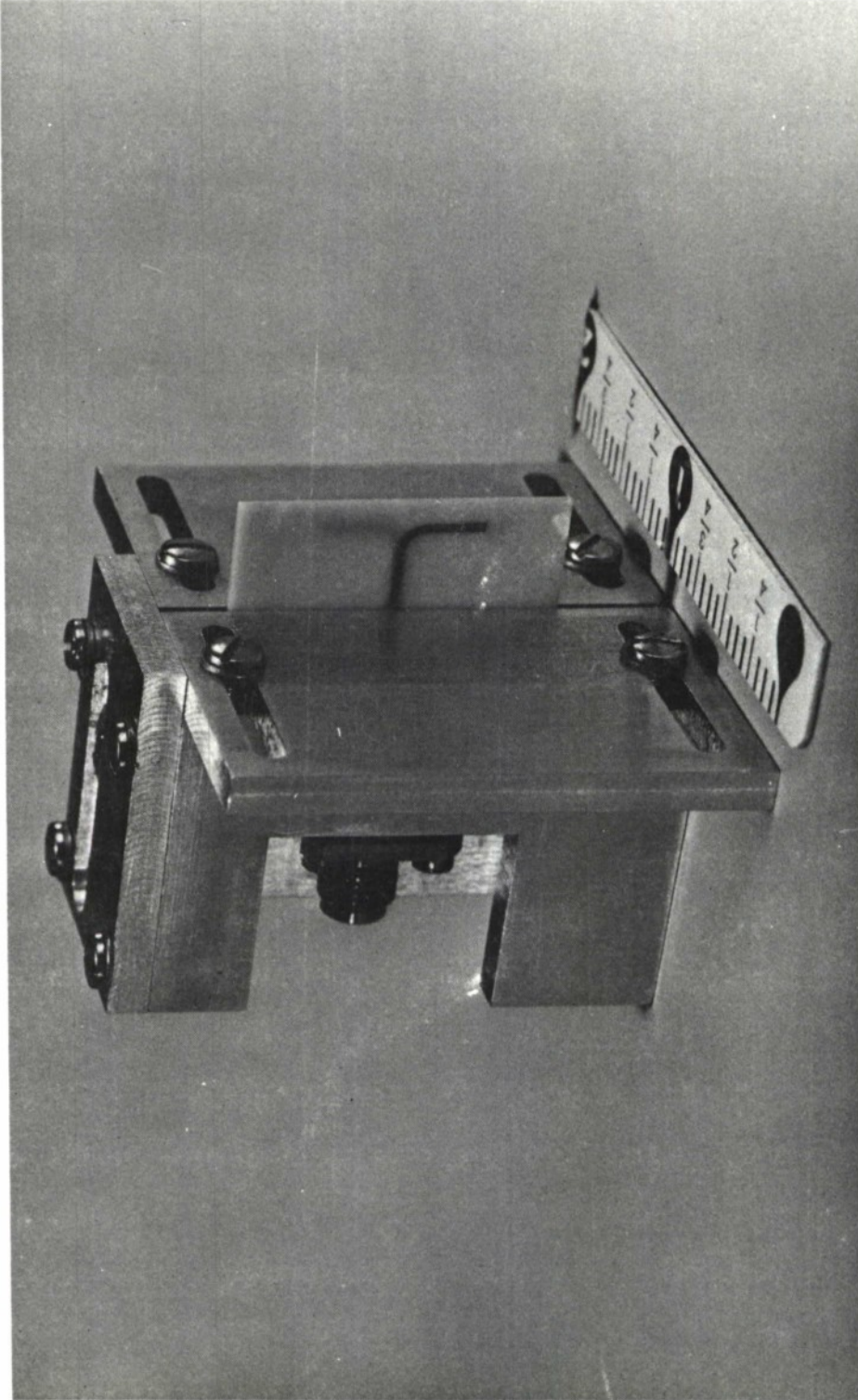


Figure 48 - Microstrip T-Dipole

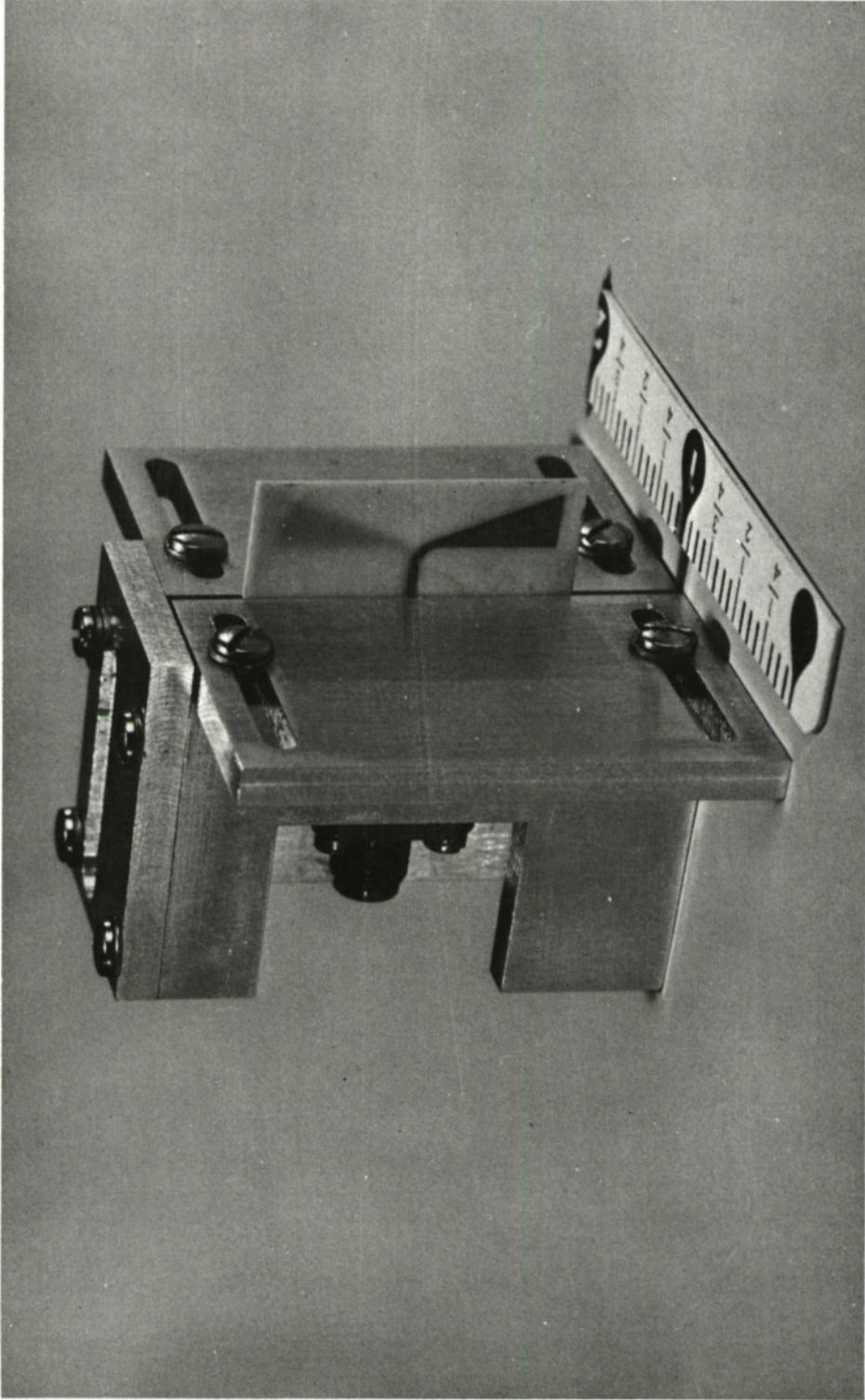


Figure 49 - "Bow Tie" Microstrip Dipole

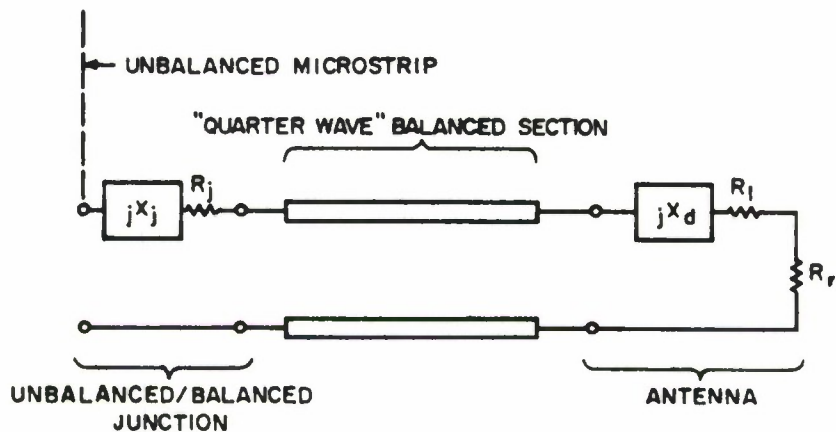


Figure 50 EQUIVALENT CIRCUIT OF DIPOLE AND MATCHING SECTION

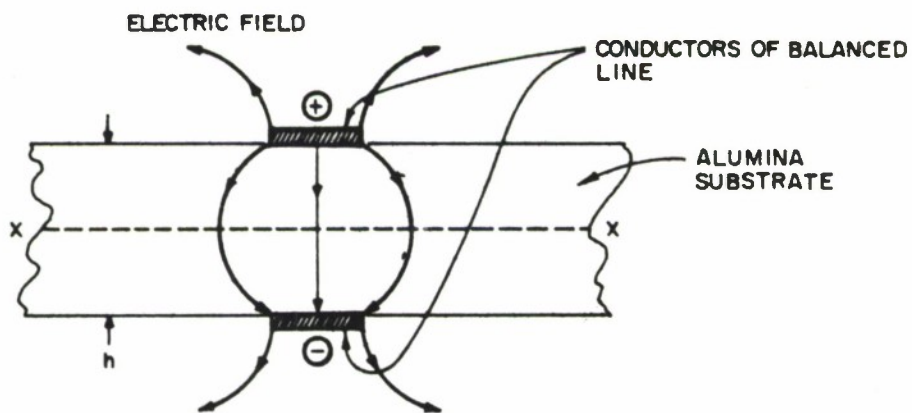


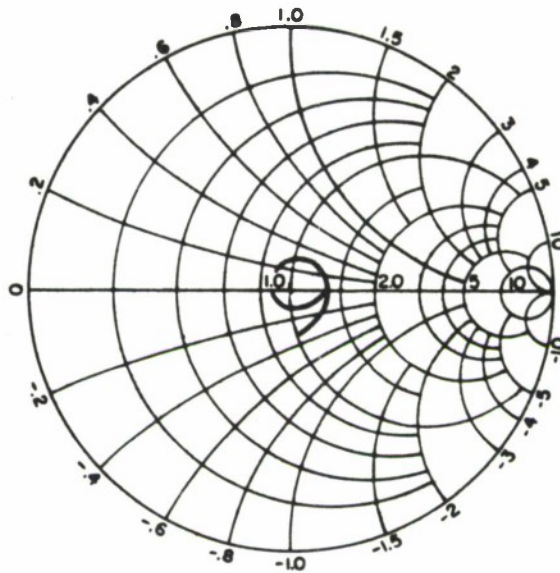
Figure 51 EQUIVALENCES BETWEEN BALANCED AND UNBALANCED MICROSTRIP LINES

1A-32,689

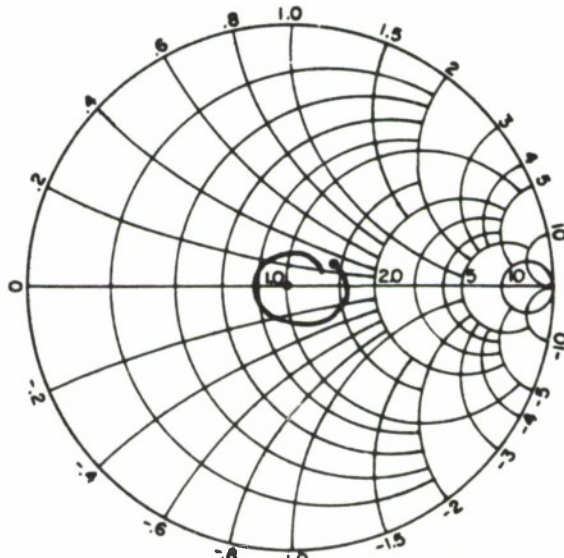
Since the effective dielectric constant for the dipole element was unknown, in view of the complicated electric field pattern, the resonant length was determined experimentally at 9375 MHz. The optimum length was $.372 \lambda_0$, for free space wavelength $\lambda_0 = 3.2$ cm. On the basis of a half-wave dipole an effective dielectric constant of 1.8 was thus derived for the dipole section. To match the dipole impedance, whose radiation resistance R_r is typically 73 ohms, to a 50 ohm source, the transformer impedance Z_t should ideally be 60.4 ohms, from Equation (7). In the test models (Figure-47), section MN was 50 ohm microstrip. Section NT was the balanced line transformer, whose length of $3/4$ wavelength and impedance of approximately 66 ohms were based on the effective dielectric constant and wavelength of half-height unbalanced microstrip^[54-56].

Results

The results of swept-frequency tests on the T-dipole antenna feed line using a tapered load to terminate sections MN or MNT (Figure-47) are shown in Figure-52. The VSWR of 1.08 midband (1.41 max.) for section MN (Figure 52-a) is partly due to the input coaxial MIC section (VSWR 1.1 to 1.15) and the test load (VSWR 1.05). The increase of VSWR for section MNT to 1.24 midband (1.53 max.) (Figure 52-b) is due mainly to the impedance discontinuity at N, due to the impedance change and parasitic junction impedance (Figure 50).



SMITH CHART SCALE, VSWR 1 TO INFINITY
 a) SECTION MN (TERMINATED), 8.5-10.2 GHz
 MEASURED VSWR 1.08 TO 1.41 ± .05



SCALE SAME AS (a)
 b) SECTION MNT (TERMINATED), 8.5 - 10.2 GHz
 MEASURED VSWR 1.24 TO 1.53 ± .05

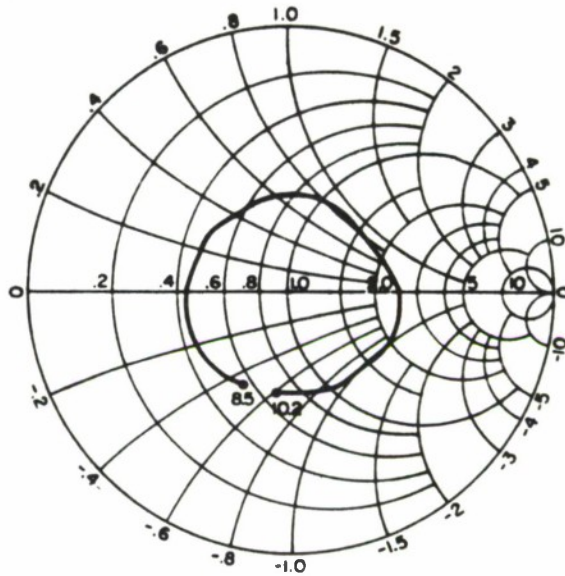
1A-32,675

Figure 52 IMPEDANCE OF T-DIPOLE CONNECTING SECTIONS

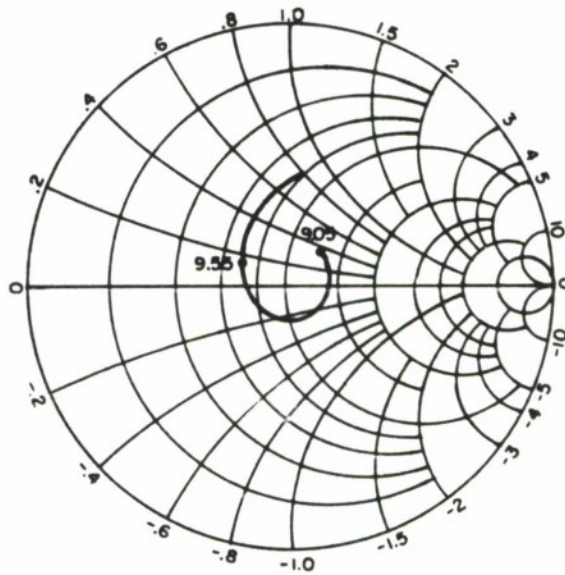
Figure 53-a shows the input impedance of the dipole and transformer section over the range 8.5 to 10.2 GHz. Although a good broadband match might require a complicated compensating network, a stub of normalized reactance $-j 0.4$ placed in section MN (Figure-46) could reduce the average VSWR to approximately 1.5 over the band 9.3 to 9.6 GHz. The tuning capacitance providing this reactance was achieved by placing thin mylar spacers between the conductors of the balanced line and the ground plane reflector plates. The dipole-to-ground spacing was fixed in the position of maximum antenna gain (approximately a quarter free-space wavelength). With the antenna so assembled (Figure-48) the input impedance (Figure-53-b) had a VSWR under 1.5 over 5% bandwidth and 1.2 over 3% bandwidth.

Radiation patterns of the above antenna were measured at 9.4 GHz. The E and H plane patterns shown in Figures 54 and 55 have half power beamwidths of 87 degrees and 114 degrees respectively. A slight skewing of the E plane pattern is attributed to possibly unequal currents in the radiating elements due to an imperfectly balanced feed, and possible radiation from the junction of the input microstrip and the transforming section. If true, the introduction of a better balun network in the feed line would be expected to eliminate the skewing. The antenna gain at 9.4 GHz was 6.7 dB.

The gain was within 0.1 dB of a matched traditional slot-fed coaxial dipole with reflector (Figure-6) as used in the array model.



SMITH CHART SCALE, VSWR 1 TO INFINITY
 a) UNMATCHED, 8.5 - 10.2 GHz



b) MATCHED, WITH REFLECTOR PLATE, 9.0 - 9.8 GHz

IA-32,676

Figure 53 IMPEDANCE OF T-DIPOLE ANTENNA

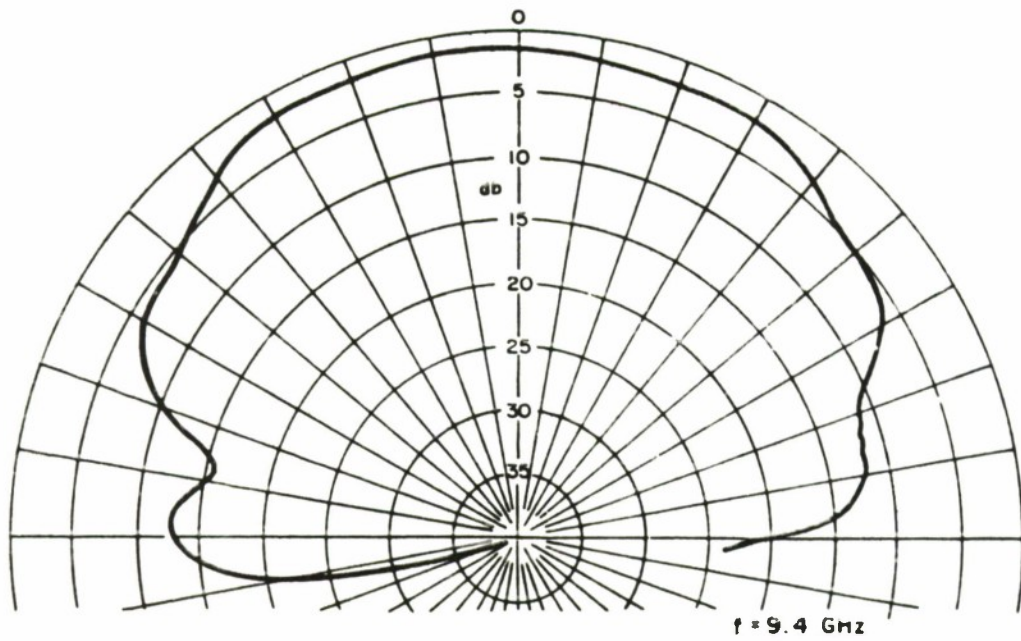
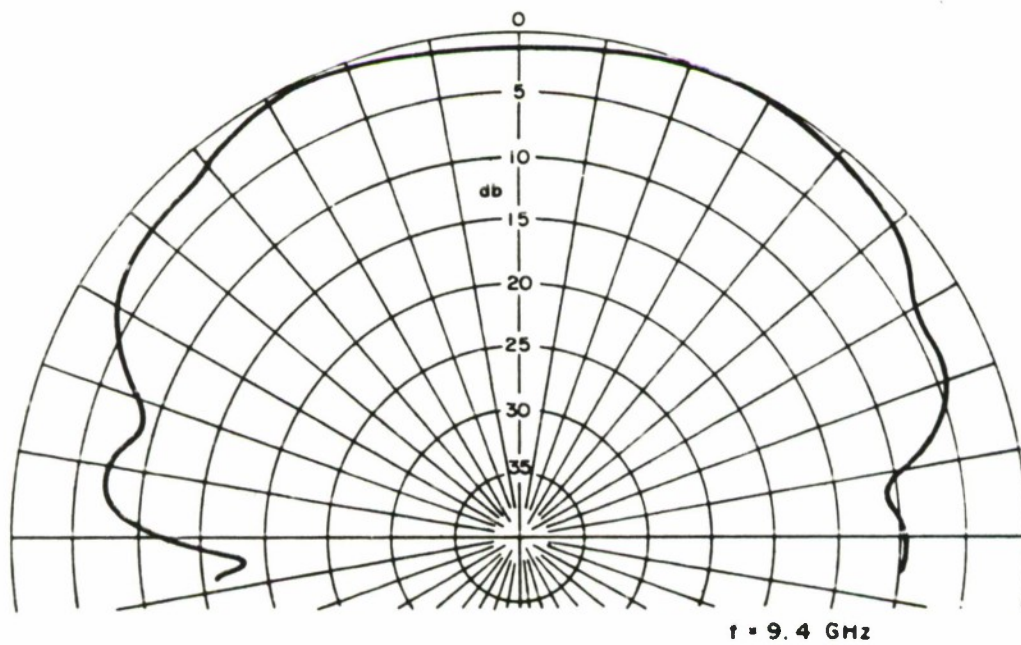


Figure 54 E PLANE RADIATION PATTERN OF T-DIPOLE WITH GROUND PLANE



IB-32,706

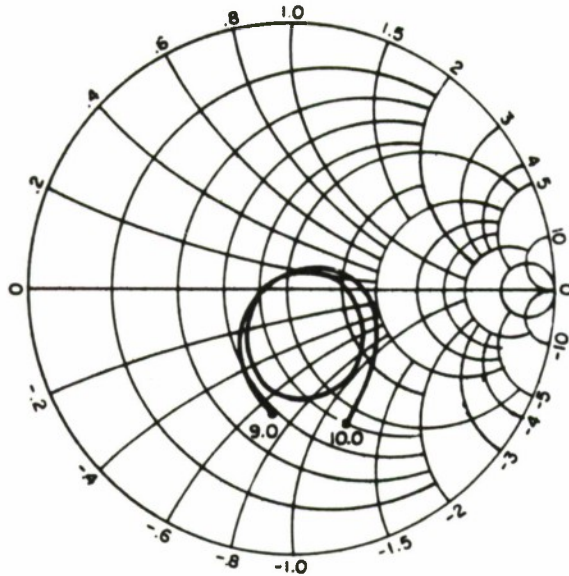
Figure 55 H PLANE RADIATION PATTERN OF T-DIPOLE WITH GROUND PLANE

The efficiency of the microstrip dipole is thus within the normal range of acceptance. Radiation patterns of the coaxial dipole were given in an earlier section (Figures-14 and 15).

The almost linear elements of the T dipole were replaced by 19 deg. tapered sections in a "bow tie" antenna (Figure-49) to check the effects on bandwidth and beamwidth. Figure-56 shows the input impedance measured, using the same matching procedure as the T-dipole. The VSWR was under 1.6 over 7% bandwidth, showing a slight improvement. Radiation patterns were measured at 9.2 GHz (Figures-57 and 58). The beamwidths in the E and H planes were 48 and 87 degrees respectively, markedly narrower than those of the T-dipole antenna. The gain increased by 2.6 dB to 9.4 dB at 9.2 GHz, and correlates with the reduction of beamwidth.

MIC TRANSMITTING MODULE

Several MIC components developed or evaluated in the course of this program were integrated to form a simple integrated transmitting module (Figure-3). This unit was equivalent to and may be compared with the MIC-coaxial module used in the array (Figure-2) employing coaxial forms of dipole, cavity oscillator, and connectors. The integrated module incorporated the 170 mW MIC avalanche oscillator and the MIC dipole antenna described earlier in this report. The circulator was orientated to provide double isolation (30-40 dB) between the oscillator and the antenna (see discussion in Appendix A).



FREQUENCY 9.0 - 10.0 GHz

IA-32,678

Figure 56 INPUT IMPEDANCE OF "BOW TIE" DIPOLE WITH GROUND PLANE

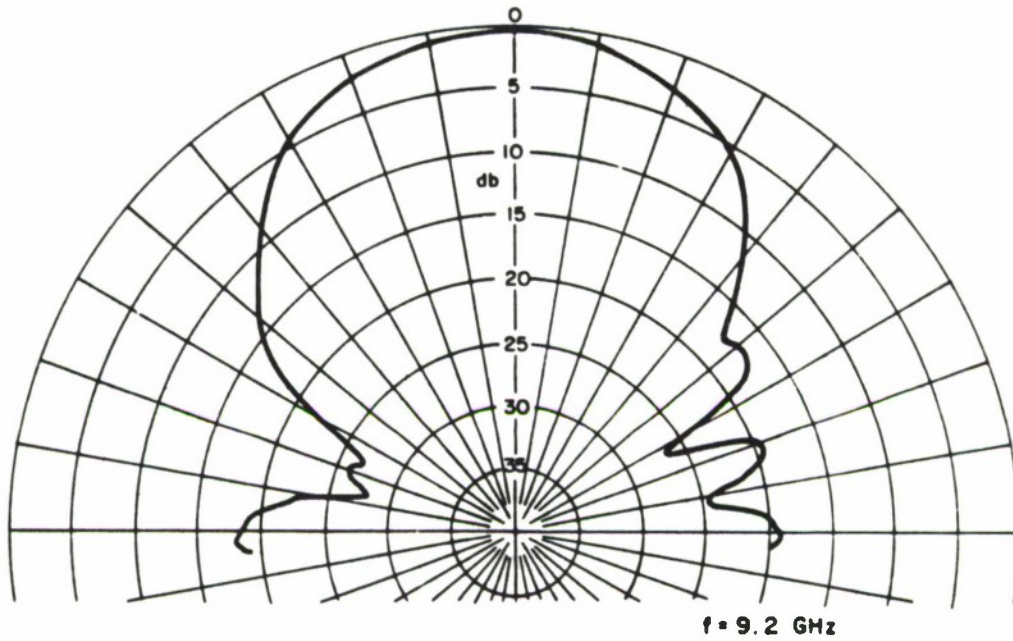


Figure 57 E PLANE RADIATION PATTERN OF "BOW TIE" DIPOLE WITH GROUND PLANE

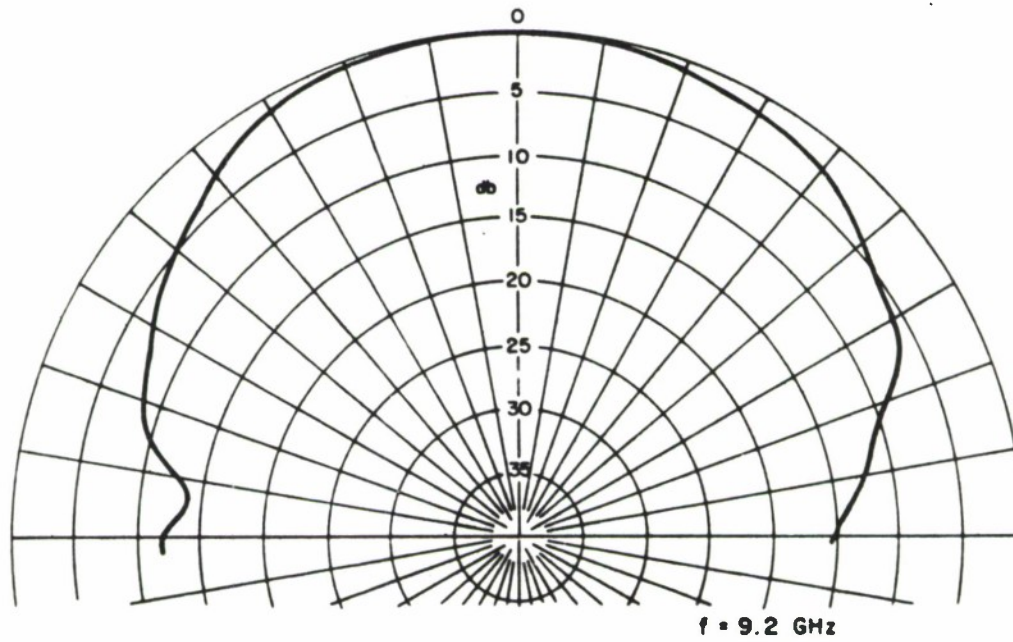


Figure 58 H PLANE RADIATION PATTERN OF "BOW TIE" DIPOLE WITH GROUND PLANE

IB-32,709

Overall performance measurements of the module were not made but individual component characteristics are reported in this and the previous report [5].

The integrated module illustrates some of the advantages of microwave integrated circuit construction techniques. The overall reduction in size and weight and the mechanical simplifications of the housings required and the reduction of interconnectors are clearly evident. The improvement of electrical performance that can result is not so obvious. The reduction of interconnector discontinuities and connecting lengths between subcomponents can result in improved bandwidths and reduced losses. Reduced phase and amplitude errors can also result from improved impedance matching. The use of separately fabricated sub-components does not usually involve any penalty, since almost reflection-free connections can be made, and this approach has possible advantages in flexibility of design, cost reduction and replacement of faulty or superseded sub-components.

MIC QUALITY MEASUREMENTS

A number of difficulties were experienced in obtaining satisfactory MIC plated alumina substrates from commercial sources. Tolerances for nominal one inch square plates of substrate thickness $25 \pm .3$ mils and surface roughness 2 or 10 micro-inches were acceptable. Plate dimensional tolerances were in some cases too

large ($1 \pm .005$ inch squares) to allow accurate alignment of abutting components and this tolerance also made mask alignment difficult in some cases. Separate abutting MIC components are desirable in some applications where replacement costs are reduced by separating components most liable to failure (those containing diodes and capacitors and assembled by hybrid fabrication). The procedure adopted was to specify $\pm .002$ inch tolerance on the long dimensions and to accept an arbitrary size of substrate (.985 inch square) due to the cutting procedure.

The adhesion of chromium-gold plating on polished substrates (2 micro-inches finish) from one vendor gave particular trouble and the need for an adequate testing procedure and specification of adhesion became apparent. A 5-10 micro-inch specification of substrate surface finish was finally used, and resulted in excellent adhesion. The latter was considered to be much more important than the slight decrease of loss associated with a finer surface finish.

The lack of electrical quality control by substrate vendors and manufacturers and the lack of agreement on measurements present problems in MIC design and production. Companies involved in component system design, and manufacture have to provide as many of the fabrication processes as possible to ensure reliability and consistency, apart from the question of economics. A common procedure is to purchase and evaluate sufficiently large batches of unplated alumina substrates to allow a program to be successfully completed.

The basic parameters necessary for MIC design are the wavelength (determined by effective dielectric constant) and the line loss at a specified impedance and frequency. These are directly determined from measurements of the bandwidth and resonant frequency of MIC resonators of known dimensions. Suitable techniques have been developed, some of which have been verified and used in our studies. The wavelength λ' in a microstrip circuit is proportional to the velocity v' of propagation along the circuit, i.e.,

$$\lambda' = v'/f.$$

For a uniform medium, the velocity is inversely proportional to the square root of the dielectric constant k , i.e.,

$$v = \frac{c}{\sqrt{k}},$$

where c is the velocity of light. For microstrip, which is a mixed medium (i.e., air with $k = 1$ and alumina with $k \approx 9.7$), either the velocity v' or an "effective dielectric constant" k' is calculated from the measurements of length and frequency and used as a basis for subsequent calculations of wavelength, using the relationships

$$v' = \frac{c}{\sqrt{k'}}$$

$$\lambda' = \frac{v'}{f} = \frac{c}{f\sqrt{k'}} = \frac{\lambda_0}{\sqrt{k'}},$$

where λ_0 is the free space wavelength.

Derivation of effective dielectric constant and loss from measurements of ring resonators^[57] has been found to be a reasonably satisfactory technique. Figure 59 shows a typical resonator and Table 10 lists the measured parameters for an unenclosed unit.

The excitation and propagation of surface waves on microstrip have been shown to become very troublesome at high frequencies. At X-band, these parasitic waves can produce spurious resonances, circuit coupling, increased loss, radiation and wavelength changes if allowed to propagate^[58]. The usual solution is to enclose the circuits in boxes small enough to prevent propagation of these waves. This unfortunately restricts the space available for the circuit layout, and can present problems. Surface wave effects with the ring resonators are small, however. The change of loss and the small change of effective dielectric constant with frequency verify this fact.

In comparison, the radiation and surface wave effects at X-band can be very serious with unenclosed, open-circuited straight resonators^[59]. For example, 50 ohm resonators spaced by ten line widths at X-band coupled strongly. Table 11 shows typical measured parameters for an unenclosed resonator made from a straight section of line and for one enclosed in a circular waveguide beyond cutoff. The Q values may be compared only qualitatively for the two types of resonators, since the sample/sample parameter variations are unknown

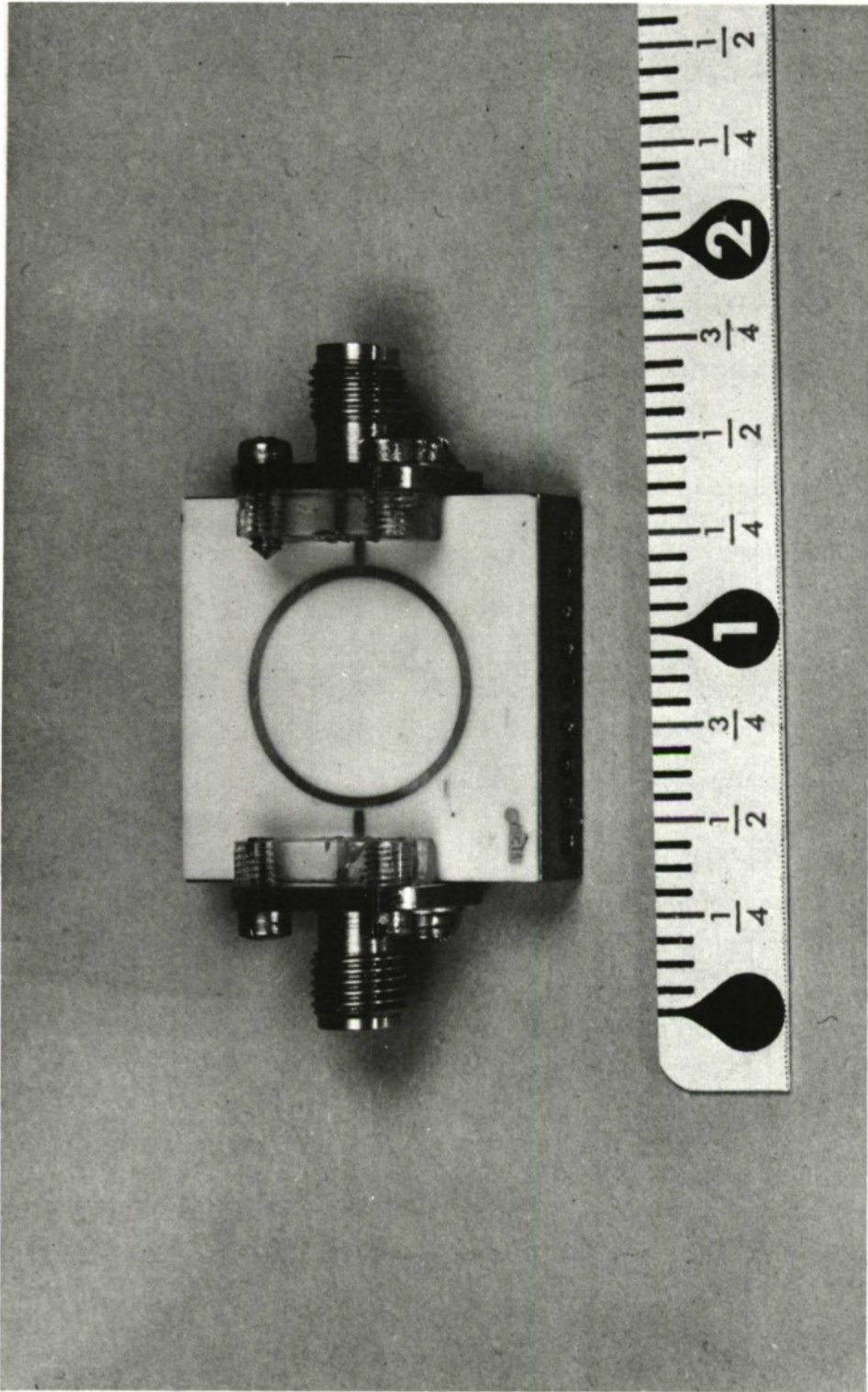


Figure 59 - Microstrip Ring Resonator

TABLE 10

Measurements on Two Ring Resonators

<u>Mode</u>	<u>f GHz</u>	<u>Unloaded Q</u>		<u>Eff. Diel. Const.</u>		<u>Loss/Inch (dB)</u>		<u>Length</u>
		<u>A</u>	<u>B</u>	<u>A</u>	<u>B</u>	<u>A</u>	<u>B</u>	
1	7.283/4	205	200	6.71	6.71	.21	.22	$3\lambda/2$
2	9.638/9	322	306	6.81	6.81	.18	.19	2λ
3	11.948/9	408	382	6.93	6.93	.18	.19	$5\lambda/2$

and the mounting configuration sometimes had a considerable effect on the Q's of the open-ended straight resonators. Mode 1, Table 11 corresponds to Mode 2, Table 10. The comparison shows the ring resonator to have a 12% higher Q. The Q of the straight resonator, Mode 1, rose by 51% when enclosed, demonstrating the large amount of radiation.

TABLE 11

Measurements on Linear Resonators

<u>Mode</u>	<u>Unloaded Q</u>		<u>Length</u>
	<u>Unenclosed</u>	<u>Enclosed</u>	
1	268	404	λ
2	350	424	$3\lambda/2$

APPENDIX A

MUTUAL COUPLING OF ANTENNA ELEMENTS

The effect of mutual coupling between elements together with the isolation (reverse coupling) of the circulators is to introduce a leakage signal into each oscillator (Figure 11). This signal is the combination of all the inter-element couplings and can be represented by a matrix including all the mutual couplings. The first-order effect is seen by considering only the coupling S_1 between adjacent elements, the circulator reverse coupling S_2 , and the oscillator voltage "gain" β (ratio of output to input locking voltages). The leakage signal δE is then

$$\delta E = K E_\ell e^{j\theta}, \quad (\text{A-1})$$

where E_ℓ is the locking voltage from the power divider and

$$K e^{j\theta} = \beta S_1 S_2 \quad (\text{A-2})$$

is the overall coupling factor between the inputs of adjacent oscillators and θ is determined by the circuit path lengths and antenna configuration. The modified locking voltage $E_\ell' = E_\ell + \delta E$ for a differential phase shift ϕ between elements is then (Figure 60)

$$\begin{aligned} E_\ell' &\simeq E_\ell + (E_\ell e^{-j\phi}) K e^{j\theta} + (E_\ell e^{j\phi}) K e^{j\theta}, \\ \text{i.e.,} \quad E_\ell' &\simeq E_\ell (1 + 2 K \cos \phi e^{j\theta}). \end{aligned} \quad (\text{A-3})$$

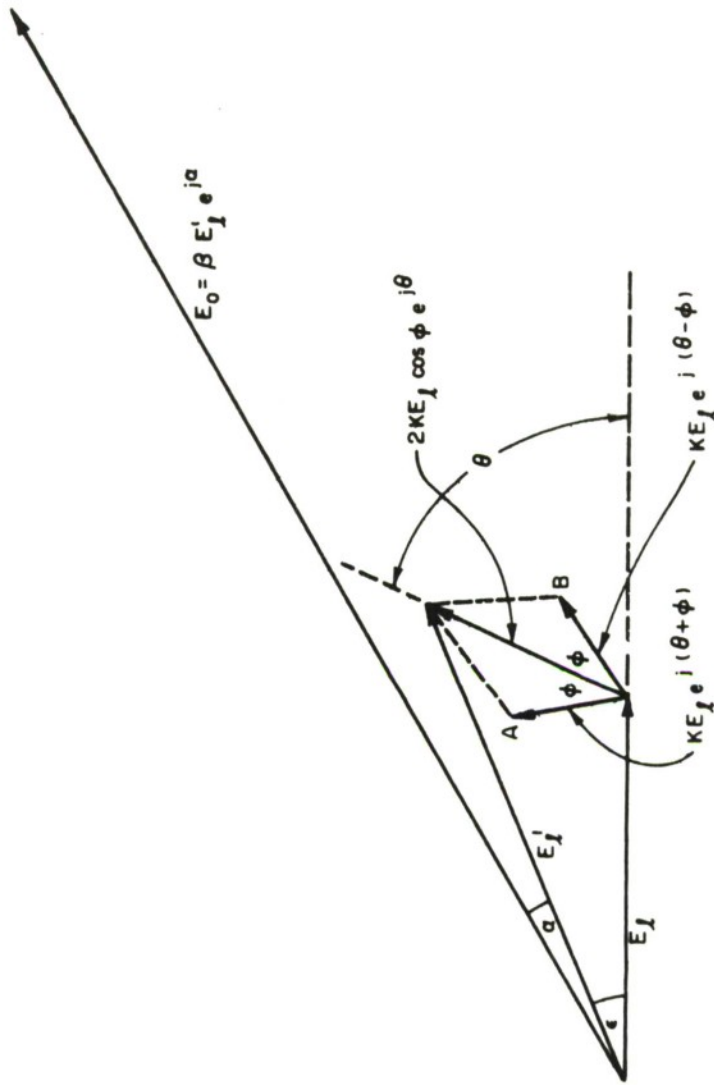
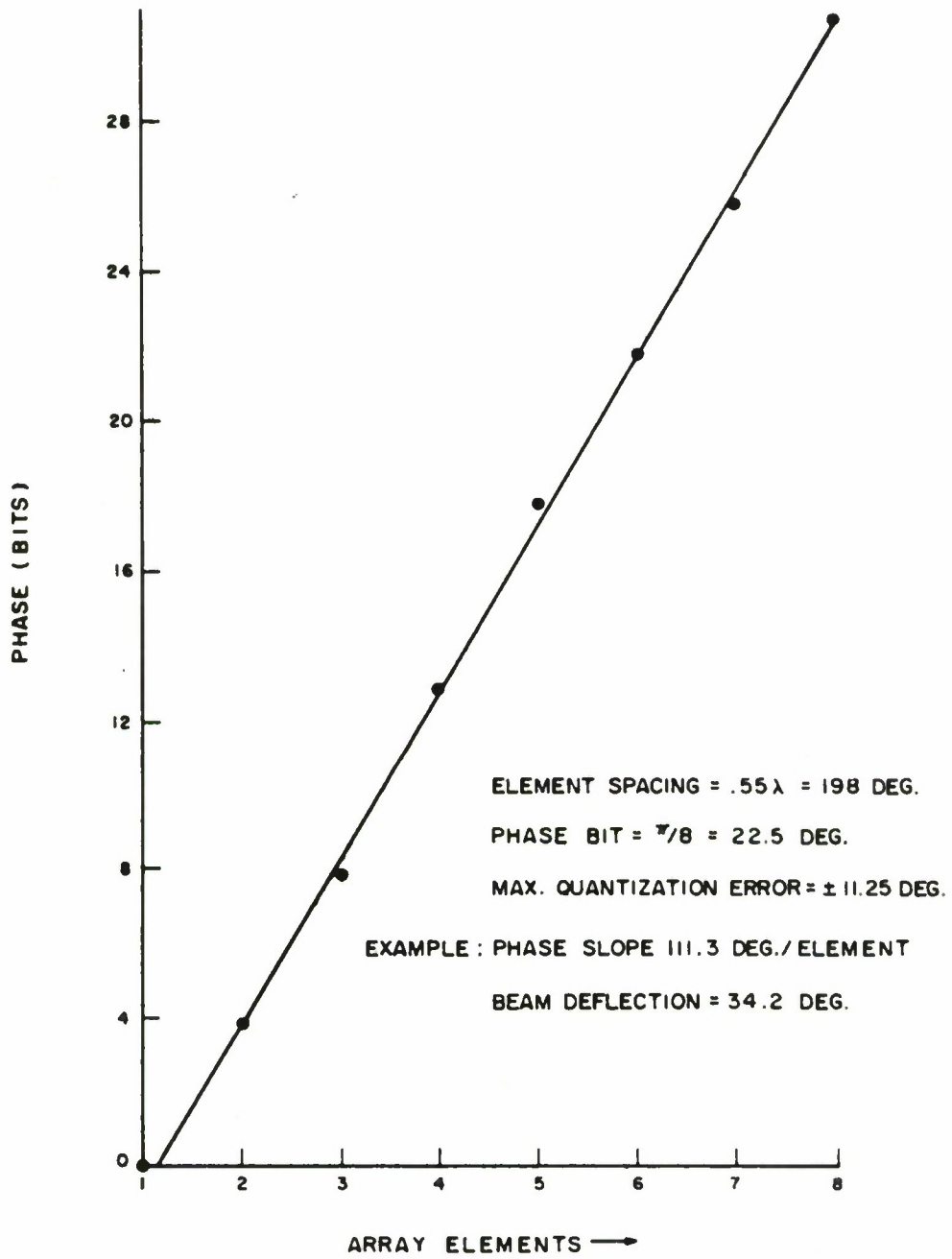


Figure 60 PHASE ERRORS IN INJECTION LOCKED OSCILLATOR

An absolute phase error ϵ can thus be produced in the output of each oscillator, relative to the locking voltage E_L . The phase error is given by

$$\begin{aligned} \epsilon &= \tan^{-1} \frac{2 K \cos \phi \sin \theta}{2 K \cos \phi \cos \theta} \end{aligned} \quad (\text{A-4})$$

and has a maximum value of $2 K$ for small K . An important point is that this absolute error is ideally (large array approximation) the same for all elements in an array since each element is ideally in the same situation. There is therefore no error in the differential phase and the resulting array radiation pattern in this case. However, there will be errors in practice since the phase increments between elements are not uniform, due to the phase steps having to approximate the uniform phase slope across the array required for a specified beam deflection. There will also be errors due to variations between components. Figures 61 and 62 show an example, illustrating the fact that the phase error due to the above mechanism may be small but not negligible. In this example there is an error of ± 11.25 deg. in half the elements (Figure 61). For element #2 with a four-unit (90°) phase differential relative to adjacent elements, the interfering phasors A and B (Figure 62-a) are seen to cancel, giving zero absolute phase error ϵ . For element #4, however, with a five-unit (112.5°) phase differential, A and B no longer cancel (Figure 62-b) and an error of a few degrees could arise. For example, the



1A-32,690

Figure 61 POSSIBLE FIT TO PHASE CURVE

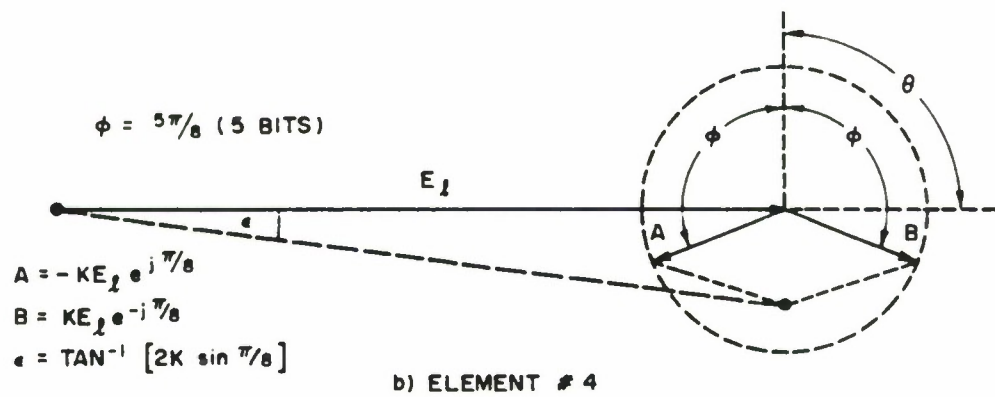
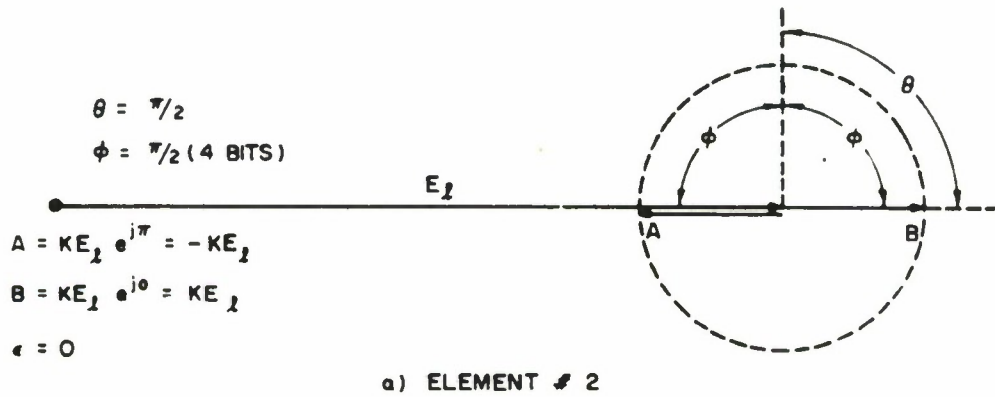


Figure 62 EFFECT OF NON-UNIFORM PHASE STEPS

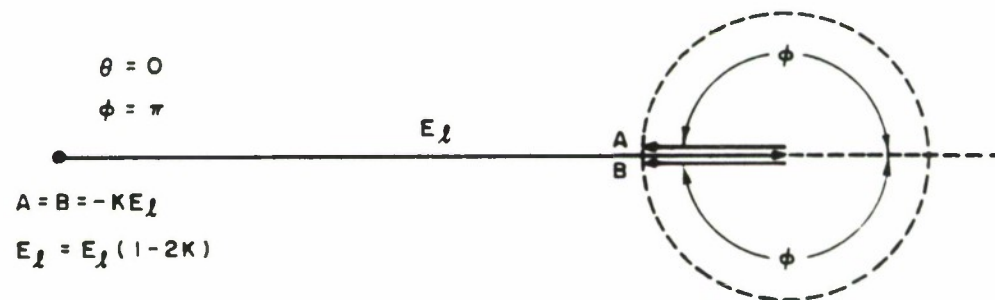


Figure 63 ANTIPHASE LEAKAGE SIGNALS

IA-32,686

parameters initially obtained in the array were $\beta = 10$, $S_1 = .16$ (16 dB antenna coupling), $S_2 = .18$ (15 dB min. circulator isolation), giving $K = .29$ and an error of 3 deg. This example is merely intended to illustrate that small but significant relative phase errors can arise, and can possibly be evaluated for specific systems. For a narrow band system, it may be possible to adjust the path lengths to give a value of coupling phase θ which minimizes the errors due to the mutual couplings. In the array model, where the circulators had inadequate isolation, and the absolute phase error was excessive, the expedient was taken of reducing the mutual coupling by incorporating baffles as described elsewhere in this report. This approach would almost certainly not be taken in a real system, where better circulators (triple circulators if necessary) would be used and baffles might be impractical.

A further phase error can result from the dependence of the phase-lock error α on the injection level E_λ . Simplifying Equation (B-4), Appendix B, for small α ,

$$\alpha = 2 Q \frac{E_o}{E_\lambda} \cdot \frac{\delta f}{f} \text{ radians,} \quad (\text{A-5})$$

where E_o , E_λ are the oscillator and lock signal voltages and the other symbols are defined in Appendix B. If the phase of the leakage signals is such that E_λ is changed by $\Delta E_\lambda = \pm 2 K E_\lambda$ (Figure 63),

then α will be changed by $\Delta\alpha$, where, from Equation (A-5),

$$\frac{\Delta\alpha}{\alpha} \approx - \frac{\Delta E_{\ell}}{E_{\ell}} \approx \pm 2 K . \quad (\text{A-6})$$

For example, taking the bad case of $K = .29$ as before, with possible values of $Q = 30$, $\Delta f = \pm 3$ MHz, $\beta = E_o/E_{\ell} = 10$, $f_o = 9$ GHz; then $\alpha = \pm 12$ deg., $\Delta E_{\ell}/E_{\ell} = \pm .58$ and $\Delta\alpha = \pm 7$ deg. These errors are reduced by ensuring low values of loaded Q , locking gain and open loop frequency error. The latter necessitates the use of a temperature-compensated and/or temperature-controlled oscillator to stabilize the frequency to within about 1 part in 10^4 .

The tolerable peak phase error can only be specified in terms of the error distribution across the array and the sidelobe criteria for the array radiation pattern. The phase error curve along the array can be broken down into its sinusoidal Fourier components. Each component, having a peak phase deviation ϕ_n , produces a pair of sidelobes in the radiation pattern whose separation increases with the number of cycles of the phase error component across the array and whose amplitude is $\phi_n/2$ (for small angles in radians). For example, the error curve for Figure 61 is a triangular spatial waveform with a peak value of half a bit (.2 radian). The fundamental sine wave component has a peak value of .16 radian giving sidebands of .08 (-22 dB). In practice, such periodic errors would be avoided by adding randomness to the selection of the phase increments.

APPENDIX B

PHASE-CODED INJECTION-LOCKED OSCILLATOR

Adler's basic equation for the injection-locked oscillator^[34] relates the phase difference α between the locking signal of the frequency f_l and power P_l , and the locked oscillator signal of unlocked frequency f_o and power P_o ,

$$\alpha = \sin^{-1} \frac{2\delta f}{B}, \quad (\text{B-1})$$

where δf is the unlocked frequency difference

$$\delta f = f_o - f_l,$$

and B is the lock bandwidth of the oscillator, given by

$$B = \frac{f}{Q} \sqrt{\frac{P_l}{P_o}}. \quad (\text{B-2})$$

This can also be expressed as

$$B = \frac{f}{Q\beta}, \quad (\text{B-3})$$

where β is the lock gain of the oscillator

$$\beta = \sqrt{\frac{P_o}{P_l}}.$$

The phase error can also be expressed as

$$\alpha = \sin^{-1} \left[\left(\frac{2Q\beta}{f} \right) \delta f \right], \quad (\text{B-4})$$

where Q , β , f are nominally fixed design parameters. Equation (B-4) shows that for small phase error, the circuit requirements are

low Q (tight coupling between oscillator and load), low lock gain, and a small percentage unlocked frequency difference. The latter implies the use of temperature compensation or control. The problems of achieving these requirements raise the question of the alternative use of a wideband amplifier and the appropriate tradeoffs.

Mackey extended Adler's theory to describe the transient response of an injection-locked (klystron) oscillator to a change of the injected signal^[35]. The instantaneous angular beat frequency (rate of phase change) is given by the transcendental equation

$$\frac{d\alpha}{dt} = -\pi B \sin \alpha + 2\pi\delta f . \quad (B-5)$$

From Equation (B-5), Mackey determined the transient response by solving for the phase difference between the oscillator and the injection signal. His solution describes the response of the oscillator when the locking signal is switched on with an initial phase difference $\alpha(0)$ with respect to the free-running oscillator. The solution also describes the case of a phase step function of the locking signal by an amount $\alpha(0)$. A special case to his solution is when the frequency of the free-running oscillator is equal to that of the injection source. The phase difference between the injected signal and the oscillator is then given as a function of time as

$$\alpha(t) = 2 \tan^{-1} \left(e^{-\pi B t} \tan \frac{\alpha(0)}{2} \right), \quad (B-6)$$

where $\alpha(0)$ is the initial phase difference between the injection signal and the free-running oscillator signal.

Figure-64 is a plot of $\alpha(t)$ against πBt with $\alpha(0)$ as a parameter. For the case of the phase code modulation shown in Figure-65 we have the following initial conditions when a 90° phase step is applied*:

- a) oscillator and locking source frequencies are equal.
- b) $\alpha(0) = 90^\circ$.

Since we require $\alpha(t) \approx 0$, Equation (B-6) simplifies to give

$$\pi Bt \approx 1 \ln \frac{114.6 \tan \alpha(0)/2}{\alpha(t) \text{ (degrees)}}, \quad (\text{B-7})$$

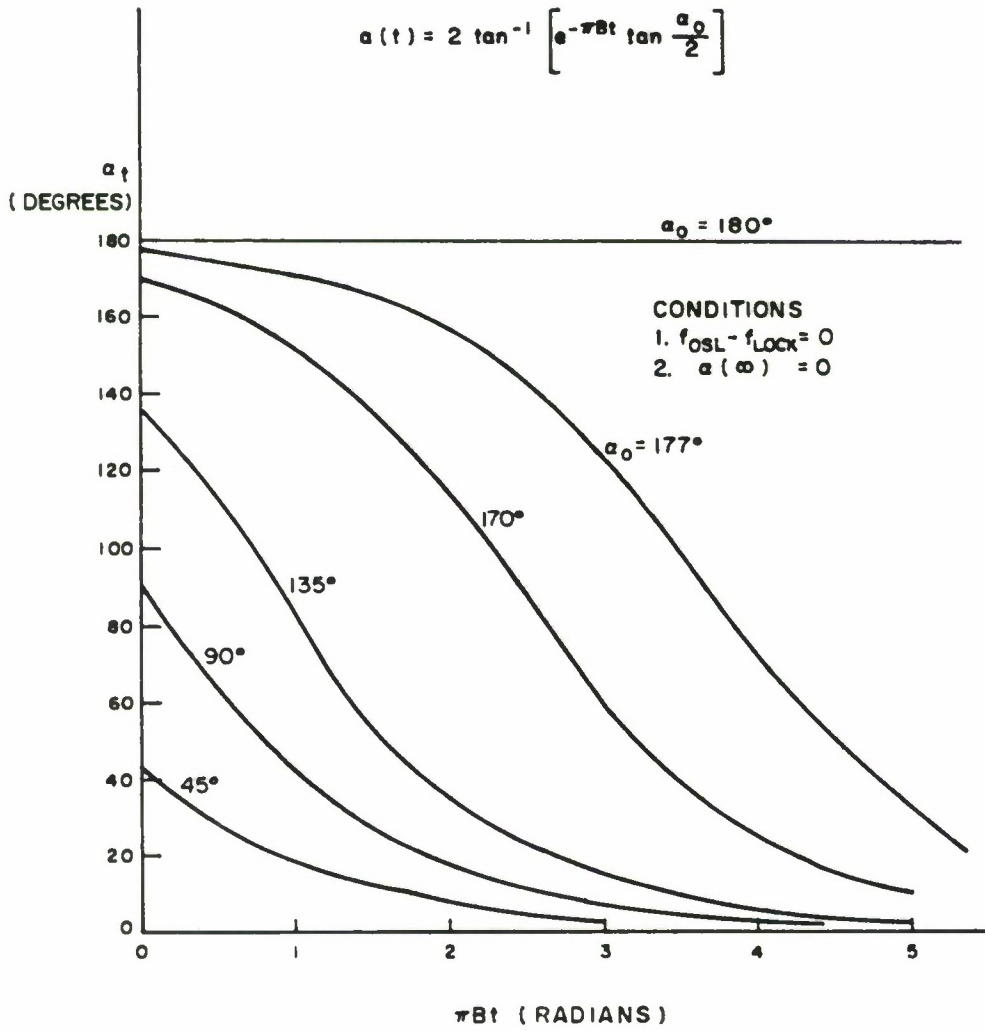
and for a phase code with $\alpha(0) = 90^\circ$,

$$t \approx \frac{733}{B} \log \frac{114.6}{\alpha(t)} \text{ ns}, \quad (\text{B-8})$$

for B in MHz and $\alpha(t)$ in degrees.

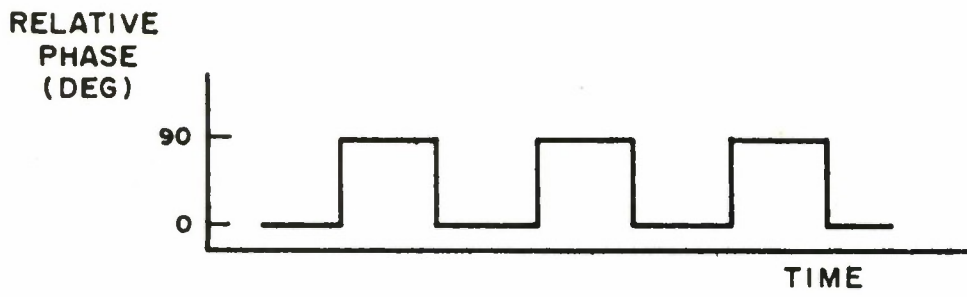
To minimize the phase distortion the modulation bit length must be large compared with the phase response time. Alternatively, for a specified modulation rate the distortion is minimized by increasing the lock bandwidth, which will reduce t . This is done either by lowering the oscillator Q or increasing the injection ratio. For example, let $B = 150$ MHz, $\alpha(0) = 90^\circ$ and $\alpha(t) = 2^\circ$. From the

*A phase step of 90° was chosen for these tests because the analytic relationships were well defined. Although the expression "binary phase coding (BPC)" is normally taken to mean a phase code $0 - \pi - 0 - \pi$ ----, the 90° case may also be considered a binary phase code.



1A-32,685

Figure 64 LOCKED OSCILLATOR TRANSIENT RESPONSE



IA-32,074

Figure 65 PHASE MODULATION

graph, $\pi Bt \approx 4.5$ and $t \approx 9.6$ ns, or from Equation (B-5), $t = 9.4$ ns.

Hence the modulation frequency must be much less than 105 MHz.

Figure 66 shows the phase modulation of the oscillator in the above example, for a bit rate of 25 MHz.

For the case where $\alpha(0) = 180^\circ$, Figure 64 shows that synchronization theoretically would not occur ($\alpha(\infty) \neq 0$). When the injection signal is (hypothetically) instantly reversed in phase the oscillator may either increase or decrease its phase in order to move towards the new phase-lock condition. The direction and response time taken in reality are determined mainly by the finite phase slope of the injection signal pulses between states. A typical response is shown in Figure 44. In his paper, Mackey discusses, in practical terms, this case where $\alpha(0) = 180^\circ$ and also the case where the oscillator and locking source frequency are not equal.

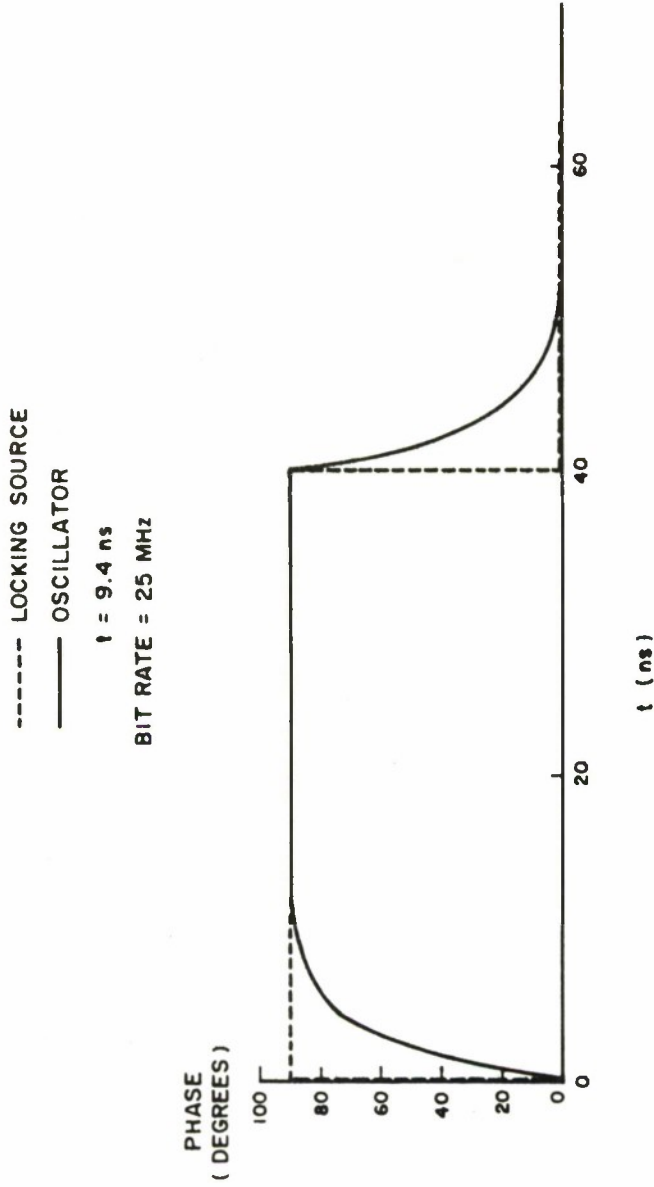


Figure 66 LOCKED OSCILLATOR PHASE FOR 90° PHASE CODE

APPENDIX C

SIMPLIFIED DESCRIPTION OF DIODE OSCILLATOR OPERATION

IMPATT OSCILLATORS

An avalanche diode derives its unique properties by operating in a mode that produces a negative conductance. The origin of this negative conductance is presented below in a simplified physical approach for a Read diode. But, first some background information is desired.

'When a carrier (electron or hole depending on doping) moves in the direction that an electric field tends to push it, the field does work on the carrier, and the field thus gives up energy. When a carrier moves opposite to the direction that an electric field tends to push it, the opposite occurs: i.e., the carrier pumps energy into the electric field. The basic procedure involved in the Read diode--or, for that matter, for transistors or vacuum tubes as well--is that of obtaining a situation in which a dc field pushes the carrier in a direction opposite to that of an ac field. Thus, energy is expended by the DC field and is absorbed by the ac field."^[60]

Since, by definition, an AC field reverses direction, a technique is needed in order to realize a net transfer of energy. The technique for accomplishing this in the Read diode is unique in that it does

not require a third electrode as with transistors. The elimination of the third electrode simplifies the fabrication of the device to be used at microwave frequencies. One of the fundamental limitations of operating transistors at high frequencies is the time it takes for carriers to diffuse across the base region from the emitter to the collector. (Transit time $\ll 1/f_0$.)

Impact avalanche has the property that, as long as the critical field is exceeded in a region, the particle current through the region will grow exponentially with time. For fields below the critical field, the current decays exponentially to a small steady-state value.

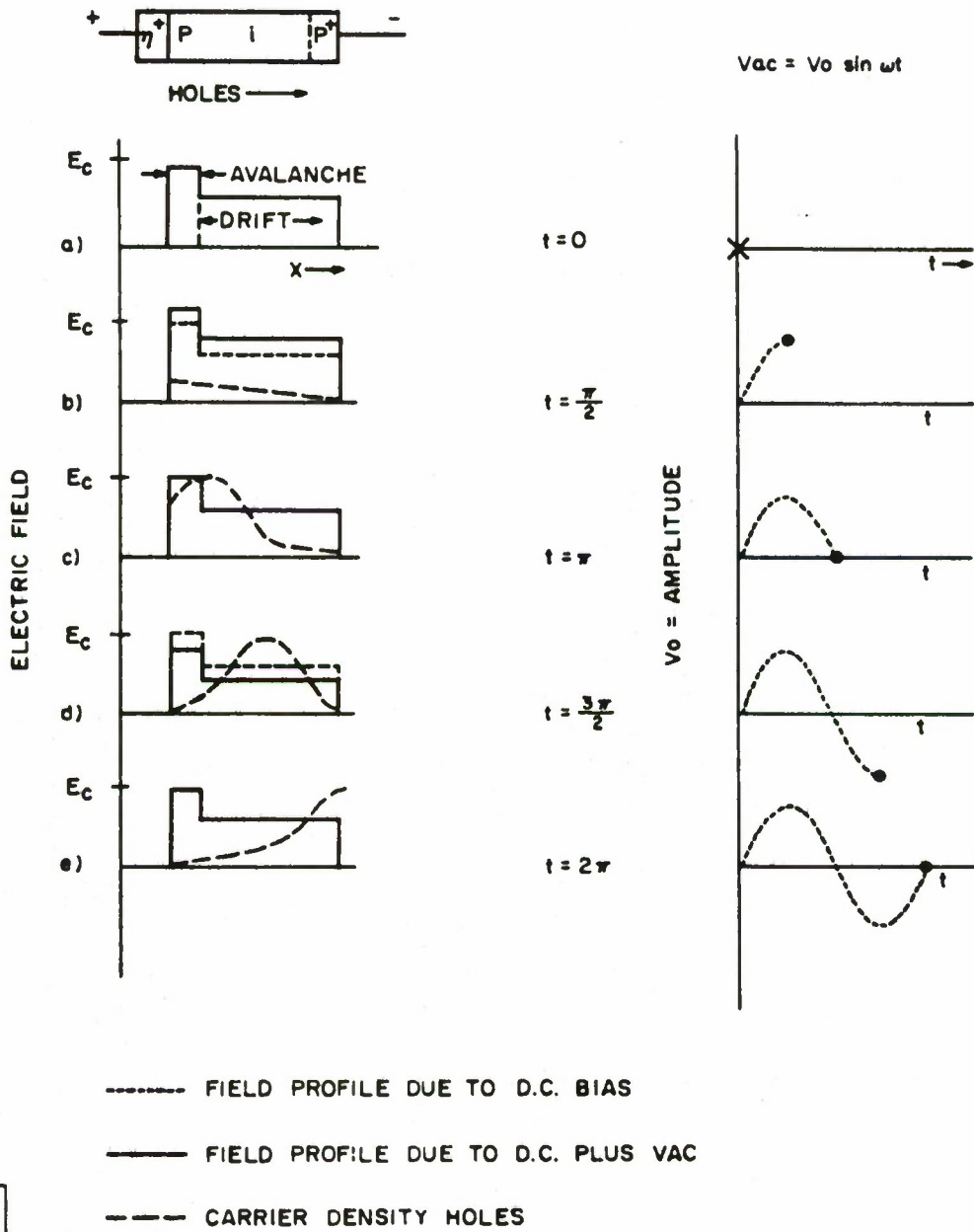
Referring now to a Read diode and to the various field patterns which develop across the biased diode (Figure 67), a simplified approach to the energy interchange will be presented.

First, a high reverse dc bias is applied to the diode which produces an electric field (E) in the diode. Under this condition and at time $t = 0$, no current flows except for a small reverse saturation current.

Since noise is always present in electronic circuitry, it is reasonable to assume that a small ac voltage (V_{ac}) is also present across the diode terminals. For extremely short intervals of time we can assume that $V_{ac} = V_0 \sin \omega t$. At time $t = 0$ the electric field (E) vs. distance across the diode and the V_{ac} would appear as

shown in Figure 67-a. At time $t = 0$, the small number of carriers (holes) present in the thin avalanche region begin to multiply and grow exponentially. As carriers are generated within this thin region, they are continually swept out by the electric field.

When a quarter cycle of V_{ac} has passed, the charge-density distribution and the E field will be as shown in Figure 67-b. Here the field in the diode is determined from the dc bias (E_{DC}) plus $|V_{ac}|$ the total of which is greater than the voltage required to produce avalanche breakdown, i.e., $E_{dc} + |V_{ac}| > E_{critical}$. Therefore the charge density starts to grow exponentially. As it continues to grow, more and more carriers are fed into the drift region. However, these carriers are drifting at the wrong time of the cycle and they are having work done on them by the ac field. Ideally, we wish they were not there, but relatively speaking they are few in number, i.e., although the number of carriers produced in the avalanche region has been growing exponentially with time, the starting concentration was so small that few carriers are actually present. After an additional quarter cycle, the situation is as shown in Figure 67-c. Throughout this time period the current in the avalanche region has been growing. Also note that just at this time, when the ac field is about to be oppositely directed to the dc field (and drifting carriers would put energy into the AC field), there is a large concentration of carriers ready to drift through the drift region of the diode. This concentration is the end result of



IA-32,683

Figure 67 OPERATION OF IMPATT OSCILLATOR

the growth and is cut off when the electric field in the avalanche region goes below the critical value. ($E_{\text{field}} - |V_{\text{ac}}| < E_c$). When the ac field goes another quarter cycle the charge density is as shown in Figure 67-d. Note that the field due to V_{ac} is opposite the dc field. As long as this AC field is smaller than the DC field (so that carriers will not turn around and go the wrong way), carriers crossing the drift space at this time will put energy into the AC field. Finally, when the full cycle has been completed, the concentration of carriers is just about to make its exit before the AC field can get very large in the wrong direction (Figure 67-e).

"This circumstance is not fortuitous but is a direct result of Read's prescription of making the drift region of such extent that the carrier transit time through it is one half period of the frequency at which the device is to operate".

$$f = \frac{1}{2\tau} \quad \tau = \text{carrier transit time.}$$

Thus we have a net transfer of energy into the AC field from the dc field, and the AC voltage can grow. In an appropriate circuit, self-sustained oscillation can be obtained.

GUNN AND LSA OSCILLATORS

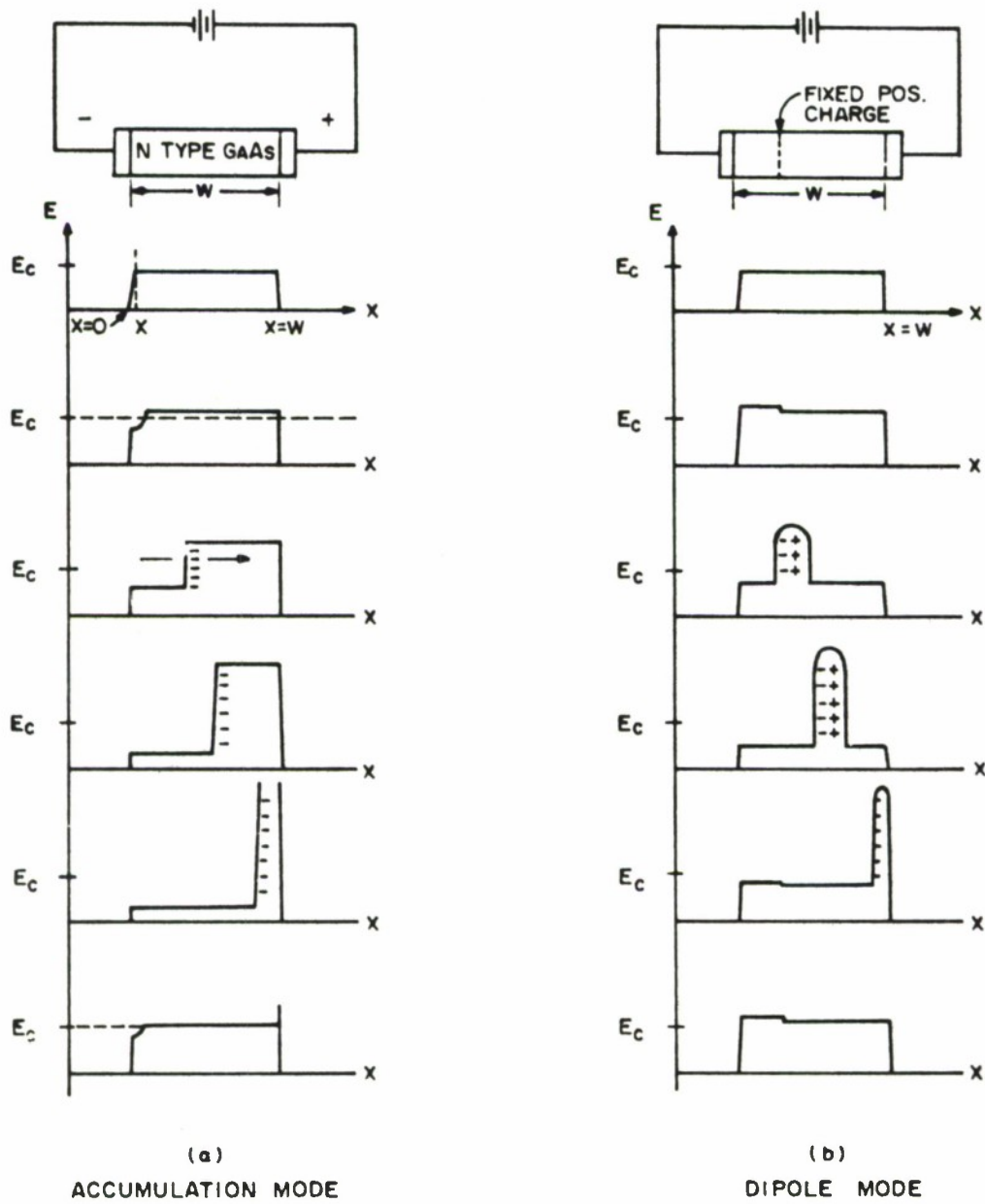
As was stated earlier, the Gunn oscillator is a transferred electron device working in a particular mode. Its operation is based on a class of semiconductor that exhibits high and low mobility

conduction bands.(defined earlier). Attention here will focus on the mechanics of the domain growth and travel through the semiconductor.

Figure 68-a illustrates the domain growth and travel in a Gunn diode. The sample of bulk material (n type G_aA_s) is connected to a DC supply by means of ohmic contacts. When DC voltage is applied, electrons enter the material at the source or negative electrode and exit at the drain or positive electrode.

When the voltage is below the critical field the device behaves as a simple resistor. As the bias is increased so that $V > E_c$ the electrons enter the source electrode faster than they leave. The field from $X = 0$ to $X = X_1$ is greater than E_c and the mobility is low. Therefore, a layer of electrons starts to form at $X = X_1$ and builds up as it moves toward the drain electrode. As soon as it is collected the process repeats itself.

The operation just described is referred to as an accumulation mode which is extremely unstable and very sensitive to doping fluctuation. If, however, one provides within the bulk material, a positive space charge or a region depleted of electrons a dipole or high-field-domain mode will form. An intentional doping fluctuation will have the effect of producing a positive field or positive charge accumulation. However, since a negative accumulation will also be present, a dipole will result and propagate through the sample, as illustrated in Figure 68-b.



IA-32,682

Figure 68 OPERATION OF GUNN OSCILLATOR

Since the applied dc voltage is constant, the area under the curves of Figures 68-a and 68-b will be constant. Therefore, when the dipole reaches the drain electrode there is, for a brief moment, an accumulation mode that causes the field across the sample to increase above E_c . With the field above E_c , conditions are again right for the start of a new dipole.

The process described above produces a current waveform the shape of which could resemble the one shown in Figure 69. Many different shapes have been observed, but this one is considered to be the classical output waveform of a bulk effect device.

The waveform consists of spikes of current, each corresponding to the absorption of a domain at the anode. The smaller peaks result from minor inhomogeneities in the specimen which can vary greatly from sample to sample. The frequencies with which the spikes of current can be generated can be quite high (X-band) depending on the length of the material.

The frequency of the Gunn oscillator is determined by the high field domain drift velocity V_d and the width of the diode (w), making the Gunn oscillator, like the avalanche, transit-time-limited.

$$\text{frequency} = \frac{V_d}{w} .$$

This frequency may be shifted almost over an octave band by adjusting the resonant circuit frequency which affects the position of the domain formation in the semiconductor.

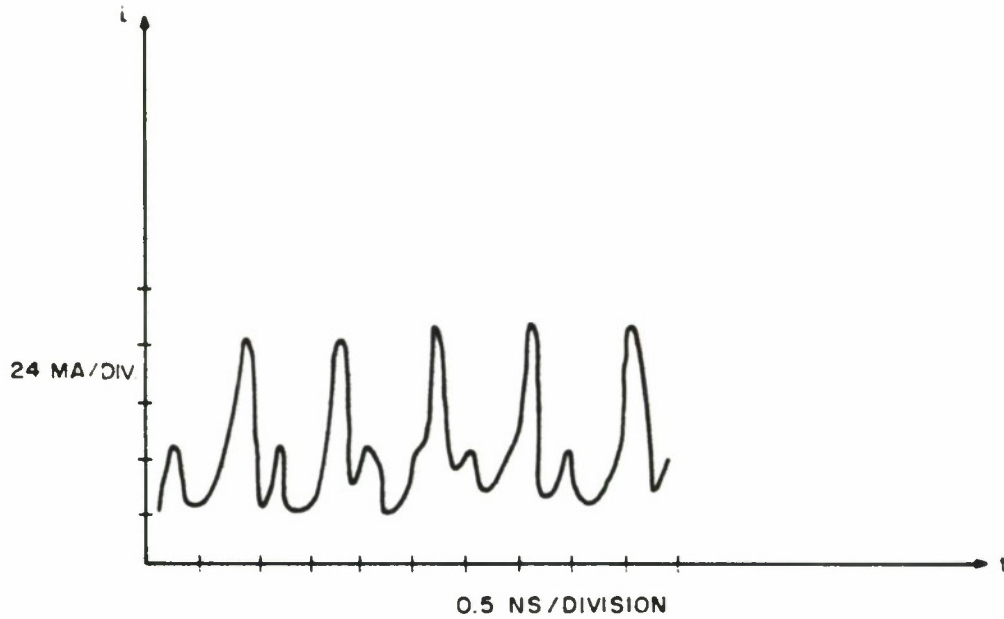


Figure 69 GUNN OSCILLATOR CURRENT WAVEFORM

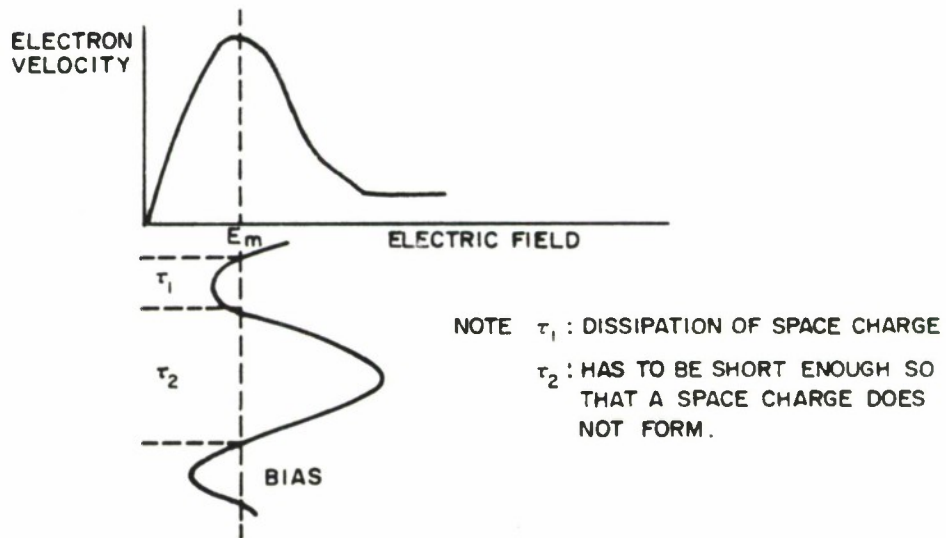


Figure 70 OPERATION OF LSA OSCILLATOR

IA-32,681

As previously discussed, when a transferred electron device is biased above the critical field, a differential negative conductivity is observed, but the inherent instability of a bulk sample results in the formation of accumulation and dipole charges and the negative conductivity therefore cannot be utilized over the entire sample: i.e., with the formation of a space charge the surrounding electric field drops below the critical voltage into the positive resistance region thereby eliminating that portion of the bulk material from exhibiting negative conductance.

In the LSA mode, however, a far greater percentage of the bulk material is forced to exhibit negative conductance. Therefore, most of the device contributes to the energy transfer of dc to RF.

'To understand the operation of the LSA mode, let us consider a Gunn device operated in a cavity whose resonant frequency is several times higher than the intrinsic frequency of the diode. The bias voltage applied to the device is set at several times the threshold voltage, and the high-frequency voltage swing across the device is large enough to reduce the voltage below the threshold for a short part of each cycle. (The resonant circuit is initially lightly loaded at the LSA frequency. Oscillations first start at the Gunn frequency and then shift to the frequency of the LSA mode. Once LSA oscillations have started,

the circuit can be more heavily loaded to increase efficiency and output power.) This large voltage swing is obtained by lightly loading the device at the LSA frequency. With a proper choice of frequency and doping, the electric field across the device rises from below threshold to several times the threshold value so quickly that an accumulation layer does not have time to grow into a high field domain".^[61]

For example, in Figure 68-b the high field domain is still hardly visible in the first two frames.

"The electric field over most of the device is uniform and changes in synchronism with the terminal voltage. Therefore, the field remains above the threshold over most of each cycle, and most of the device exhibits the negative resistance. If the frequency increases, the distance over which the accumulation layer travels decreases, and more electrons contribute energy to the load. Thus the efficiency in this mode increases with frequency".^[61]

Therefore, for LSA operation the voltage must swing below the threshold voltage and stay there long enough to dissipate the space charge that tries to grow each cycle. Also, the part of the voltage swing that is above the threshold voltage must not last too long or a space charge will build up and form a domain (Figure 70). Because

the space charge is not allowed to completely form, this mode of operation is referred to as Limited Space-Charge Accumulation. Another important aspect of this mode is that it is not transit time limited. It derives its ability to transform DC to AC directly from the negative differential drift velocity of the individual electron with respect to electric field rather than to the movement of a space charge across the device.

REFERENCES

1. A. Gold, "Trends in Phased Array Systems," *Microwave Journal*, 13, No. 9, p 8, September 1970.
2. *Microwave Journal*, MIC's/Phased Arrays, 12, No. 9, September 1970. See especially; B. T. Vincent et al, "Microwave Integrated Circuits for Phase Array Applications," p 53. Also, H. T. MacFarland et al, "The Role of Solid State in Phase-Array Radars," p 63.
3. V. J. Higgins et al, "The Utility and Performance of Avalanche Transit Time Diode and Transferred Electron Oscillators in Microwave Systems," *Microwave Journal*, 12, No. 7, p 37, July 1970.
4. D. R. Ayer et al, "The Evolution of Strip Transmission Line," *Microwave Journal*, 12, No. 5, p 31, May 1969.
5. B. D. Campbell et al, "Microwave Solid State Sources and Integrated Circuits--Report for Fiscal Year 1969," MITRE Technical Report No. 1761, 17 November 1969. Also USAF Systems Command, Electronic Systems Division, ESD-TR-70-138, Contract F19(628)68-C-0365, Project 7150, May 1970.
6. W. Wasylkiwskyj, "Mutual Coupling and Element Efficiency for Infinite Linear Arrays," *Proc. IEEE*, 56, No. 11, p 1901, November 1968 (Special issue on Electronic Scanning).
7. J. D. Kraus, Antennas, Ch. 4 and 11, McGraw-Hill, New York, 1950.
8. Special Issue on Semiconductor Bulk-Effect and Transit Time Devices. *IEEE Trans.*, ED-13, No. 1, January 1966.
9. Second Special Issue on Semiconductor Bulk-Effect and Transit Time Devices. *IEEE Trans.* ED-14, No. 9, September 1967.
10. W. T. Read, "A Proposed High Frequency Negative-Resistance Diode", *The Bell System Technical Journal*, March 1958.

11. B. Hoefflinger, "Recent Developments on Avalanche Diode Oscillators," *Microwave Journal*, p 101, March 1969.
12. T. K. Gaylord, "Gunn Effect Bibliography," *IEEE Trans.*, ED-15, No. 10, October 1968.
13. T. K. Gaylord, "Gunn Effect Bibliography," *IEEE Trans.*, ED-16, No. 5, May 1969.
14. B. C. DeLoach, Jr., et al, "Device Physics of TRAPATT Oscillators," *IEEE Trans.*, ED-17, No. 1, January 1970.
15. R. Blau, "A Microwave Integrated Circuit Avalanche-Diode Oscillator," *MTT Letter*, p 196, March 1968.
16. S. G. Liu et al, "High Power K-Band Silicon Avalanche Diode Oscillators," *Proc. IEEE Letters*, p 919, June 1970.
17. J. F. Reynolds et al, "High Efficiency Transferred Electron Oscillators," *Proc. IEEE Letters*, p 1692.
18. G. Gibbons et al, "High Efficiency Avalanche-Diode Oscillators and Amplifiers at X Band," *Proc. IEEE Letters*, p 512, March 1970.
19. W. J. Evans, "Circuits for High Efficiency Avalanche-Diode Oscillators," *IEEE Trans.*, MTT-17, No. 12, p 1060, December 1969.
20. W. J. Evans et al, "CW Silicon TRAPATT Operation," *Proc. IEEE Letters*, p 284, February 1970.
21. J. W. Gewartowski, "Power Combination With Diode and Circuits Array," *IEEE International Convention Digest*, 70C 15, p 242, March 23-26, 1970.
22. C. B. Swan et al, "Composite Avalanche Diode Structures for Increased Power Capability," *IEEE Trans.*, ED-14, pp 584-589, September 1967.
23. J. G. Josenhans, "Diamond as an Insulating Heat Sink for a Series Combination of IMPATT Diodes," *Proc. IEEE*, 56, pp 762-763, April 1968.

24. S. G. Liu, J. J. Risko, "Stacked Avalanche-Diode Microwave Oscillators," Int'l. Electron Devices Meeting, Washington, D.C., October 1969.
25. H. Fukui, "Frequency Locking and Modulation of Microwave Silicon Avalanche Diode Oscillators," Proc. IEEE, 54, pp 1475-1477, October 1966.
26. F. Ivanek, V.G.K. Reddi, "X-Band Oscillator and Amplifier Experiments Using Avalanche Diode Periodic Structures," 1969 ISSCC Digest, 12, pp 80-81, February 1969.
27. J. J. Sie, W. J. Crowe, "A One Watt CW Avalanche Diode Source or Power Amplifier," 1969 Int'l. Microwave Symposium, Dallas, May 1969.
28. I. Tatsuguchi, "A Frequency-Modulated Phase-Locked IMPATT Power Combiner," 1970 Int'l. Solid-State Circuits Conference, February 1970.
29. C. W. Lee et al, "High Power X-Band Integrated GaAs Avalanche Diode Amplifier," Government Microcircuit Applications Conference Digest of Papers, 1, p 30, October 1970.
30. S. G. Liu, "Microstrip High-Power High-Efficiency Avalanche Diode Oscillator," IEEE Trans., MTT-17, No. 12, December 1969.
31. S. G. Liu, "Stacked High Power Avalanche Diode Oscillators," IEEE Letters, p 707, April 1969.
32. K. L. Kolyebue et al, "The Design of Broadband Frequency Doublers Using Charge Storage Diodes," IEEE Trans, MTT-17 p 1077, December 1969.
33. A. T. Botka et al, "Microwave Integrated Circuit Front End for Low Power Radars," International Solid-State Circuits Conference, p 50, 1968.
34. Denison et al, "An X-Band Integrated Circuit Marine Radar Beacon," European Microwave Conference, 8-12, September 1969.

35. R. Blau, "A Microwave Integrated Circuits Avalanche Diode Oscillator," *MTT Letters*, p 196, March 1968.
36. J. W. Amoss, "Frequency Modulation of Avalanche Transit Time Oscillator," *IEEE Trans.*, MTT-15, No. 12, p 742, December 1967.
37. M. I. Grace, "Varactor-Tuned Avalanche Transit-Time Oscillator with Linear Tuning Characteristics," *MTT Letters*, p 44, January 1970.
38. M. Dyoyk, "Ferromagnetically Tunable Gunn Effect Oscillator," *Proc. IEEE Letters*, p 1363, August 1968.
39. F. J. Rosenbaum et al, "Gunn Effect Swept Frequency Oscillator," *Proc. IEEE Letters*, p 2165, December 1968.
40. M. Omori, "Octave Electronic Tuning of a Gunn Diode Using a Yig Sphere," *Proc. IEEE Letters*, p 97, January 1969.
41. M. I. Grace, "Magnetically Tunable Transit-Time Oscillator," *Proc. IEEE Letters*, p 771, April 1968.
42. R. Adler, "A Study of Locking Phenomena in Oscillator," *Proc. IRE and Wave and Electron*, 34, p 351, June 1946.
43. D. D. Khandelwal, "Injected Signal Characteristics of High Power Avalanche Diode Oscillators," *Proc. IEEE Letters*, p 928, June 1970.
44. H. R. Holliday, "The Effect of Operating Parameters and Oscillator Characteristics Upon the Phase Angle Between a Locked X-Band Gunn Oscillator and its Locking Signal," *IEEE Trans.*, ED-17, No. 7, p 527, July 1970.
45. G. King, "Frequency Modulation of Gunn Effect Oscillator," *IEEE Trans.*, ED-14, No. 10, October 1967.
46. J. R. Ashley et al, "Measured FM Noise Reduction by Injection Phase Locking," *Proc. IEEE Letters*, p 155, January 1970.
47. "Stable X-Band Gunn Source Takes Unregulated Input Voltages," *Microwaves*, p 118, October 1969.

48. W. K. Kennedy, "Yig-Tuned Bulk GaAs Oscillators," Watkins-Johnson Application Note 100308, November 1969.
49. D. A. Fleri et al, "Amplifying Properties of Gunn Oscillator in Injection Locked Mode," Proc. IEEE Letters, p 1205, June 1969.
50. K. Sugawara, "A Wide-Band 4 GHz Esaki-Diode Injection Locked Oscillator," Proc. IEEE Letters, February 1969, p 215.
51. B. Glance, "Microstrip IMPATT Oscillator with High Locking Figure of Merit," Proc. IEEE Letters, p 2052, November 1969.
52. J. R. Vaughn, "The Injection-Locked Voltage-Tunable Magnetron," Microwave Journal, p 45, October 1968.
53. R. C. Mackey, "Injection Locking of Klystron Oscillators," IRE Trans. Microwave Theory and Techniques, p 228, July 1962.
54. Microwave Journal Handbook and Buyer's Guide, February 1969, p 65.
55. T. G. Bryant et al, "Parameters of Microstrip Transmission Lines and of Coupled Pairs of Microstrip Lines," Worcester Polytechnic Institute, July 15, 1968. Also IEEE Trans., MTT-16, December 1968.
56. H. A. Wheeler, "Transmission Line Properties of Parallel Strips Separated by a Dielectric Sheet," IEEE Trans., MTT-13, No. 3, p 172, March 1965.
57. C. P. Hartwig, "Basic Parameters of Microstrip Transmission Lines," IEEE International Convention Digest, p 426, March 23-26, 1970.
58. C. P. Hartwig et al, "Frequency Dependent Behavior of Microstrip," IEEE International Microwave Symposium Digest, No. 68C38, p 110, May 20-22, 1968.
59. R. A. Pucel et al, "Losses in Microstrip," IEEE Trans., MTT-16, p 342, June 1968.

60. B.C. DeLoach, Jr., "Avalanche Transit-Time Microwave Diodes," Microwave Semiconductor Devices and Their Circuit Application, H. A. Watson, ed., C1969, p 475.
61. M. Uenohara, "Bulk Gallium Arsenide Devices," Microwave Semiconductor Devices and Their Circuit Applications, H. A. Watson, ed., C1969, pp 521-522.
62. Arnold et al, "MIC Applications to Radar Systems," Microwave Journal, p 42, July 1969.
63. Bandy et al, "MERA Modules--How Good in an Array," Microwaves, August 1969.
64. S. March, "Microwave Micromin Bibliography," (1951-1968), Microwaves, 8, No. 12, p 59, December 1969.
65. S. March, "Microwave Micromin Bibliography," (Cont. 1968-September 1969), Microwaves, 9, No. 1, January 1970.
66. K. K. N. Chang, "High Efficiency Avalanche Diode Microwave Sources", IEEE International Convention Digest, 70C15, March 23-26, 1970, pp 240-241.

DOCUMENT CONTROL DATA - R & D

(Security classification of title, body of abstract and indexing annotation must be entered when the overall report is classified)

1. ORIGINATING ACTIVITY (Corporate author) The MITRE Corporation Bedford, Massachusetts 01730		2a. REPORT SECURITY CLASSIFICATION UNCLASSIFIED	
		2b. GROUP	
3. REPORT TITLE MICROWAVE SOLID STATE SOURCES AND INTEGRATED CIRCUITS - FINAL REPORT			
4. DESCRIPTIVE NOTES (Type of report and inclusive dates)			
5. AUTHOR(S) (First name, middle initial, last name) Bruce D. Campbell, Peter J. Benson, Alfred L. Murphy, Ved P. Nanda, Ronald S. Steriti			
6. REPORT DATE JULY 1971	7a. TOTAL NO. OF PAGES 164	7b. NO. OF REFS 66	
8a. CONTRACT OR GRANT NO. F19(628)-71-C-0002	8b. ORIGINATOR'S REPORT NUMBER(S) ESD-TR-71-229		
b. PROJECT NO. 702B	8c. OTHER REPORT NO(S) (Any other numbers that may be assigned this report) MTR-2028		
c.			
d.			
10. DISTRIBUTION STATEMENT Approved for public release; distribution unlimited.			
11. SUPPLEMENTARY NOTES		12. SPONSORING MILITARY ACTIVITY Electronic Systems Division, Air Force Systems Command, L. G. Hanscom Field, Bedford, Massachusetts 01730	
13. ABSTRACT This report describes the completion of the studies, initiated in FY 69, carried out to assess the practicability of applying microwave integrated circuits and solid state fundamental oscillators to future sensor subsystems for radar and communications, including data relay. The X-band eight-element phased array was evaluated, a simple MIC module including a printed antenna was constructed and studies were carried out of avalanche diode oscillator modulation characteristics, MIC IMPATT avalanche diode oscillators, MIC antennas, and MIC evaluation techniques.			

KEY WORDS	LINK A		LINK B		LINK C	
	ROLE	WT	ROLE	WT	ROLE	WT
CRYSTAL OSCILLATORS						
DATA LINKS						
DATA TRANSMISSION						
GUNN DIODES						
MICROWAVE EQUIPMENT						
MICROWAVE INTEGRATED CIRCUITS						
MICROWAVE OSCILLATORS						
OSCILLATORS						
RADAR RECEIVERS						
TELECOMMUNICATIONS						
TELEMETRY						